Making Single-cell Electroporation with Microelectrodes Predictable and Reproducible

by

Bradley Alan Lambie

B.S. Chemistry, Edinboro University of Pennsylvania, 2000

Submitted to the Graduate Faculty of

Arts and Science in partial fulfillment

of the requirements for the degree of

Doctor of Philosophy in Analytical Chemistry

University of Pittsburgh

2010

UNIVERSITY OF PITTSBURGH

This thesis was presented

by

Bradley Alan Lambie

It was defended on

March 26th, 2010

and approved by

Dr. Shigeru Amemiya, Associate Professor, Department of Chemistry (University of

Pittsburgh)

Dr. Adrian Michael, Associate Professor, Department of Chemistry (University of Pittsburgh)

Dr. Owe Orwar, Professor, Department of Biophysical Chemistry (Chalmers Univeristy of

Technology)

Dr. Stephen Weber, Professor, Department of Chemistry (University of Pittsburgh)

Making Single-cell Electroporation with Microelectrodes Predictable and Reproducible

Bradley Alan Lambie, PhD

University of Pittsburgh, 2010

Electroporation is the creation of transient pores in a membrane by the application of an external electric field. When using microelectrodes, which can be used to electroporate single-cells, for applying an electric field to the cell, there is a question of how much voltage to apply. Unlike in bulk electroporation where hundreds of volts may be applied between electrodes, a rather small voltage is applied to a microelectrode in single-cell electroporation. In the single-cell experiment with microelectrodes, a substantial fraction of the voltage does not exist in solution because it is lost at the microelectrode/solution interface. This problem is the same as the classical electrochemist's problem of knowing the 'iR' drop in solution and correcting for it to obtain true interfacial potential differences. Therefore, we have used current interruption experiments to determine the iR drop in solution near microelectrodes. Because the electric field produced by microelectrodes is inhomogeneous, computer simulations were preformed to understand the electric field distribution. Results of the current interruption are validated by comparing two independent measurements of the resistance in solution: one value results from the measured iR drop in conjunction with the known applied current. The other value results from a measured solution conductivity and a computer simulated cell constant. This paper shows how to calculate the approximate current required to electroporate a cell with a microelectrode of a particular size, shape and distance from the cell. Carbon fiber microelectrodes were used to electroporate single A549 cells using the current calculated.

TABLE OF CONTENTS

LIST OF TABLES

LIST OF FIGURES

PREFACE

1.0   INTRODUCTION: ELECTROPORATION

A better understanding of the parts, single cells, leads to a better understanding of whole, regulation of metabolic processes, response to stimuli, etc. Because of this, the analysis of single cells is of great importance to the scientific community. Recently the analysis of single cells has become more practical due to the miniaturization of laboratory equipment and the increased sensitivity of detection methods. The current methods used for determining concentrations of solutes in a single cell generally mean death to the cell. The methods include physically smashing or grinding cells and lysing the cells[1-5]. These methods when performed on single cells also have apparent flaws when one is concerned about the cytoplasmic concentration of a specific molecule, because of the possibilities of this molecule being present in organelles and/or in storage vesicles within the cell. When the cells are physically smashed or ground, the compartmentalization from the presence of organelles and other barriers is destroyed. Because of the destruction of these barriers, species within the cell that would not normally be found together are allowed to come in contact with each other. This decompartmentalization leads to the production of molecules that would not naturally be produced because of the mixing of these different areas[6]. The same decompartmentalization and production of unnatural species occurs when cells are lysed, but the amount produced is lessened due to the shortened time between decompartmentilzation and analysis[6]. The same methods used for single cell sampling are used when one wants to look at a cell's response to a stimulus, with a control group and a

stimulated group. This can lead to biased results because of inhomogeneities in the two cell cultures.

What is required is a way to open a window into a cell without the destruction of this compartmentalization, measure the concentration of the desired species, and then close this window to allow the cell to continue to function normally. Electroporation, the creation of transient pores in a membrane[7-9], may be a viable technique for the analysis of single cells.

Our hypothesis is that electroporation can be used to extract molecules out of a cell, because one can control the concentration of these molecules in the buffer solution on the outside of the cell. By making the concentration of the molecules of interest dramatically lower or zero in the buffer solution when compared to their cytoplasmic concentration, these molecules will diffuse through the electropores due to of the concentration difference[10].

The detection of the molecules that are extracted from the cell has to be sensitive, because the quantity of a specific molecule that diffuses through the electropores is minute. The detection of the electroactive molecules that diffuse out of these electropores is possible with electrochemical detection. A similar type of experiment, using patch clamp and carbon fiber microelectrodes, was used to measure cytosolic catecholamines that diffused out of single chromaffin cells because of a concentration difference.

The use of electroporation to open a window in the cell membrane is advantageous, because when electroporation is done properly, the pores created spontaneously reseal. After the pores reseal the stimulus can be applied, and the same cell can be electroporated again. This would avoid any of the inhomogeneities that arise because of the analysis of two different cell cultures. The use of this technique would also be quite useful when one wants to look at the

effects on a cell that has been repeatedly stimulated, to see if each successive response is the same as prior stimulations.

There are several aspects of microelectrode single cell electroporation that are not well understood, due to the infancy and lack of research on the technique. One of these aspects we hope to clarify is the electric field produced by the micro/nanoelectrodes. We have begun investigating this using a computer simulation program, FEMLAB now Comsol Multiphysics, which is discussed in more detail later in the paper. It is important to calculate the electric field produced by the microelectrode at the membrane because of the inhomogeneity of the electric field produced by microelectrodes. Knowing the electric field at the membrane is important to understanding the fundamental physical basics of electroporation. The theoretical membrane voltage is useful because the statically defined membrane voltage needed to reach the electroporation threshold is known for numerous cell lines from batch electroporation experiments. With the single cell approach, we will have the ability to determine whether the voltage required to electroporate is dependent on the variables, such as where on the membrane the field is applied, where the cell is in its growth cycle, etc.

Once we determine the electric field required, how does a researcher know how to apply this field in practice? There are several factors that affect the drop in potential between the two electrodes. A generalized diagram and graph of the potential drop is shown in Figure 1. First is the drop in potential at the microelectrode due to the positive electrode's double layer impedance. This large drop is followed by a much smaller gradual drop in the electric potential. This smaller gradual drop arises from the resistance of the solution between the positive electrode and cell membrane. Next is another small drop in potential across the cell membrane due to an accumulation of excess positive charges on the membrane's exterior and negative

charges on the membrane's interior. There is not a drop in potential inside the cell because very little current travels through the cell. Then, there is another small drop in potential due to the accumulation of excess negative charges on the membrane's exterior and positive charges on the membrane's interior at the other pole of the cell. Another small gradual drop occurs because of the resistance of the solution between the membrane and negative electrode. Finally, there is another large drop due to the negative electrode's double layer resistance.   This simple picture holds true if the field in the absence of the cell would be homogenous.   In single cell electroporation, the field is not homogeneous, so the picture below is oversimplified.
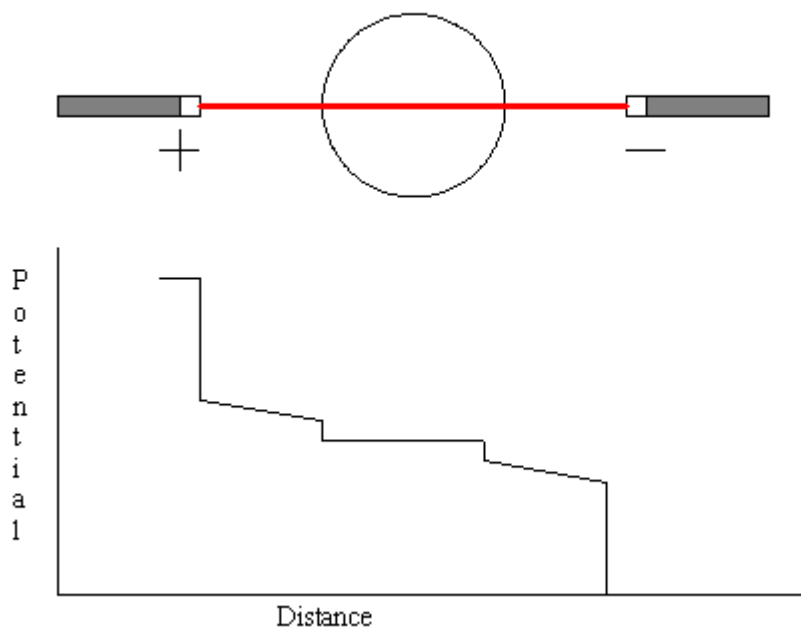
Figure 1. A generalized diagram of the electrode/cell setup and a graph of the potential profile it would create.

We have begun to investigate these drops in the electrical potential using current interruption experiments, which are discussed in more detail later. There are no papers on the application of current interruption to micro/nanoelectrodes at this time to my knowledge, so our

use of this technique is novel. The use of current interruption will allow one to compensate for the voltage drop due to the solution resistance in the applied voltage. Clarification of this aspect will enable microelectrode electroporation and all other types of electroporation to be better understood and hopefully more reproducible.

1.1   BASIC PHENOMENOLOGY

1.1.1   Membrane Voltage

Pores in electroporation are created due to the dielectric breakdown of the cell's or liposome's membrane. The membrane voltage at which this occurs varies with cell type or the lipid or lipids one uses to make the liposomes that are to be electroporated. The theoretical transmembrane voltage, V_m, can be calculated at different locations of a spherical cell or liposome membrane in a homogeneous electric field that is applied for duration t, can be calculated from the following equation[11],

$$V_m = 1.5 \, r_c \, E \cos \alpha \, [\, 1 - \exp(-t/\tau_m) \,] \tag{1}$$

where, r_c is the radius of the cell, E is the electric field strength, α is the angle in respect to the orientation of the electric field, and τ_m is the membrane relaxation time. τ_m can be calculated from the equation below[11]

$$\tau_m = r_c \, C_m \, [\, (R_{int} + R_{ext}) / 2 \,] \tag{2}$$

where, C_m is the membrane capacitance, and R_{int} and R_{ext} are the resistivities of the intracellular and extracellular fluids.

5

1.1.2 Pore Formation

The formation of pores in the bilayer lipid membrane by the applied external electric field is not fully understood at this time. The most widely accepted hypothesis for the formation of these pores is a three stage process[12]. The pores begin in the closed stage and as the external field is applied the lipids in the membrane rearrange to create a hydrophobic pore. A hydrophobic pore is characterized by the hydrocarbon tail of the lipids lining the interior walls of the pore. As the pore radius increases in size, up to about 5-10 nanometer, due to the external electric field still being applied the hydrophobic pore converts into a hydrophilic pore. This conversion is characterized by the rearrangement of the lipids so that the charged head groups line the interior walls of the pore. This process is depicted in figure 2 below[12].

Weaver, J.C., Electroporation of cells and tissues.
IEEE Transactions of Plasma Science (c) 2000 IEEE
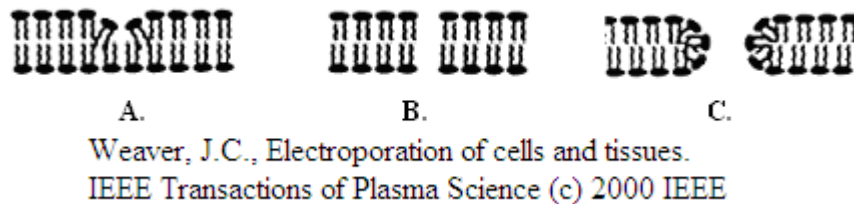
Figure 2. Most widely accepted hypothetical pore formation process A. Rearrangement begins with thinning of membrane. B. Hydrophobic pore, hydrocarbon tail line interior of pore. C. Hydrophilic pore, charged heads line interior of pore.

The dynamics of pore formation and closure where measured on a cell analog, giant unilamellar vesicles, which are similar in size to that of mammalian cells with a temporal resolution of ~30 μs by Dr. Riske.[13] Earlier experiments had been done on lipid vesicle, but with their size is much small than that of mammalian cells, but there observations were indirect and membrane tension and curvature could have had a significant role.[14-17] The formation of hydrophilic

pores were shown to be on the timescale of ~175 μs and resealed on the timescale of ~10 ms, when the giant unilammelar studied are assumed to initially be tension-free.[13]

While the pores one has created due to the applied external field are open, molecules that are normally impermealible can pass through the pores created in the cell's membrane. The transfer of molecules through these pores is due to the concentration gradient between the interior and exterior of the cell. By using electroporation, it is possible to load cells by transfering molecules from outside of the cell through the pores created into the cell's interior. The main restriction on which molecules can be loaded is size; they have to be able to fit through the created pores. This restriction causes the loading of some larger molecules impossible by this method, at this time, or to be loaded at a low efficiency or concentration. The same restriction applies to the molecules coming out of the cell; they also have to fit through the created pores.

1.2   TYPES OF ELECTROPORATION

1.2.1   Batch Electroporation

There are two major types of electroporation that are performed on cells: batch and single cell electroporation. Batch or bulk electroporation is performed on numerous cells suspended in a conductive buffer between two plate electrodes, as seen in figure 3 below[12].
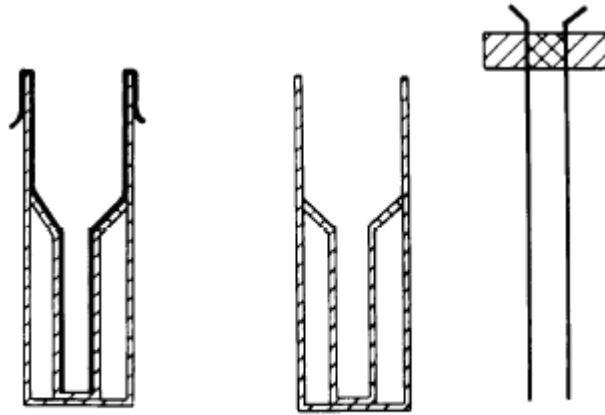
Weaver, J.C., Electroporation of cells and tissues.
IEEE Transactions of Plasma Science (c) 2000 IEEE

Figure 3. Cross sectional drawing of a typical place electrode electroporation apparatus made to fit into a cuvette.

Plate electrodes generally have a minimum spacing of 1-2 mm, and cuvette volumes of 10-100 μL[8]. The use of these plate type electrodes has both advantages and disadvantages. The advantages are that one can perform electroporation on many cells at the same time, and the electric field in the conductive buffer is for practical purposes homogenous. The disadvantages are the need for high field strengths, 10-12 kV/cm, and a statistical distribution of those cells that are impermeable, reversibly permeable, and irreversibly permeable is produced. This is due to the fact that the different cell membranes are not totally homogeneous, and the field strength varies by location with respect to the working electrode. Parameters and phenomena in these types of experiments should be considered average values. Another disadvantage arises because the electrodes have a high cross-sectional area, which cause a large current in the solution between the electrodes, high IR drops at the electrode surfaces, and significant changes in solution temperature.

1.2.2   Microchip-based Electroporation

Electroporation on single cells are performed using two different methods: microchip-based devices[12, 18-21] and micropipette type experiments[11, 22, 23]. Microchip-based devices that are used for single cell electroporation are related to batch electroporation in the sense that one can electroporated many cells in a short period of time. As seen below in figure 4, this type of setup is not very well designed to measure quantitatively a molecule's uptake or release from a cell or liposome. In figure 4[21], the left fluid inlet introduces a dilute cell suspension into the device. The second fluid outlet reduces the pressure on the bottom side of the micro hole, until a cell or liposome covers the hole, restricting or stopping the buffer solution from flowing through it. After the cell is in place, a voltage with the proper parameters, for that cell, is applied across the two electrodes causing the cell or liposome to electroporate. After the pores created by the cell's electroporation have closed, the third fluid inlet increases the pressure on the bottom side of the micro hole, until the cell is resuspended in solution. The last fluid outlet removes the cell suspension that has been electroporated from the device.

The microchip-based devices are however, very useful in determining the electric potential needed to electroporate a given type of cell, and to determine the time the pores are open for a given set of parameters used to electroporate the cell. It is possible to measure these two things using the microchip-based devices because when the cell or liposome is in place over the micro hole between the top and middle layers the resistance between the top and bottom electrode increases greatly. This dramatic increase occurs because the lipids that the membranes are composed of have a conductance of about 10^4 times lower than the buffer typical solution, in which they are suspended[8]. Once the cell is electroporated this resistance drops noticeably because the current can now travel through the cell, which has a typical conductance similar to

the surrounding buffer solution. This noticeable resistance drop also allows one to conclude that pores have been created in the membrane. During the experiment the voltage between the two electrodes can be determined by a potentiostat. With the dimensions of the microchip based device and the voltage needed to electroporate the cell, one can simulate the potential that was needed to electroporate that specific cell's membrane with a computer program. When the created pores close the resistance between the top and bottom electrodes will increase approximately back to its original value. The drop in resistance due to the opening of pores in the membrane and then increase in resistance due to the closing of the pores makes it possible for one to measure how long the pores were open.
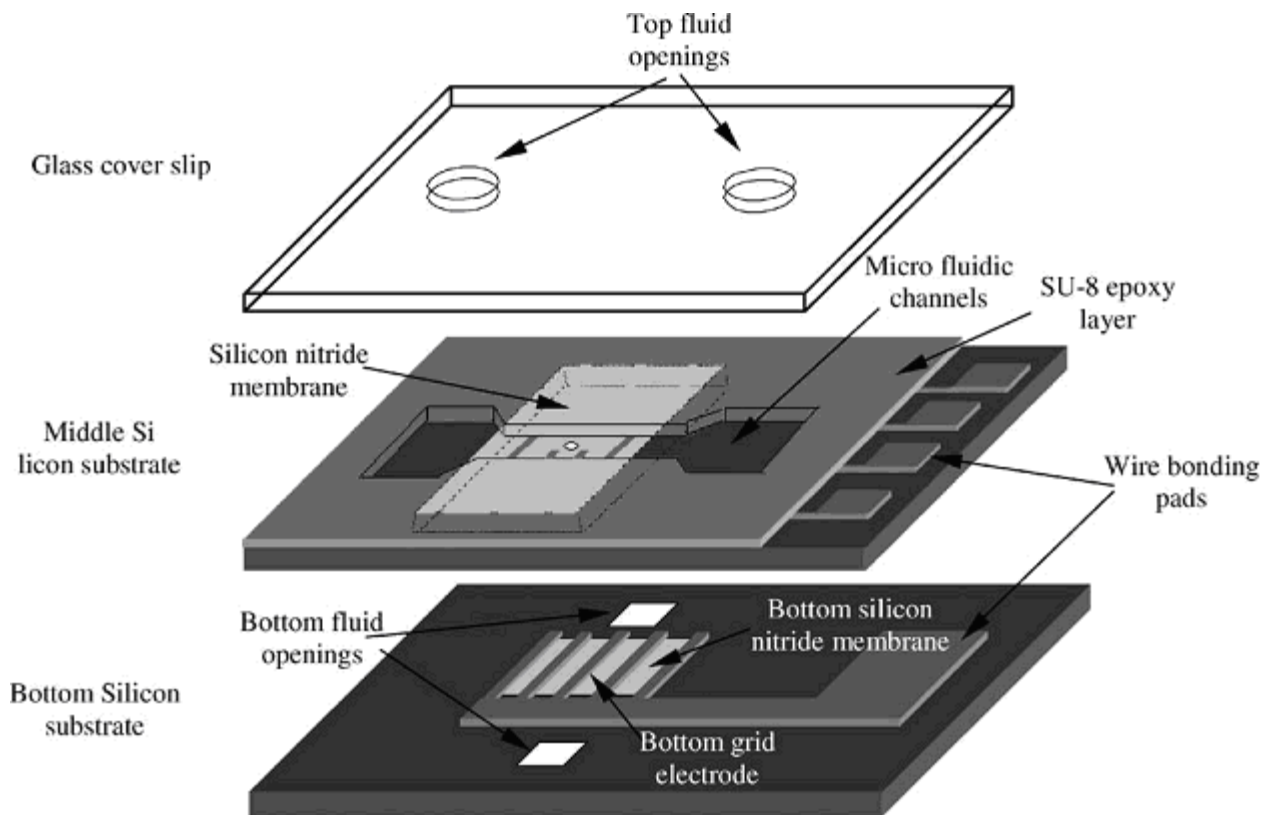
Figure 4. Cross sectional view of a typical microchip-based single-cell electroporation device.

1.2.3　　　Microelectrode Electroporation

The microelectrode type of single cell electroporation is the type of electroporation that is the focus of this research. This type of electroporation is much better suited to make quantitative measurements of a molecule's uptake or release from a cell. The research was preformed on adherent cell lines. The working microelectrode would be place closely to the immobilized cell and the counter electrode would be far away in the cell bath solution, as seen below in figure 5. Non-adherent cells can be immobilized with a micropipette device and a working microelectrode is placed closely to it. The construction and use of this immobilization device will be described in more detail later. The positioned working microelectrode would be well placed to measure the electroactive species as they are released from the cell. In order for a quantitative measurement to be made, one would consequently have to make adjusts to the measurements of electroactive species released to compensate for the diffusion of the electroactive species released from the cell that would not be detected by the working microelectrode. The use of computer simulations to calculate the release of the electroactive species from the cell that will not be detected by the working microelectrode would be required.
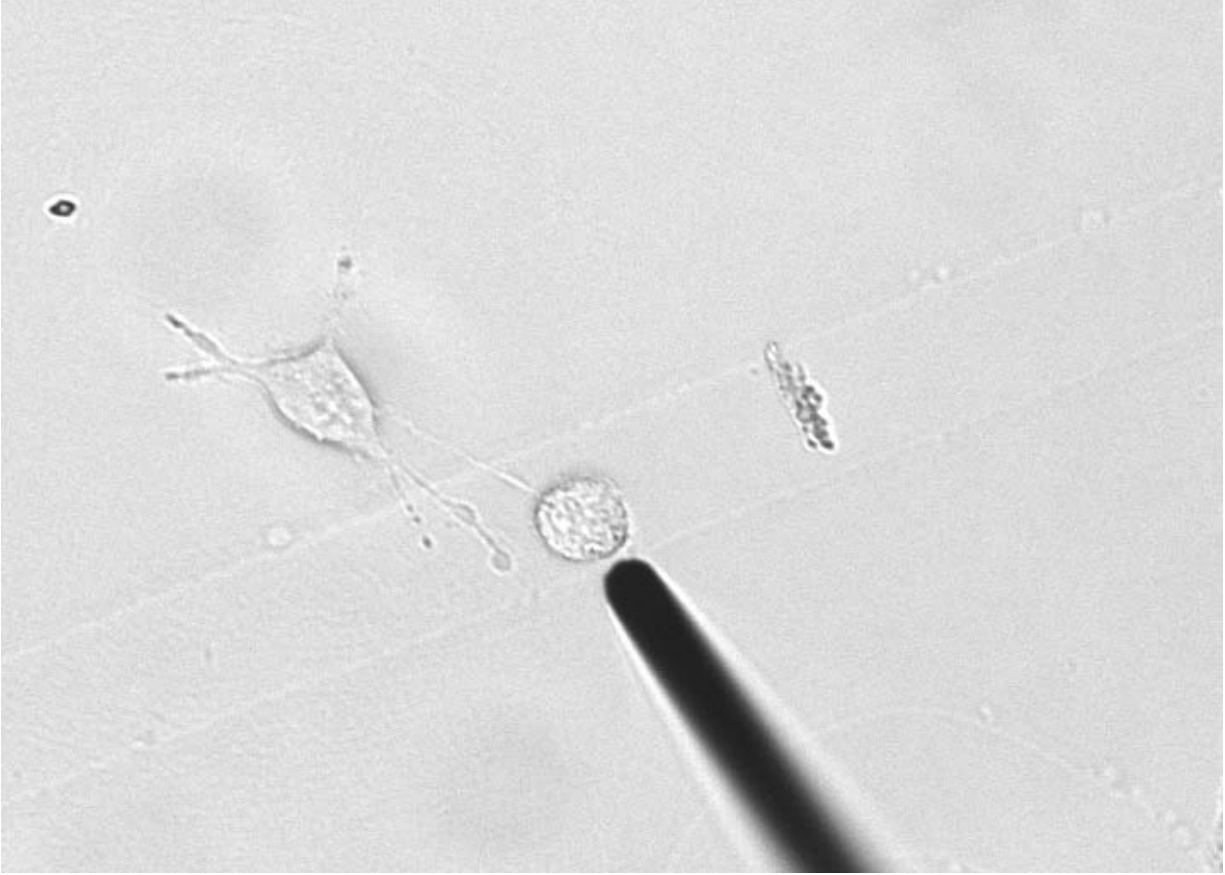
Figure 5. An adherent cell (A549) with a 10 μm carbon fiber microelectrode placed closely to electroporate it.

A disadvantage of using this type of electroporation is that the electric field produced by the micro or nanoelectrodes used is not homogenous, like the one produced by the plate electrodes in batch electroporation. This problem becomes apparent when one tries to solve equation 1 for this experimental set up. One has to know the electric field to calculate the theoretical transmembrane voltage needed to electroporate the cell in question. The solution to this problem will be approached by the use of computer simulations and current interruption experiments.

1.3   MAJOR CURRENT CLINICAL USES OF ELECTROPORATION

Electroporation is a versatile technique, which can be used to improve the transport of small and medium polar molecules across a membrane[7, 24-29], transfection of DNA and nucleic acids[24, 30-40]. An example of how electroporation has improved the first two techniques, transport and transfection, is shown in the next two paragraphs.

1.3.1   Cancer Treatment

There are several current clinical applications and numerous others under investigation. The most widely used clinical application of electroporation is its use in the enhancement of drug delivery to cancerous tumors, electrochemotherapy. The most commonly used and effective cancer treatment drug used is bleomycin[26]. Numerous other cancer treatment drugs have also been tested[26, 28, 35, 41-45], such as cisplatin, actinomycin D, daunorubicin, doxorubicin, etoposide, paclitaxel, etc. The reason bleomycin is the most studied is because it showed the greatest increase in cytotoxicity when coupled with electroporation in preclinical studies[26], enhancement of 300-700 fold. In clinical trials, a complete response, cure rate after once-only treatments were between 9 and 100% depending on the techniques used for administration of bleomycin and electroporation. There were also trials with more than one treatment that showed increased complete response rates.   This type of cancer treatment has shown to be less deleterious to the health of the patients treated. This is because the amount of anti-cancer drug administered in electrochemotherapy is, in most instances, far less than that used in one treatment, rather than an entire cycle, of conventional chemotherapy[26].

1.3.2   Transfection, Gene Therapy, and Nucleic Acid Vaccines

Electroporation has also emerged as a leading technique for developing nonviral transfection, gene therapies, and nucleic acid vaccines. The first use of electroporation to incorporate plasmid DNA (herpes simplex thymidine kinase) into cells (mouse lyoma) was done by Neumann.[46] Electroporation is being explored because of the inefficiency and/or toxicity of the existing viral and nonviral gene delivery methods[19, 20, 24, 31, 34-39, 47-49]. Even though virus-based systems enhance delivery efficiency, recombinant viral vector-based treatments have been associated with complication caused from highly complex and evolved viral biology and/or host-parasite interactions[40]. The inefficiency of *in vivo* clearance and formulation/manufacture complexities often compromise the utility of nonviral delivery systems. Direct injection followed by electroporation has increased efficiency 10 to 1,000 fold compared to direct injection alone. The major complication experience at this time is the inactivation of free polynucleotides via endo- or exonucleolytic cleavage in the extracellular media. The use of lipidic delivery systems, polymeric delivery agents, and viral packaging tend to provide protection from endonucleolytic degradation in the extracellular media[40]. The use of electroporation has been shown to be approximately ten times as effective chemical transfection.[46, 50]

2.0   INITIAL APPROACH

2.1   CARBON FIBER MICROELECTRODES

2.1.1   Versatile detection

Carbon fibers can be used to make microelectrodes that have the ability to detect many electroactive species[51-54]. The choice to use carbon fiber microelectrodes is due to their versatility and low cost of production. Not only can the unmodified microelectrodes be used to detect numerous electroactive species, but these microelectrodes can be modified easily to lower the limits of detection, and even detect more electroactive species[55-62]. Some of the electroactive species that can be detected by unmodified carbon fiber microelectrodes include dopamine[52], catechol[54], 3,4-dihydroxybenzoic acid (DHBA)[54], steriods[51, 53, 63, 64], and numerous others.

2.1.2   Fabrication of 10 μm Carbon Fiber Microelectrodes

Carbon fiber microelectrodes used were constructed using a multiple step fabrication process. A carbon fiber microelectrode made this way is depicted in figure 6. 1) First is the threading of a 10 μm carbon fiber (Thornell Carbon Fiber, P-55 3K, Amoco Performance Products, Inc., Greenville, SC) into a glass capillary tube (Sutter Instruments, Co., Novato, CA). The capillaries

used are made of borosilicate glass and have the following dimensions; outer diameter (o.d.): 1 mm, inner diameter (i.d.): .75 mm, and a length of 10 cm. This can be facilitated by immersing the capillary in acetone, which allows the carbon fiber to be threaded more easily into the capillary. 2) The glass capillary threaded with the carbon fiber is then pulled using a vertical micropipette puller (Narishing, Tokyo, Japan). The carbon fiber that now connects both sides of the pulled capillary is cut, creating two pulled capillaries with a carbon fiber protruding from the pulled end of the two capillaries. 3) The carbon fiber/glass junction is now sealed by backfilling the tip of the capillary with a low viscosity epoxy (Spurr Epoxy, Polysciences, Inc., Warrington, PA). The backfilling process uses a 1 ml syringe (Henke-Sass Wolf GmbH, Tuttlingen, Germany) with a needle (PrecisionGlide 21G2, Becton Dickinson & Co. Franklin Lakes, NJ) connected to an approximately 8 cm length of fused silica capillary (Polymicro Technologies, Phoenix, AZ) with an i.d. of 248 μm and o.d. of 364 μm. The fused silica capillary is held in place by epoxy (5 Minute Epoxy, *ITW*Devcon, Danvers, MA). The epoxy that was delivered into the tip of the pulled capillary is cured at $70^{o}C$ for 8 or more hours. 4) After the epoxy is allowed to cure the protruding carbon fiber is trimmed with a scalpel to a length of about 1 mm using a microscope under a magnification of 45. 5) The capillary is then backfilled with mercury to insure an electrical contact between the carbon fiber and the copper wire inserted into the unpulled end of the capillary. The unpulled end of the capillary is sealed with poster sticky tack to hold the copper wire in place and to prevent the mercury from escaping from the capillary.

16
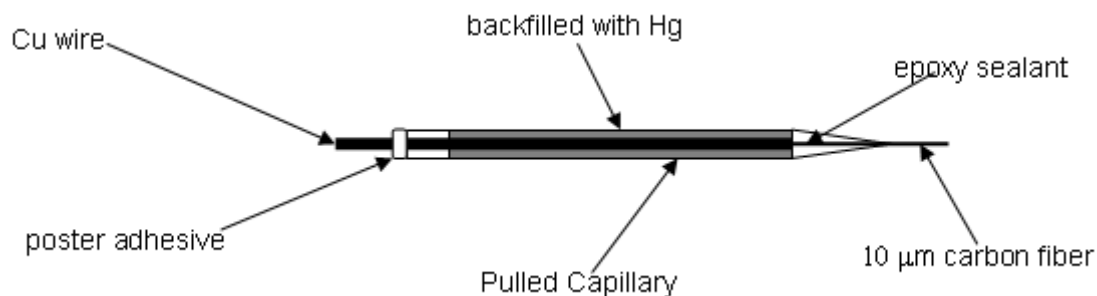
Figure 6. A representation of a carbon fiber microelectrode made using the above procedure.

2.1.3   Testing of the Microelectrodes

After the construction of the 10 μm carbon fiber microelectrode is complete, the second part of the fabrication process is the testing of the microelectrodes. This is to insure that the microelectrodes work properly, before being electrochemically etched to a smaller size. Before being tested the microelectrodes are cleaned by ultrasonification (Cole-Parmer Instrument Co. Model 8845-4, Chicago, IL) for ~10 minutes in isopropanol (EM Science PX1835-3, Darmstadt, Germany), which has been cleansed with deactivated carbon (Fisher Scientific C170-500, Fair Lawn, NJ). The microelectrodes are allowed to air dry prior to being tested. The microelectrodes are tested by cyclic voltammetry with a computer control potentiostat (BAS Epsilon EC ver.1.30.64, Bioanalytical Systems, Inc., West Lafayette, IN); a typical scan is shown below in figure 7. A 0.1 M potassium chloride (Mallinkrodt AR 6858, Paris, KT) solution for the blank, and 0.1 M potassium chloride and 10 μm potassium ferricyanide (Fisher Scientific P-232, Fair Lawn, NJ) solution are used to test the microelectrodes. For each scan the applied potential initially starts at -100 mV, is linearly scan up to 600 mV, and then back to the initial potential of -100 mV versus a silver/silver chloride (Ag/AgCl) electrode at a scan rate of

17

200mV/s. Microelectrodes that have a current of less than 150 nA are considered not to work properly and are discarded at this stage.

Microlectrode Prior to Etching
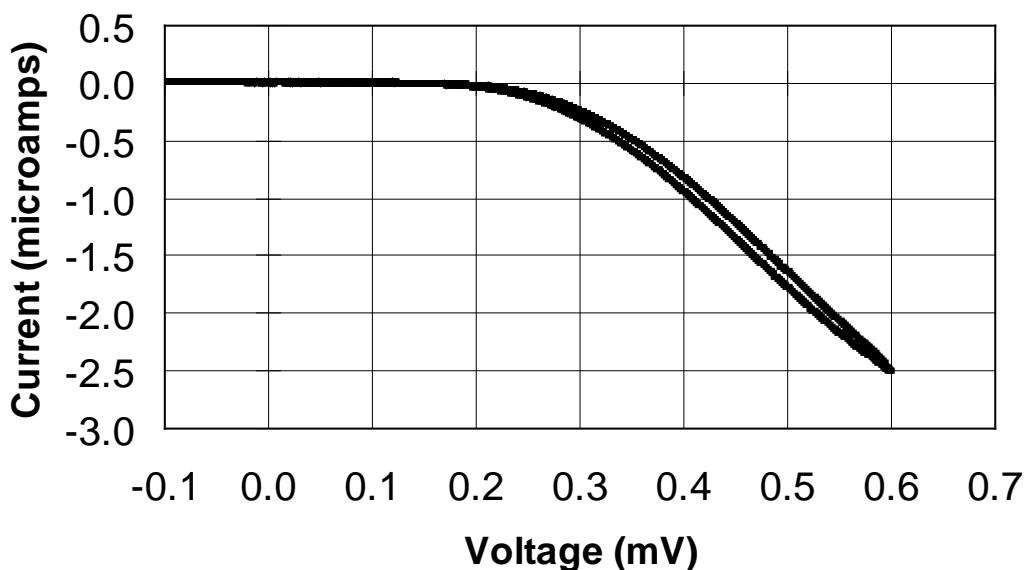
Figure 7. A plot of a typical cyclic voltammetry experiment on a 10 μm carbon fiber microelectrode. The conditions are as follows; 10 μM potassium ferricyanide and 0.1 M potassium chloride solution swept from a potential of -100 mV to 600 mV and back at a rate of 200 mV/s versus a silver/silver chloride electrode.

2.1.4 Etching of Carbon Fiber Microelectrodes

The microelectrodes are cleaned with isopropanol and allowed to air dry again prior to etching, which is the third step of the fabrication process. The microelectrodes are electrochemically etched in an in-house built cell following procedure by Schulte[52]. The main modification made to their procedure was to replace the "U"-shaped Pt counter electrode with a Pt tube, and is

18

shown below in figure 8. This modification was made to create a more homogenous electric field around the carbon fiber microelectrode that is being etched.
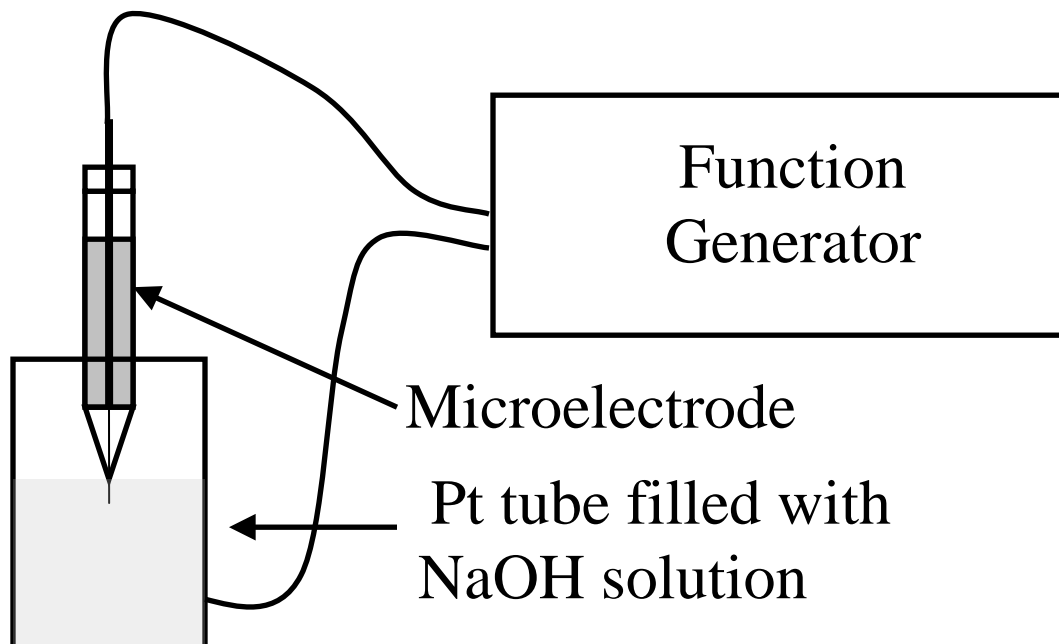
Figure 8. In-house built setup for electrochemical etching 10 μm carbon fibers.

The in-house cell consists of a 1.0 mm o.d. and 0.8 mm i.d. platinum tube connected to a copper wire, which is incased in PTFE/FEP dual shrink plastic (Small Parts Inc., Miami Lakes, FL). A 45 Hz, 3.9 V peak to peak, bipolar square wave is created by a synthesized function generator (Stanford Research System Model DS5345, Sunnyvale, CA), which is connected to the copper wire of the electrochemical cell and metal wire of the microelectrode. The square wave is monitored by an oscilloscope (LeCroy 9410, Chestnut Ridge, NY) and a computerized digital oscilloscope program (National Instruments 5911, Austin, TX). The solution used for etching was 0.1M, 0.075M, or 0.05M sodium hydroxide (NaOH), depending on which run is in question. The carbon fiber was dipped into the NaOH solution, being sure not to immerse the carbon

fiber/glass junction, with the aid of a Stereomaster Zoom Microscope with Boom Stand (Fisher Scientific, Pittsburgh, PA) and micromanipulator (Narishinge Co. MN-151, Tokyo, Japan). The square wave electrical pulse was applied until the microelectrode was no longer in contact with the NaOH solution. This was determined by the connected oscilloscope's signal, it would change from the applied square wave to noise.

The desired result was to take a cylindrical 10 μm carbon fiber microelectrode and electrochemically etch it to a cylindrical microelectrode of a desired diameter, ~1 μm or less. The etching of the microelectrodes was first performed with 0.01M NaOH etching solution like that used in the Schulte paper. Unfortunately, this did not decrease the diameter of the microelectrode as much as desired. This was most likely due to the decrease in volume of the Pt tube compared "U"-shaped counter electrode. This problem was first addressed by replacing the NaOH solution between several etchings on the same microelectrode. Replacement of the solution was time consuming and it also did not decrease the microelectrode's diameter as much as expected. Next increasing the concentration of the NaOH solution to 0.1 M was tried to decrease the diameter of the microelectrodes. This adjustment worked, but a new problem arose. Most microelectrodes were completely etched away reproducibly leaving a conical electrode of ~3 μm, instead of a cylindrical microelectrode, when etched for 10 minutes. The microelectrodes were cone shaped because the NaOH solution level in the platinum tube decreases gradually as the square pulses by the function generator were applied. The gradually decrease in the NaOH solution was due to the gaseous products in the electrochemical reaction that takes place during the etching process, the reaction is shown below:

$$C_{(s)} + Na^+_{(aq)} + OH^-_{(aq)} + H_2O_{(l)} \longrightarrow CO_{2(g)} + H_{2(g)} + Na^+_{(aq)} \tag{3}$$
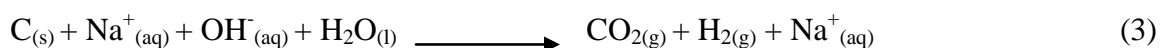
The production of gas bubbles, a drop in the height of the NaOH solution, and the shape of the microelectrode were all observed with the microscope used to position the microelectrode. The time the microelectrodes were etched for was varied to find an etching time that would reproducibly reduced the microelectrode diameter to 3 μm or less. An etching time was not found that gave reproducible results. Figure 9 shows the relationship between etching time and signal produced by the microelectrode.
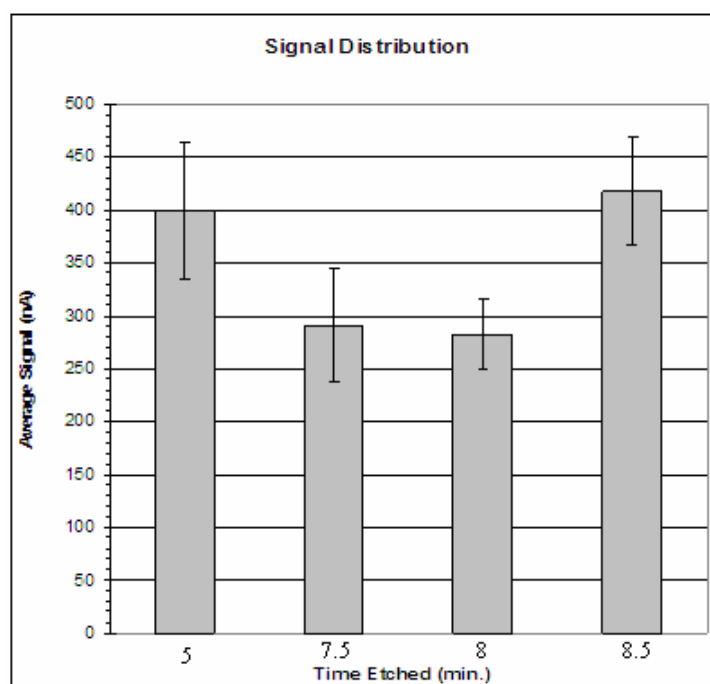
Figure 9. Bar graph of the absolute value of the average signal for microelectrodes etched in 0.1 M NaOH for different lengths of time. Error bars are confidence intervals.

This suggested the possibility that a 10 fold increase of the NaOH solution concentration was too great of an increase in concentration. Etching trials of NaOH solution concentrations of 0.05 M and 0.075 M were started with similar preliminary results (data not shown). These etching trials and computer simulations with FEMLAB, which allows one to simulate the potential gradient in a solution produce by microelectrodes of different geometries, were done in parallel. These computer simulations showed (described more fully below) that microelectrode geometry only

21

had a minor effect on the potential gradient produce by the microelectrodes. With microelectrode geometry only having a minor affect on the potential gradient it produces, microelectrodes reproducibly made with a conical geometry were acceptable, how the microectrode geometry affects the potential gradient is discussed later. Figure 10 shows the relationship between the concentration of the NaOH solution used to etch the microelectrodes and the cyclic voltammetry signal produced by them.
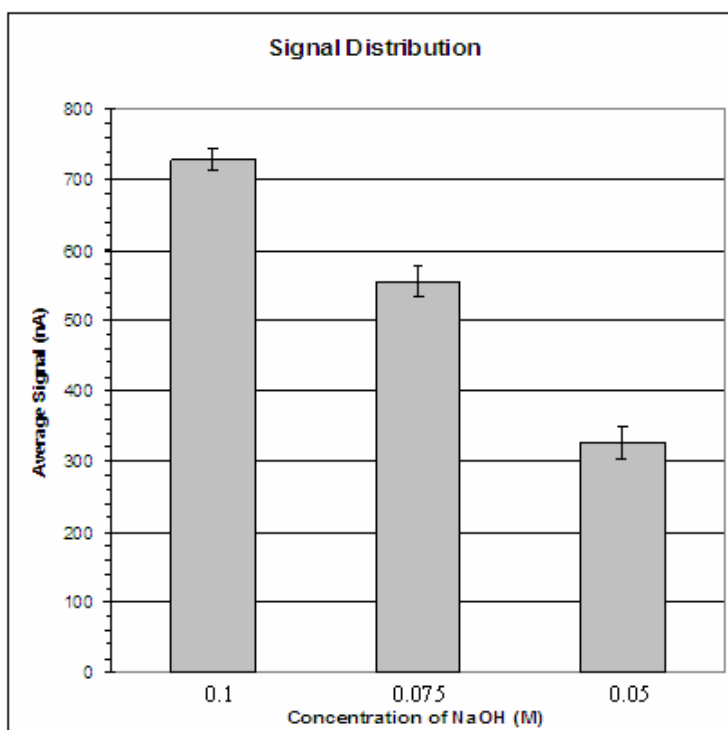
Figure 10. Bar graph of the absolute value of the average signal for microelectrodes etched in different concentration of NaOH. Error bars are confidence intervals.

A plot of a cyclic voltammetry experiment on a microelectrode after etching is shown in figure 11.

Microelectrode After Etching
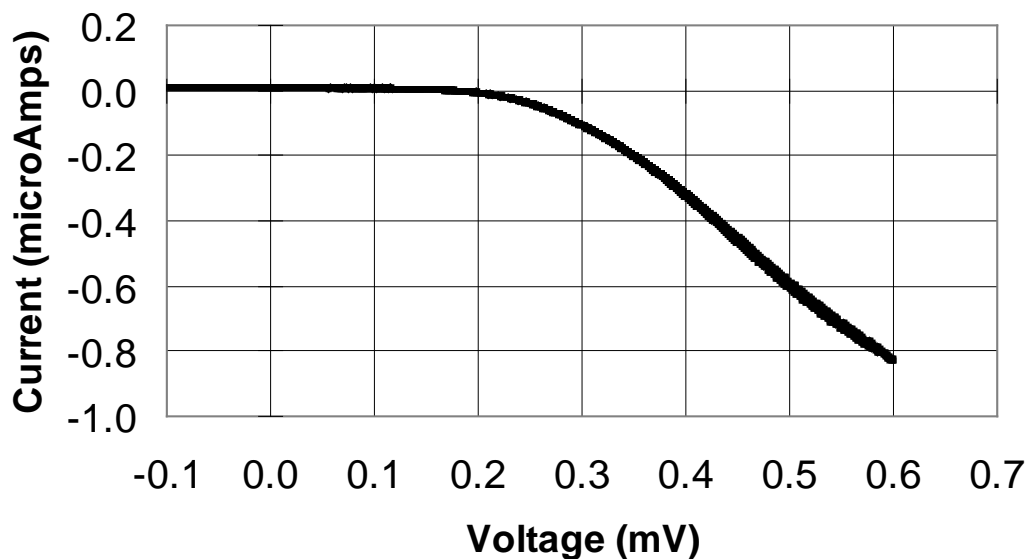
Figure 11. Graph of a cyclic voltammetry experiment done with the same microelectrode as in figure 7, but after etching. The conditions are as follows; 10 μM potassium ferricyanide and 0.1 M potassium chloride solution swept from a potential of -100 mV to 600 mV and back at a rate of 200 mV/s versus a silver/silver chloride electrode.

The same microelectrode and experimental conditions that were used for this cyclic voltammetry were used in the experiment that is shown in figure 7 above. One can see from that graphs that there is a reduction in the current; the post-etched signal is about one third of the microelectrodes pre-etched signal. With the microelectrode surface area being the only experimental parameter changed, one can conclude the post-etched microelectrode has less surface area than the original microelectrode. This conclusion is supported with statistical analysis, which can be seen in Appendix A.

2.2 POTENTIAL DROP IN SOLUTION

Electroporation results when cells are placed in an electric field of the proper strength[65-67]. Transient pores are formed in the cell membrane that allows molecules to diffuse in and out of the cell based on their chemical potential gradient. Parameters of the experiment, such as the threshold voltage drop over the cell and the related field required for electroporation, can be determined experimentally using bulk electroporation because of the homogenous electric field existing between two parallel electrodes, figure 12 a). At microelectrodes, the electric field in solution is inhomogeneous, figure 12 b).
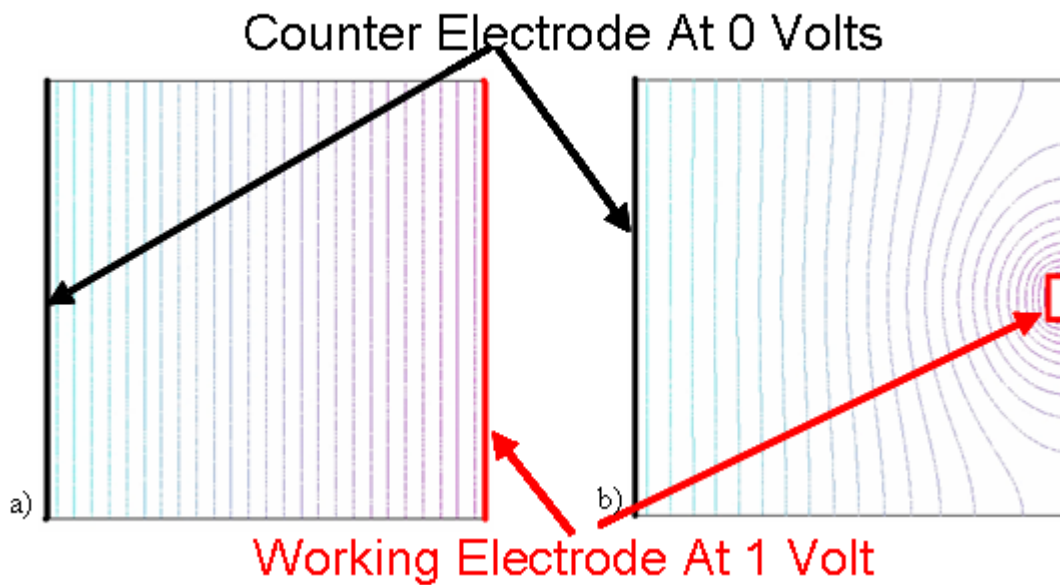
Figure 12. **a) The electric field produced by the planar working electrode, on the left, is homogeneous, as shown by the evenly spaced equipotential lines. b) The electric field produced by the working microelectrode, on the right, is not homogeneous.**

The electric field drops of rapidly with increasing distance from the microelectrode. Thus, electroporation with microelectrodes can achieve high resolution, figure 13 a) and b).
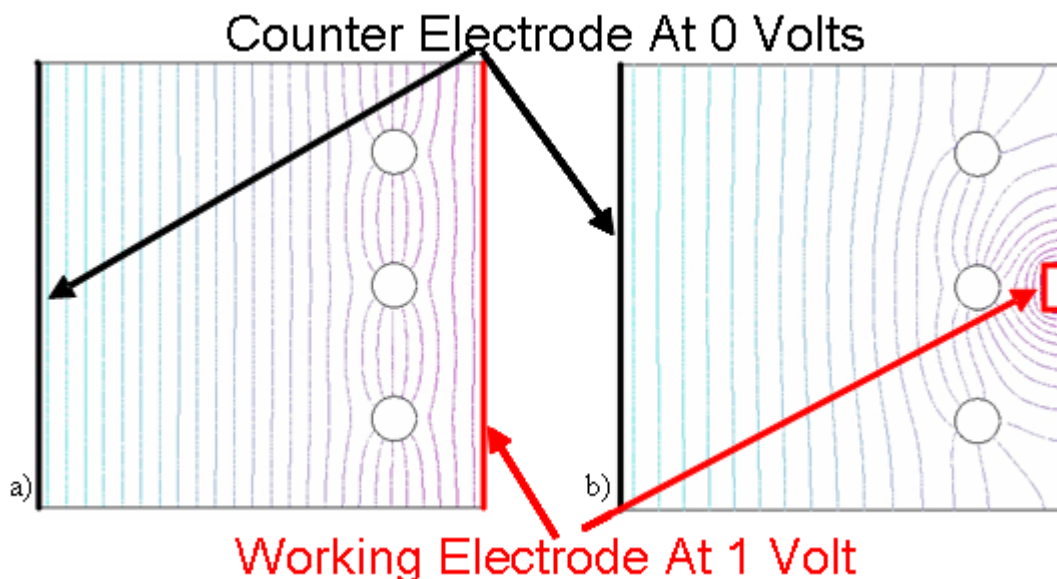
Figure 13. a) The homogeneous electric field produced in bulk electroporation permits the three cells, the empty circles, to feel the same electric field. c) The inhomogeneous electric field produced by a microelectrode causes the electric field felt by the middle cell to be stronger than the other two cells.

Unfortunately, to make microelectrode-based single-cell electroporation a predictable experiment both the shape of the electric field and the total voltage dropped through solution must be known. Of course, this is the same voltage that is termed 'iR drop' in electrochemical circles. Once the iR drop is known, the field at any point in the solution can be known from doing a calculation of the shape of the field by finite element analysis

In principle, the iR drop in solution could be controlled experimentally by controlling the current applied to the microelectrode, and combining the current, i, with a known resistance of the electrolyte solution. This resistance, however, is not trivially determined. The resistance of a solution depends on the resistivity of the medium and a geometric factor (called the 'cell constant' by electrochemists) of the working microelectrode/electrolyte solution/counter electrode system, which is discussed below.

2.2.1   Simulation Setup

The computer simulations were performed in FEMLAB, now Comsol Multiphysics, in the Conductive Media DC with axial symmetry (2D) model. FEMLAB uses a version of Laplace's equation,

$$-\nabla \cdot (\varepsilon \nabla V)=0 \tag{4}$$

in its calculations of this model.

The geometric shape and boundary conditions for these simulations are shown in figure 14.
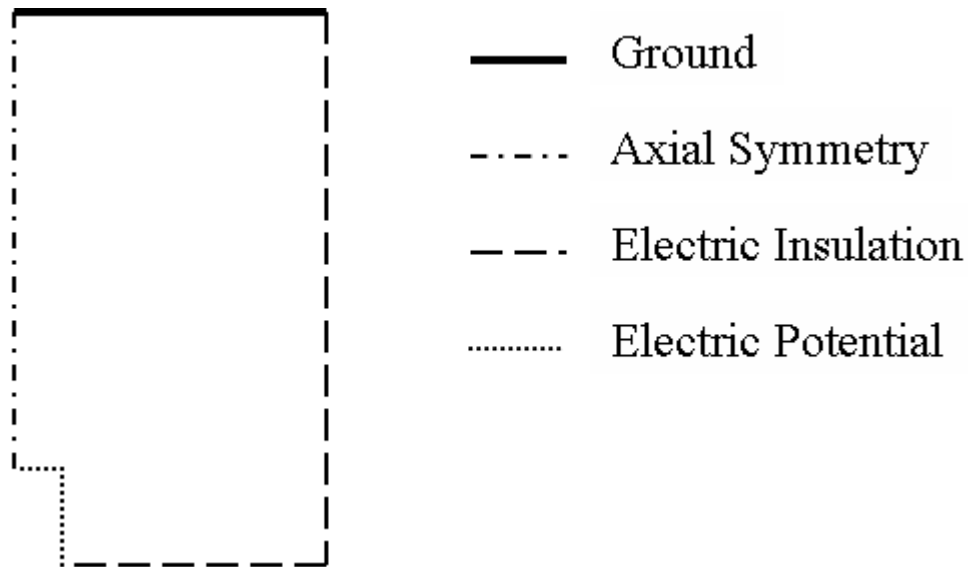
Figure 14. The boundary conditions and geometry used to simulate the electric field and to help calculate cell constants. The relative size of the microelectrode, for which the boundary condition is potential, is increased for visibility. In this geometry, the microelectrode has approximately an infinite insulating plane. The dimensions of the electric field simulations were in a cell 5 cm by 2.5 cm. Theses simulations had 80,000 – 120,000 elements, depending on the length of the microelectrode simulated. The global mesh parameters for the simulations were set to the predefined mesh size of 'finer'. The mesh around the microelectrode is refined by creating a subdomain, 5 mm by 2.5

mm, around the microelectrode and specifying a maximum element size of 50 μm and a growth rate of 1.15 in that subdomain. The mesh around the microelectrode was then selectively refined further until the size of the elements bordering the microelectrode were 1 μm or smaller. The extremely fine mesh around the microelectrode is required because of the high gradient of the electric field in this region. A two dimensional model was used to represent a three dimensional geometry because of the symmetry around the z axis. This helped reduce computation time and the amount of memory used by the simulations.

2.2.2   Simulation Results

The electric fields for disc, conical, hemispherical and cylindrical microelectrodes protruding from an insulating plane, as well as for a cylinder with an insulating 'sheath' were calculated in FEMLAB. All of the microelectrodes in these simulations had a diameter of 10 μm. The lengths of the conducting portion of the conical, cylindrical, hemispherical, and insulated microelectrodes were all 5 μm. The potential as a function of distance from the tips of the electrodes are compared in Table 1 (a more extensive tabulation can be found in Appendix B). The potentials were similar for the disc, cylindrical, hemispherical, and insulated geometries but the potential profile for the conical geometry is significantly different.

Table 1. A comparison of the potential in volts simulated for different microelectrode geometries at various distances from the tip of the microelectrodes. All of the microelectrodes simulated had a diameter of 10 μm and a length of 5 μm (excluding the disc geometry) with 1 volt applied to the microelectrode. In the 'insulated' geometry, the cylinder has a 5 μm thick insulating layer that extends 1 mm down the microelectrode shaft.

Distance from the Microelectrode Tip (μm)	Conical	Disc	Hemispherical	Cylindrical	Insulated
1	0.6901	0.8755	0.8325	0.9036	0.8915
2	0.5809	0.7597	0.7141	0.8127	0.7895
5	0.4058	0.5029	0.4972	0.5988	0.5526
10	0.2725	0.2976	0.3330	0.4020	0.3439
25	0.1645	0.1269	0.1668	0.1999	0.1509
50	0.0752	0.0642	0.0912	0.1089	0.0765

The potentials 5 μm from the tip of the microelectrodes of various lengths, which were calculated in FEMLAB, are compared in Table 2. In the context of electroporation, the key factor is the total potential difference across the cell. Taking a typical cell to be 20-40 μm in diameter if the microelectrode-cell distance is 5 μm, the range of potential differences seen by a cell depends somewhat on the cell diameter, somewhat on the microelectrode length, and somewhat on the shape of the microelectrode. In no case, however, is the dependence a strong one. This bodes well for reproducibility of electroporation using microelectrodes. In this regard, it is interesting to note the very small dependence of the potential at a 5 μm distance (Table 1) on microelectrode length for the conical shape.

Table 2. The potential in solution, in volts, at 5 μm from the tips of the microelectrodes (at 1.0 V). The microelectrode lengths for the hemispherical and conical geometries are the total of a hemispherical and conical tip (both 5 μm) plus the length of the cylindrical shaft.

Microelectrode Length (μm)	Conical	Hemispherical	Cylindrical	Insulated
5	0.4058	0.4972	0.5988	0.5526
10	0.4742	0.5440	0.6260	0.5852
15	0.5027	0.5655	0.6417	0.6049
25	0.5334	0.5897	0.6606	0.6290
50	0.5686	0.6208	0.6841	0.6591
100	0.5981	0.6465	0.7049	0.6854
500	0.6518	0.6935	0.7438	0.7346
1,000	0.6709	0.7102	0.7577	0.7521

2.3   CALCULATING THE CELL CONSTANT FOR MICROELECTRODES

2.3.1   Simulation Setup

The same computer simulation program, FEMLAB now Comsol Multiphysics, was used to calculate the cell constants for the microelectrodes. The cell constant simulations were also performed in the Conductive Media DC with axial symmetry (2D) model and they were solved for the same equation. The geometric shape and boundary conditions were also similar to that of the electric field simulations. The cell dimensions of the cell constant simulations were in a cell 1 m by 0.5 m and had 180,000 – 220,000 elements, depending on the length of the microelectrode. The global mesh parameters for these simulations were also set to the predefined mesh size of 'finer'. The mesh around the microelectrode is refined by creating a subdomain, 5 mm by 2.5 mm, around the microelectrode and specifying a maximum element

size of 50 μm and a growth rate of 1.15 in that subdomain. The mesh around the microelectrode was then selectively refined further until the size of the elements bordering the microelectrode were 1 μm or smaller. The extremely fine mesh around the microelectrode is required because of the high gradient of the field in this region. The mesh bordering the ground in the cell constant simulations was also selectively refined, because the electric field close to this boundary is required for calculating the cell constant.

2.3.2   Simulation Results

The following equation was used to calculate the cell constant (κ) for the microelectrodes:

$$\kappa = \frac{\int \vec{E} dz}{\int \vec{E} dA} \tag{5}$$

The numerator is the integral of the electric field ($\vec{E}$) over the z axis. The denominator of the equation is the integral of the electric field ($\vec{E}$) normal to an isopotential line over the area through which the current flows. The numerator of equation 5 is equal to ΔV. With this substitution and by setting the potential of the microelectrode at 1 volt versus the ground electrode, the numerator is 1 with the units of volts in equation 5. The denominator is calculated very close to the planar counter electrode with the following equation:

$$\int \vec{E} dA = \sum_0^n \left(\left(\frac{\overrightarrow{E_{r_n}} + \overrightarrow{E_{r_{n-1}}}}{2} \right) \pi \left(r_n^2 - r_{n-1}^2 \right) \right) \tag{6}$$

where $\vec{E}_{r_n}$ is the field at the nth radius, r_n.

The calculated cell constant of an electrochemical cell is dependent on the size and shape of the microelectrodes. Numerous simulations were done with only the length of the microelectrode being altered. These simulations were done for the three common diameters of carbon fibers commercially available, 5, 7, and 10 μm. The general geometry for these simulations can be seen in figure 14. Values of $1000/\kappa$ fit well to a power law, equation 7, as seen in for 10 μm diameter electrodes in figure 15.

$$1000/\kappa = A*|x|^p + y^0 \qquad (7)$$

Coefficients for the three microelectrode diameters are in Table 3. With these equations, calculating a reasonably accurate cell constant for a microelectrode of specific dimensions can easily be obtained without a computer simulation.
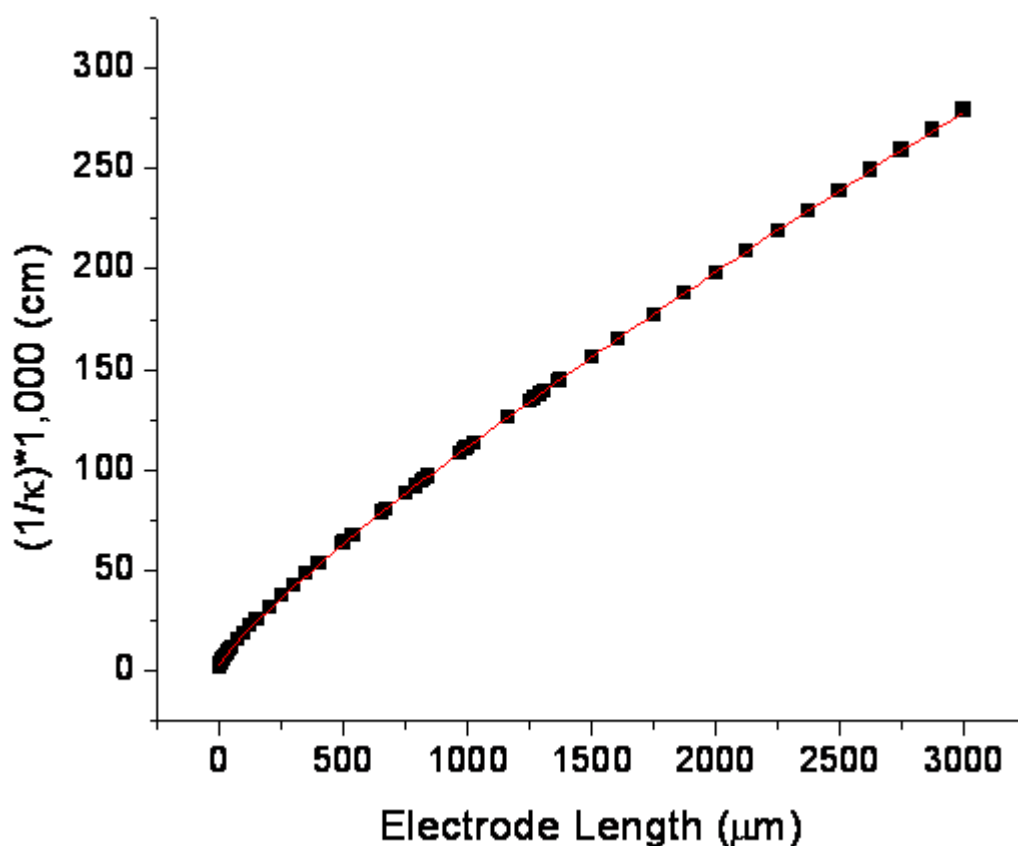
Figure 15. A plot of the cell constant calculated from FEMLAB simulations versus the microelectrode length for 10 μm diameter microelectrodes. The squares indicate the values from the simulations and the line is from a fitted first order power equation.

Table 3. The values for the fitted power law equation, $1000/\kappa = A*|x|p + y^0$, for the three common diameter of commercially available carbon fibers. The variable 'x' is the length of the microelectrode in micrometers. The value for y^0 was set to the value of $(1/\kappa)*1,000$ for a disc microelectrode of the given diameter. The units of $1000/\kappa$ are cm.

Microlectrode Diameter	5 μm	7 μm	10 μm
R^2	0.99996	0.99996	0.99996
A	0.28441	0.30707	0.33151
	$\pm$ 0.0038	$\pm$ 0.00414	$\pm$ 0.0028
P	0.8468	0.84314	0.83992
	$\pm$ 0.00179	$\pm$ 0.00178	$\pm$ 0.00112
y^0	1.0163	1.43001	2.24273

Changes in the cell constant were also observed as a result of making more subtle changes in the shape of the microelectrode, such as roughness of the microelectrode surface, thickness of the microelectrode's insulating layer, and the roundness and sharpness of the microelectrode tip. Results of the calculations are shown in Table 4.

Table 4. Common geometrical properties of microelectrodes and the effect they have on the cell constant. Ideal: smooth sides with perpendicular face. Pointed tip: the last 5 μm is conical. Rounded tip: the last 5 μm is hemispherical. Rough sides: the microelectrode has a wave (± 0.285 μm) that repeats every 5 μm.

Microelectrode Length	Ideal	Pointed Tip	Rounded Tip	Rough Sides	Insulated
5 μm	265.78 cm^{-1}	386.94 cm^{-1}	308.31 cm^{-1}	267.55 cm^{-1}	221.18 cm^{-1}
10 μm	201.98 cm^{-1}	244.76 cm^{-1}	224.08 cm^{-1}	202.40 cm^{-1}	164.65 cm^{-1}
15 μm	166.58 cm^{-1}	190.99 cm^{-1}	179.69 cm^{-1}	166.76 cm^{-1}	135.02 cm^{-1}
25 μm	126.81 cm^{-1}	138.62 cm^{-1}	132.27 cm^{-1}	126.82 cm^{-1}	102.72 cm^{-1}
50 μm	83.49 cm^{-1}	87.66 cm^{-1}	85.46 cm^{-1}	83.39 cm^{-1}	68.33 cm^{-1}
100 μm	52.45 cm^{-1}	53.84 cm^{-1}	53.11 cm^{-1}	52.36 cm^{-1}	43.76 cm^{-1}
500 μm	15.66 cm^{-1}	15.75 cm^{-1}	15.71 cm^{-1}	15.63 cm^{-1}	13.86 cm^{-1}
1,000 μm	8.96 cm^{-1}	8.98 cm^{-1}	8.97 cm^{-1}	8.94 cm^{-1}	8.11 cm^{-1}

The short microelectrode (10 μm) had the most significant changes in the cell constant. This was not a surprise because applying the same changes to the tip for each microelectrode causes the largest relative change in the 10 μm microelectrode's surface area. Tip geometry is insignificant for microelectrode lengths > 100 μm.

3.0   CURRENT INTERRUPTION

The iR drop at microelectrodes can be determined by a technique called current interruption[68-70]. This technique determines the value of the voltage drop in solution for a given application of current. This technique works by applying a constant current to an electrochemical cell, and quickly switching this current off, figure 16.

Current Source Switch   **Current Source** Switch

V1   V2

V1=V1⁰exp(-kt) V2=0

$$V1 = V1^0 exp(-kt) \quad V2 = 0$$
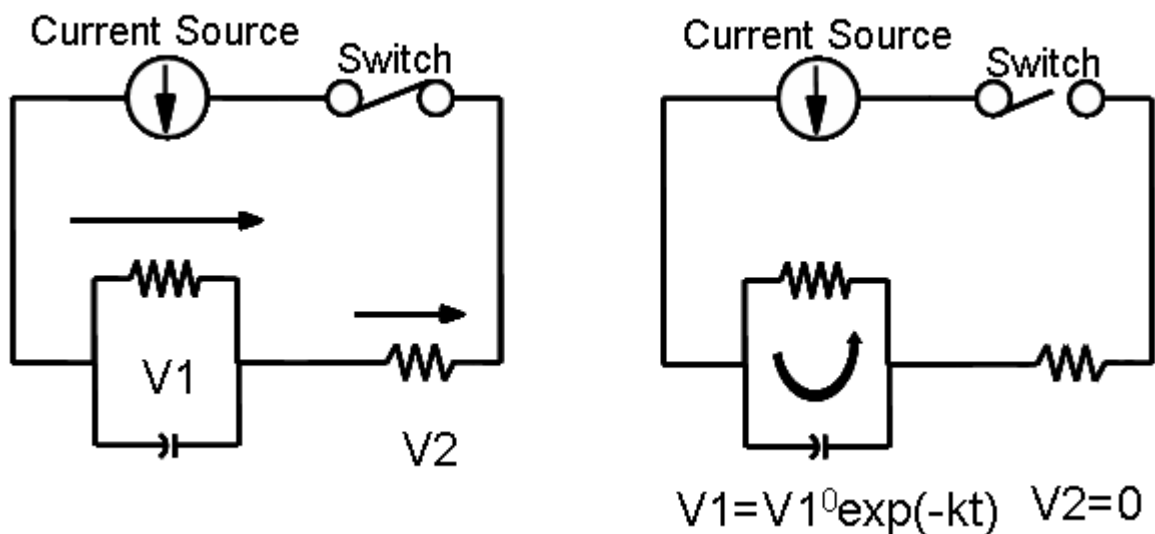
Figure 16. In the left figure, the switch is closed; current flows through both resistors (resulting in voltage V1 and V2), and charges the capacitor. In the right figure, the switch is open; current (discharge of the capacitor) only flows through the left resistor resulting in V1, which would decay exponentially, and no current flowing through the right resistor.

The output signal created by this has two distinct regions: 1) an instantaneous drop and 2) an exponential decay, figure 17. The instantaneous drop is due to the solution resistance whereas the exponential decay is attributed to the electrode's impedance.
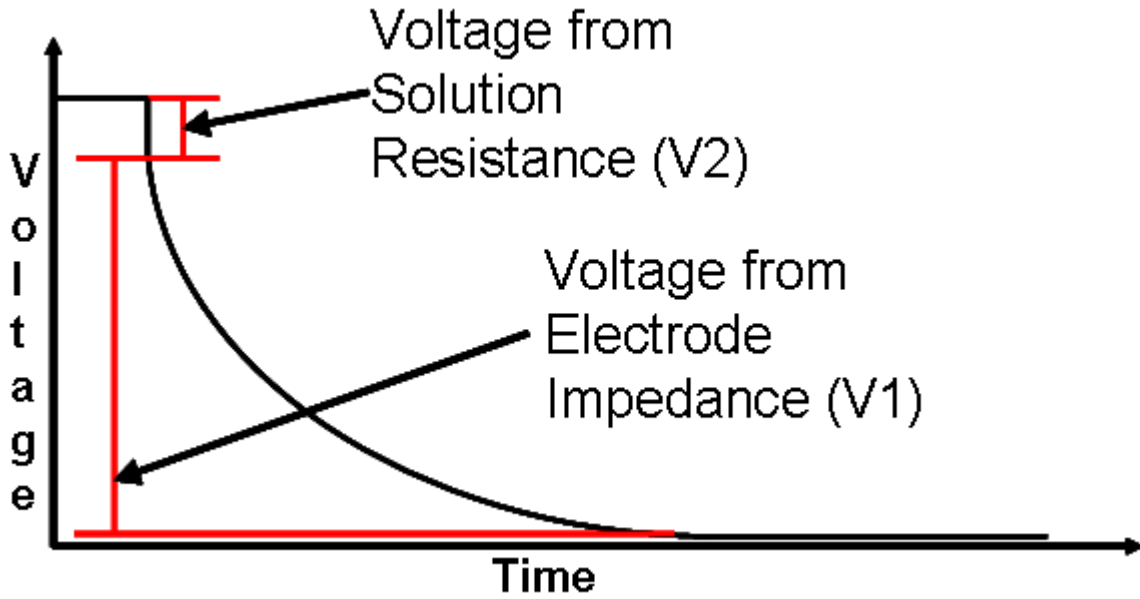
Figure 17. An idealized signal that would be produced by a current interruption experiment.

3.1 TESTING A MODEL SYSTEM

One can model the microelectrode-solution interface and solution, namely with simple electronic components, two resistors and a capacitor. The behaviors of these types of electronic components are well understood. The total resistance of resistors in series can be calculated by the following equation,

$$R_T = R_1 + R_2 + R_3 \ldots + R_n \tag{8}$$

where R_T is the total resistance, R_1 is the resistance of resistor #1, R_2 is the resistance of resistor #2, R_3 is the resistance of resistor #3, and R_n is the resistance of the nth resistor. One also can calculate the total resistance of a circuit, given one knows the current applied to the circuit and the voltage given off by the circuit using this equation,

35

$$R_T = E/I \qquad\qquad (9)$$

where E is the applied voltage and I is the current. The discharging and charging of a capacitor is given by the next equation,

$$I = (E/R)\, e^{(-t/RC)} \qquad\qquad (10)$$

where t is time in seconds, and C is the capacitance of the capacitor. A representation of a microelectrode setup using resistors and a capacitor is shown in figure 18 and will be referred to as a dummy cell.
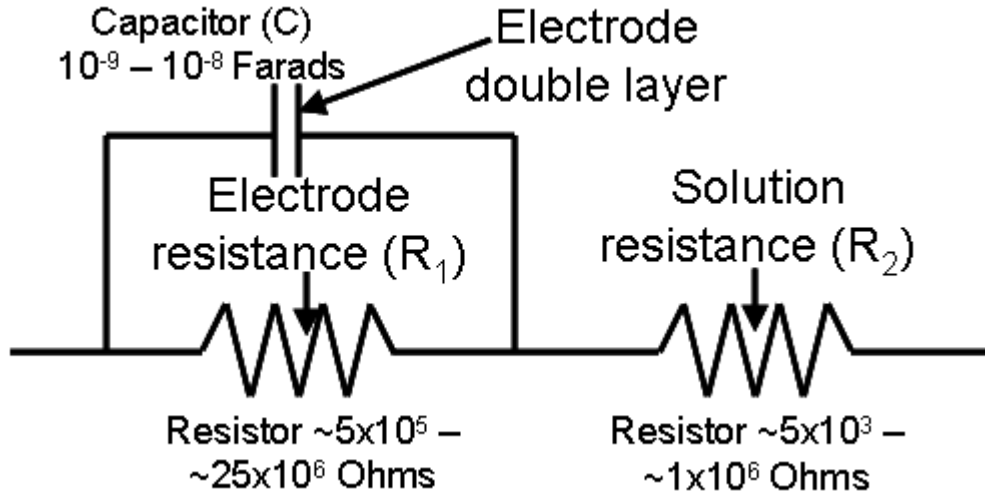
Figure 18. A diagram of a dummy cell with value ranges of the resistors and capacitors used in experiments.

The purpose of the dummy cells is to check the accuracy of experimental values with that of measured values for the solution resistances. The results for the different dummy cells can be found in Appendix C. A graph of the output voltage for dummy cell # 4 is shown in figure 19 below. One can easily see in this figure the part of the voltage drop that is due to the solution resistance, and the part that is due to the microelectrode resistance, because of the voltage drop from the microelectrode decays exponentially.
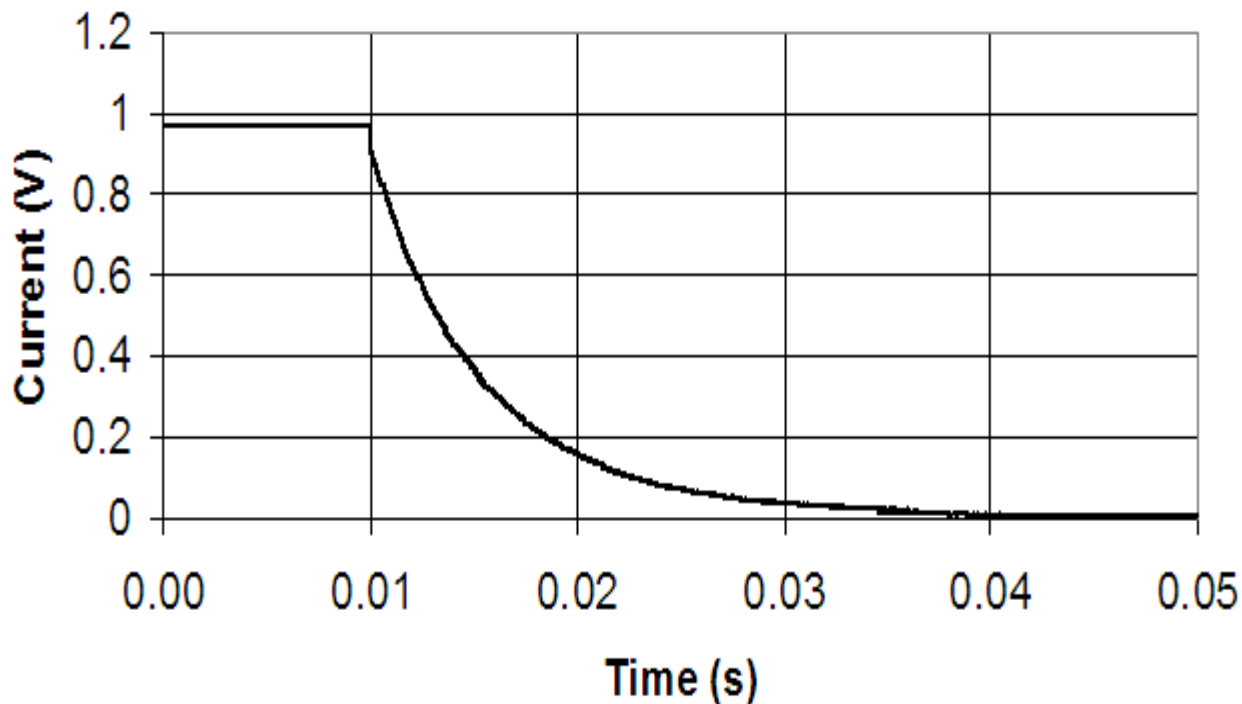
Figure 19. Plot of voltage drop from current interruption experiment using a dummy cell. The dummy cell had an microelectrode capacitance of 11.63 nF, an microelectrode resistance of 477 kΩ, and a solution resistance of 23.9 kΩ,

3.2   REDUCTION OF NOISE

In our lab we are able to know the current applied to the microelectrode by using an electronic circuit that converts applied voltage to current. This electronic circuit converts one volt to ten microampere of current. The voltage applied to the circuit has been controlled by a wave function generator and a standard 9 V battery in our lab. The output voltages of these two devices were checked by an oscilloscope, with the wave function generator being the more reproducible of the two methods. Two different triggering methods were also tested. One method was a solid state switch, which produced noise when triggered as seen in the figure

37

below. The other way the electronic device was triggered was with the wave function generator. This is done by the signal coming from the wave function generator being a one volt bipolar square wave and offsetting it by half a volt, which causes the voltage to drop from 1 volt to 0 volts. The method that used the function generator as the trigger had significantly less noise than the other method. This is shown in figure 20 below.

Function Generator Trigger
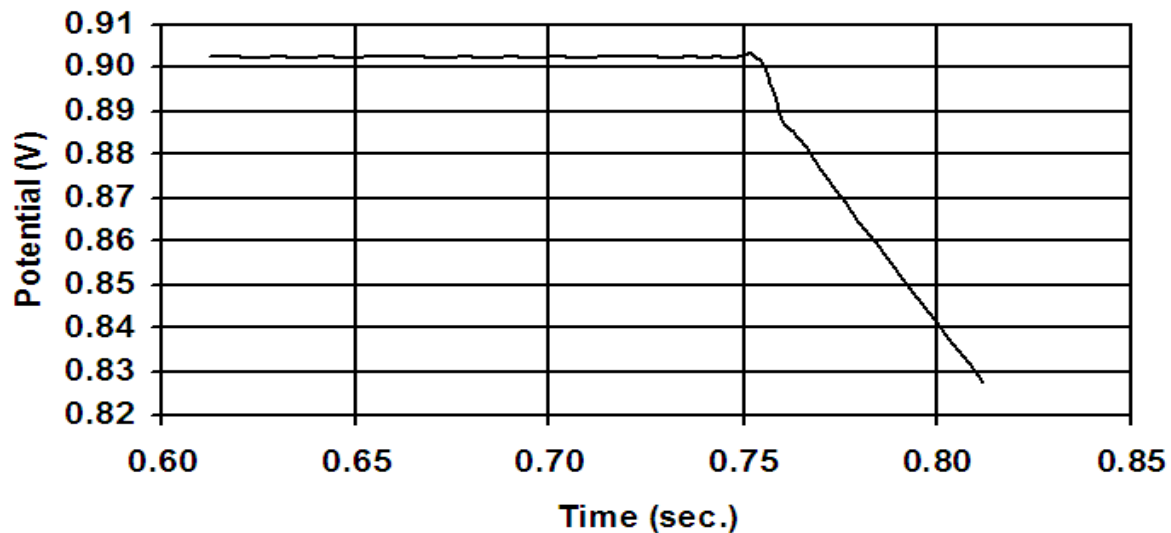
Button Trigger
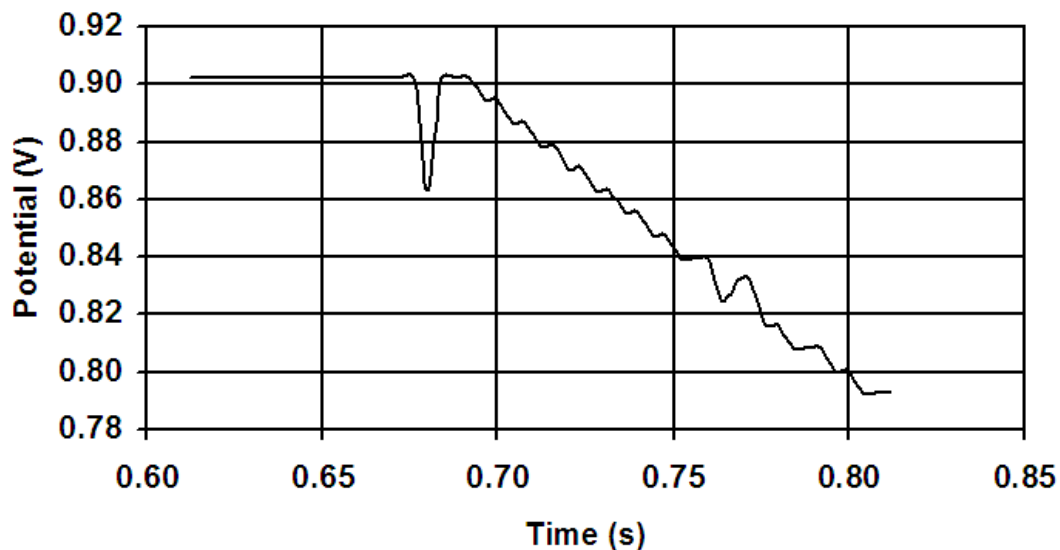
Figure 20. Plots of the same dummy cell using the two different triggering methods with the wave function generator on top and the solid state switch on bottom. The dummy cell had a microelectrode capacitance of 1.06 nF, an microelectrode resistance of 1.01 MΩ, and a solution resistance of 10.8 kΩ,

3.3   APPLICATION TO MICROLECTRODES

Current interruption works by quickly, in nanoseconds, dropping or cutting off the current applied to the microelectrode to zero. This allows one to be able to tell what voltage drop comes from the resistance of the microelectrode double layer, and what voltage drop comes from the resistance of the solution. Current interruption experiments allow one to calculate the resistance and capacitance of a microelectrode along with the resistance of the solution in which the microelectrode is placed.   This can be achieved by knowing the current applied to the microelectrode and having a plot of the measured voltage. With the use of current interruption one can derive, using Eq. 8-10, what the resistance and capacitance of a microelectrode, and the resistance of the solution are because of the way they are set up, in parallel and in series.   The resistance of the microelectrode interface with the solution is in parallel with the capacitance of the microelectrode, due to the double layer.   The current, from the discharging of the microelectrode double layer, does not go through the solution, so the solution resistance is not seen by the discharged of the double layer; it only sees the microelectrode resistance.   The resistance of the solution is not in parallel with that of the microelectrode double layer, and drops quickly, in nanoseconds, like that of the applied current.

A block diagram of the in-house built current interruption device is shown as figure 21. Examples of experimental data are also shown, figure 22.
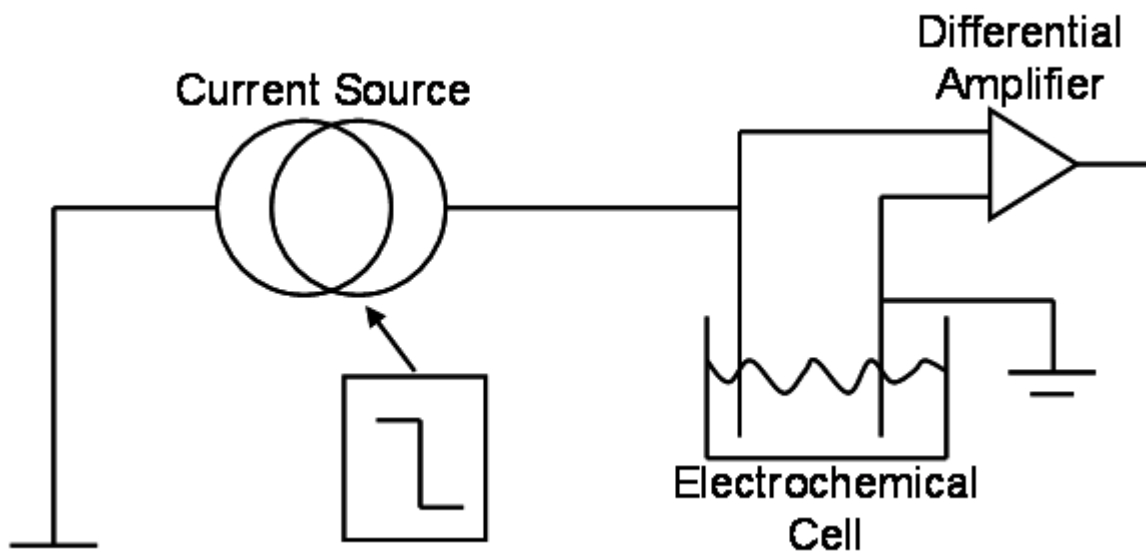
Figure 21. A block diagram of the in-house built current interruption device used in our current interruption experiments.
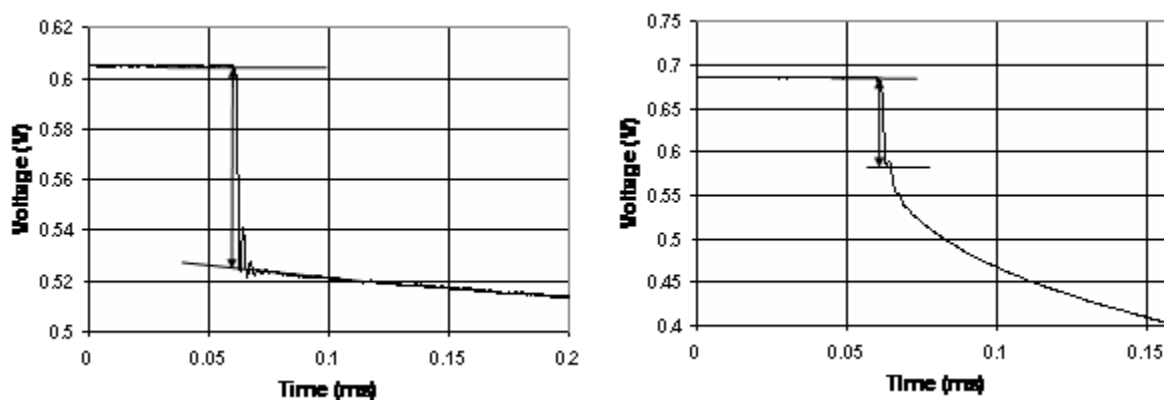
Figure 22. Plots of two current interruption experiments that were performed on 10 μm diameter carbon fibers. The lengths of the microelectrodes are approximately 415 μm for the left and 60 μm for the right plot.

The current interruption device requires a signal voltage which is converted to an applied current. A unipolar square wave from a function generator (Stanford Research Systems Model DS345) was used as the voltage source. The electrochemical cell consists of a counter electrode, working microelectrode, and a conductive solution in a container. The signal from the current interruption device is captured using a fast acquisition oscilloscope (LeCroy Model 9410), which

41

was externally triggered by the same function generator that was used as the current source. The data acquired by the oscilloscope were then passed to a computer in text file format using a GPIB connection and National Instruments software (LabWindows CVI Version 7.1). In a given experiment a typical protocol is to apply 1 μA for 10 s, drop to 0 μA ('interruption') for 10 s, and repeat 10 times. Ten transients were averaged. The results were not affected by doing a series of interruptions, but the precision was improved over single pulse experiments. In practice, the microelectrodes used in the experiments reported here varied in length from 0 to 1,600 μm. Often, cutting the microelectrode with a scalpel leaves a tip with a point. During use, the tip erodes to a hemispherical shape. This change in shape can be attributed to the higher current density at the pointed tip, which causes the carbon fiber to be etched.

3.4   RESULTS

Current interruption experiments were done with the microelectrodes of various lengths in solutions of different conductivities. The lengths of the microelectrodes were determined with the use of the microscope, camera, and computer software. The instantaneous potential drop in solution and the applied current together determine the solution resistance. These experimental resistances were then compared to the theoretical resistance derived from the simulated cell constants (κ), the measured conductivities (ρ) of the electrolyte solutions and the ohmic resistance of the microelectrode (R1). The agreement of these two values depends on the conductivity of the solution and microelectrode length, figure 23.
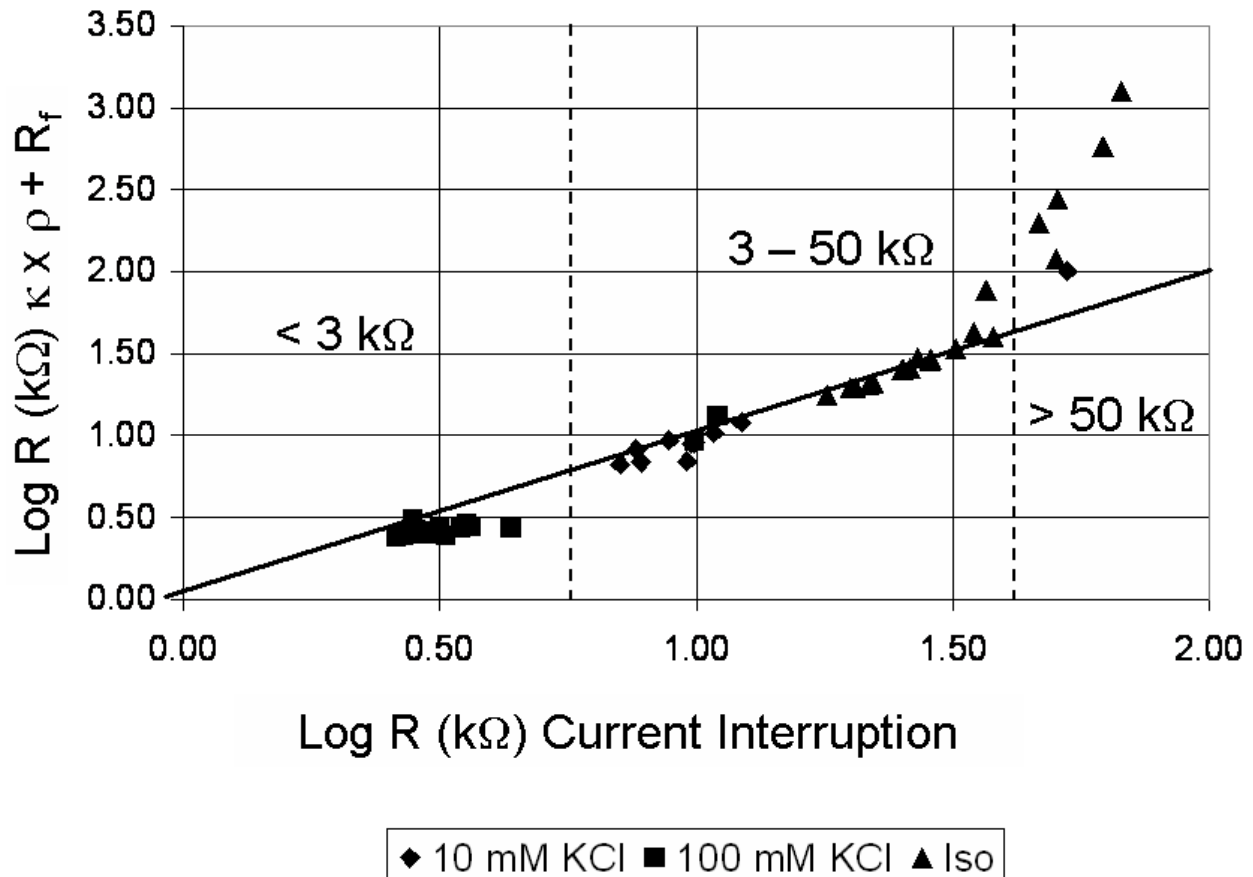
Figure 23. A log plot of the theoretical solution resistance vs. the experimental solution resistance values for current interruption experiments completed in various solutions. The diagonal line on the graph represents perfect correlation with a slope of 1. The approximate conductivities of the solutions used in the current interruption experiments: 100 mM KCl (13,000 μS/cm), 10 mM KCl (1,500 μS/cm), and Iso (350 μS/cm).

For the 10 mM KCl, the agreement for all lengths of microelectrodes tested was acceptable. Agreement was acceptable in the Iso solution for microelectrodes with a length longer than 150 μm. For the highest conductance solution, 100 mM KCl, agreement was only acceptable for microelectrodes with a length shorter than 200 μm. Agreement is good in the range of about 3 to 50 kΩ. The 'good' range includes data from each of the three electrolyte solutions. Disagreement at higher and lower resistances may be caused by the very same undesirable

43

phenomena that cause concern in an electroporation experiment. Thus, we have considered several phenomena such as local changes on pH, conductance, and temperature near the microelectrode.

3.4.1 Ohm's Law

We had anticipated better agreement. Several potential confounding effects were investigated. Is Ohm's Law being obeyed in the current interruption experiments? According to Ohm's Law an increase or decrease in the applied current should linearly affect the drop in voltage when the resistance is kept constant. Current interruption experiments were performed at various applied voltages on several microelectrodes of various lengths in the 10 mM KCl and Iso solutions. The data for the 10 mM KCl solution is shown in figure 24.
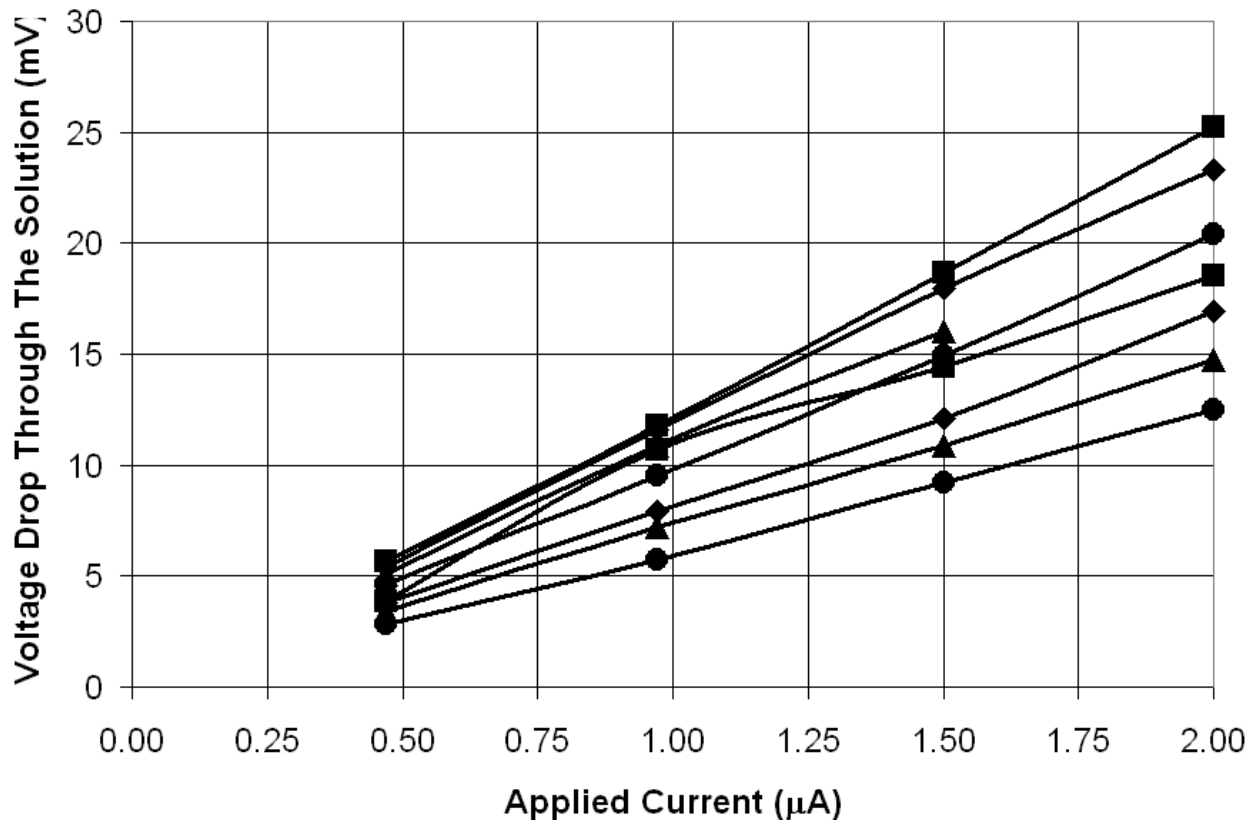
Figure 24. A plot of the voltage drop through solution at several different currents for several microelectrodes in a 10 mM KCl solution.

The positive linear correlation (average $R^2 = 0.9962$) and an intercept of -94 µV between the applied current and instantaneous voltage drop shows that Ohm's Law is being obeyed in the current interruption experiments.

3.4.2 Average Current Density

Could this lack of agreement with theory be due to the difference in the average current density applied to the microelectrode? First, current interruption experiments were performed on microelectrodes of various lengths in a 100 mM KCl aqueous solution with an applied current of 1 µA. Then, current interruption experiments were performed on microelectrodes in the same

solution, but the applied currents were adjusted so that the average current densities for the different microelectrodes were approximately the same. This was done by applying 1 μA of current to the longest microelectrode and linearly decreasing the applied current as a function of the microelectrode's surface area. The resistance values for the adjusted applied current were similar to those for the applied current of 1 μA, figure 25.
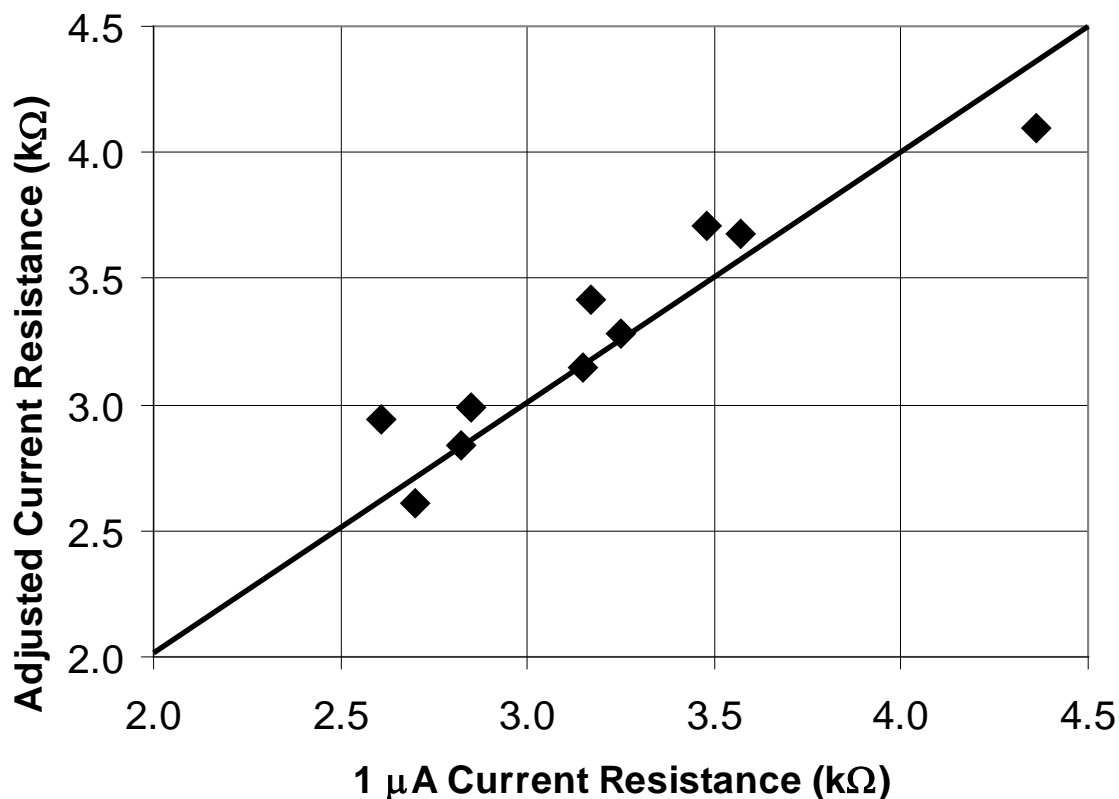
Figure 25. A plot of the calculated solution resistances from current interruption experiments performed on microelectrodes of various lengths (494 – 1,604 μm) in a 100 mM KCl solution. In the 'Adjusted current' measurements, all of the microelectrodes had the same average current density. The diagonal line shows where direct correlation would appear on the plot.

The average current density experiments were also carried out on shorter microelectrodes in the Iso solution with similar results, which are shown below in figure 26. As there is good

agreement between current interruption experiments with one μA applied and those with the adjusted current based on the length of the microelectrode in two different solutions on several different microelectrodes, it was concluded that the current density was not the caused of the lack of agreement with theory.
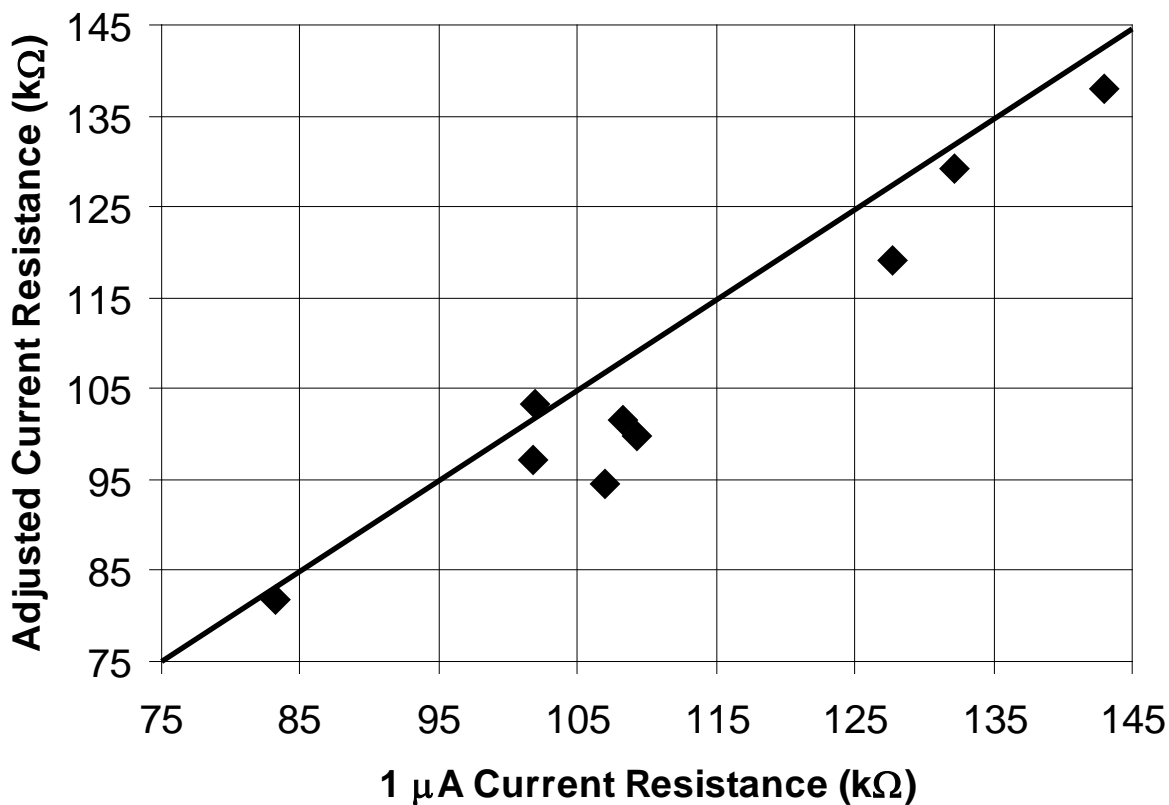
Figure 26. A plot of the calculated solution resistances from current interruption experiments performed on microelectrodes of various lengths (0 – 223 μm) in the Iso solution. In the 'Adjusted current' measurements, all of the microelectrodes had the same average current density. The diagonal line shows where direct correlation would appear on the plot.

3.4.3   Electrode Polarization

 Is the lack of agreement of the experimental resistance values from the theoretical ones due to electrode polarization? Initially, no reversible depolarizer was added to any of the solutions (10 mM KCl, 100 mM KCl, and Iso). In order to insure that polarization was not influencing the results, quinhydrone was added to the Iso solution. The concentration of quinhydrone (5 mM) was sufficient to insure that the diffusion limited current was greater than the current applied in the current interruption experiment. The solution resistance values of the experiments with quinhydrone added was within 10% of the initial experiments without any quinhydrone, figure 27. This allowed us to determined that electrode polarization was not the cause of the lack of agreement with theory.
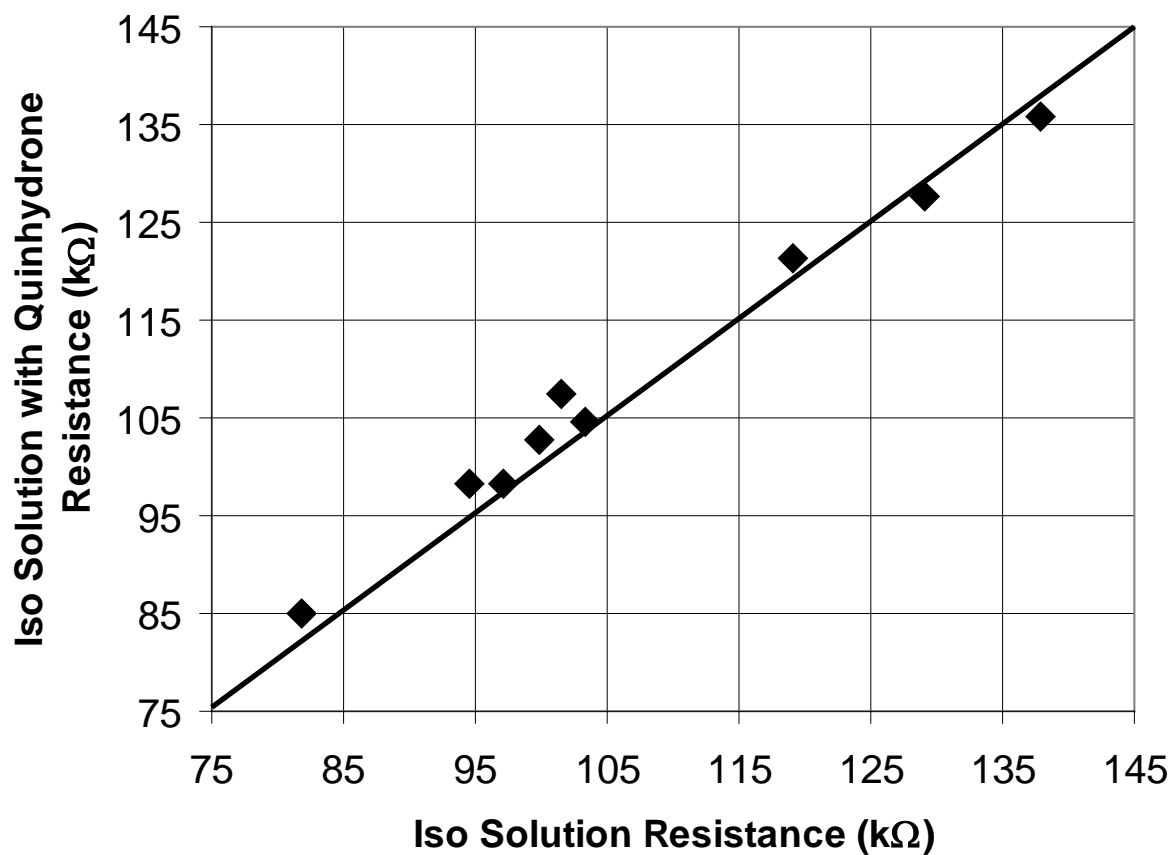
Figure 27. **A plot of the calculated solution resistances from current interruption experiments performed on microelectrodes of various lengths (0 – 223 μm) in the Iso solution with and without 5 mM quinhydrone. In both sets of experiments the same average current density was applied to each microelectrode. The diagonal line shows where direct correlation would appear on the plot.**

3.4.4 Conductivity Changes

Could changes in conductivity be the cause for this lack of agreement with theory? The conductivity of the solutions were taken before and after current interruption experiments with no significant, less than 1%, change in its value for all three solutions. The lack of a global

change in conductivity of a solution does not ensure that the local conductivity of a solution around the microelectrode does not change. This is especially true for the Iso solution that contains organic molecules, ~ 225 mM inositol, that could be oxidized into conductive ions. We determined that, in fact, electrolysis of Iso solution does increase its conductance. In a cell with two glassy carbon plate electrodes ~ 3 cm by 1 cm by 0.25 cm, and using a similar current density to that of the carbon fiber microelectrode's in 50 mL of the Iso solution in a thermostated cell (23° C) for 6 hours resulted in an 18% increase in the solution conductivity. We further carried out a 'back of the envelope' calculation to tell us what the concentration of electrolyte created by this electrolysis might be near a microelectrode. The dimensionless time in the equation for current at a cylinder, $\tau = 4Dt/a^2$ (D is diffusion coefficient, t is time, a is cylinder radius) for a typical 200 ms pulse used in electroporation is 30, and for the current interruption experiment is much larger. Thus, we are in the 'quasi-steady state' regime. We use the equation for diffusion controlled current density, with a diffusion coefficient of 1×10^{-9} m^2s^{-1}, we take n = 1, to arrive at what the concentration at the microelectrode of the species must be. With a current density of about 70 A/m^2 (1 μA at a 10 μm diameter, 500 μm long cylinder) we get a surface concentration of about 400 mM. This is clearly sufficient to lead to a resistance much lower than anticipated from the bulk conductance of the Iso solution and the cell constants (the right side of figure 23).

3.4.5   Change in pH or Temperature

Could a local change in the pH or temperature around the microelectrode be the cause for the lack of agreement between the experimental and theoretical solution resistance values? A drastic change in pH could indicate the electrolysis of water, which would increase the local

conductivity of the solution. We verified that there was not a significant change in the pH around the microelectrode with the pH indicator, methyl orange, in the Iso solution. This was done by running current interruption experiments, in which the current was applied 10 times longer than normal, under a microscope with 200 times magnification. No noticeable color change in the pH indicator was observed under these conditions. As the temperature of a solution increases, the conductivity of a solution also increases. The global temperature change of a solution is prevented by thermostating the electrochemical set-up. Computer simulations were performed to see if a local temperature change around the microelectrode is predicted. When an average current density similar to those in the current interruption experiments was applied to the microelectrode in the simulation, there was no (< 0.004 ℃) predicted temperature increase in the solution around the microelectrode for the Iso solution. When an average current density of 10 times greater than that in the current interruption experiments was applied to the microelectrode a temperature change of < 0.04 ℃ was predicted, 100 times gave a predicted temperature change of < 3.7 ℃. With out a noticeable change in pH, demonstrated by the lack of color change by the pH indicator in solution and the computer simulations predicting an insignificant temperature change at or harsher than experimental conditions, it was determined that neither the pH or the temperature change caused the lack or agreement with theory.

3.4.6   Thin Semi-insulating Layer

Could the lack of agreement between the experimental and theoretical solution resistance values be a result of a thin semi-insulating layer on the surface on the microelectrode? It would explain the disagreement on the low-resistance end with the high conductance solution. This is not unreasonable. Graphite oxide can be formed on carbon surfaces[71]. Graphite oxide is

nonconductive, but the layer it forms on an electrode surface is porous. Thus it acts as a resistive coating. The presence of such an additional resistance, if it discharged rapidly in the current interruption experiment, would add to the solution resistance, creating the bias seen in the lower left part of figure 23.

3.4.7   Computer Simulation Model

Another possible explanation could be the simplicity of the model used in the computer simulations. It does not account for any secondary electrochemical effects, such as ion concentration at the electrodes. The geometry of the computer simulation model has also been idealized. The differences between the geometry used for calculating the cell constants for the microelectrodes and the actual experimental set-up are addressed in detail in a later section.

4.0 FABRICATION OF CARBON FIBER SHORT MICROELECTRODES (LESS THAN 15 MICROMETERS)

If one does a calculation to estimate the amount of the current needed to be applied to the microelectrode to create a potential of ~250 mV across a cell, the necessity for short, ~15 μm or less, microelectrodes becomes apparent. This estimation of the current will be carried out below for two 10 μm diameter microelectrodes with the lengths of 125 μm (E_1), which is quite short when cutting the carbon fiber with a scalpel, and 15 μm (E_2). The solution to be used in the experiments will be the Iso-osmolar solution, because it has the lowest conductivity (~3.5 mmhos/cm), thus the highest resistance of the three solutions tested during the current interruption experiments. The solution resistances of the microelectrodes were determined experimentally to be about 11 kΩ (E_1) and 21 kΩ (E_2). By multiplying the solution resistance by the solution conductivity, this would give experimental cell constants of around 38.5 cm^{-1} (E_1) and 73.5 cm^{-1} (E_2). Unfortunately, the cell constant value for the short microelectrode (E_2) does not agree well with the one calculated using equation #7 above, which gives cell constants of 46.3 cm^{-1} (E_1) and 183.5 cm^{-1} (E_2). This discrepancy will be addressed in a later section. With the use of the simulated potential gradient for the microelectrodes and their calculated cell constants the currents needed would be 70.6 μA (E_1) and 13.7 μA (E_2) with a distance of 5 μm between the cell and microelectrode tip and a cell diameter of 20 μm. When using the experimental cell constants the current needed would be 84.9 μA (E_1) and 34.2 μA (E_2).

53

Applying either of the currents needed for the 125 μm microelectrode (E_1) would damage, if not completely destroy, the microelectrode but the currents needed for the 15 μm microelectrode (E_2) would not. Another reason why the use of short microelectrodes is desired is that the shorter the microelectrode the better the spatial resolution of electroporation between nearby cells.

4.1 ENCASEMENT OF THE CARBON FIBER

Carbon fibers, 10 μm in diameter and 5 cm or greater in length, are attached to a copper wire (Goodfellow Cambridge Limited, Huntingdon, England) 0.5 mm in diameter and 12 cm or greater in length, using a silver conducting paint (SPI Supplies, West Chester, PA). After the silver paint is allowed to dry, 10 minutes or longer, the copper wire/carbon fiber is threaded into a borosilicate glass capillary (Sutter Instruments, Co., Novato, CA) with a 0.75 mm inner diameter, 1 mm outer diameter, and a length of 10 cm, copper end first. Once the copper wire/carbon fiber junction is pulled slightly over half way into the capillary, it is fixed in place using Epoxi-Patch (The Dexter Corporation, Seabrook, NH) to seal the copper connector wire to the glass. The epoxy is allowed to cure overnight before the capillaries are pulled using a standard vertical micropipette puller (Narishige, Tokyo, Japan). The capillary must be positioned so that the carbon fiber/copper wire junction is about one centimeter above the heating coil of the puller. The carbon fiber protruding from the tip of the pulled capillary is cut to the desired length, ~1 mm in our case, using a microscope with an ocular micrometer and a scalpel. The seal of the glass/carbon fiber junction is reinforced by placing the glass/carbon fiber junction in a resistively heated metal loop for approximately 3 minutes. Figure 28 shows the same microelectrode before and after this sealing step.
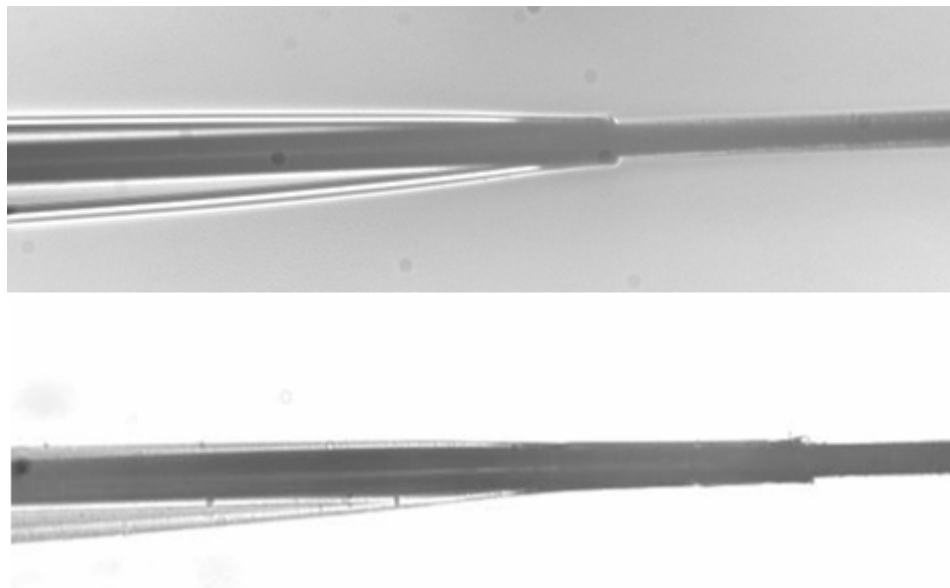
Figure 28. Image of the same microelectrode before (top) and after (bottom) sealing the glass/carbon fiber junction with the resistively heated metal loop.

The carbon fiber microelectrode is now immersed in acetone for 5 minutes. This removes the sizing compound from the carbon fiber and can be used as a preliminary indicator of a good or bad seal between the glass capillary and carbon fiber. The appearance of acetone on the inside of the glass capillary indicates a bad seal. If a bad seal is indicated, the acetone inside the capillary is allowed to evaporate before the microelectrode is resealed in the resistively heated metal loop. If a good seal is indicated, the microelectrode is then sonicated for 10 minutes in isopropanol with activated carbon, before being tested using CV in a 1 mM $K_4Fe(CN)_6$ / 0.1 M KCl aqueous solution (testing solution). After the CV, the microelectrode is then rinsed in Milli-Q water and allowed to dry before application of the photoresist.

4.2   APPLICATION OF PHOTORESIST

The Photoimage^{TM} is diluted as recommended by the manufacture and stored in a non-transparent container at room temperature. A stainless steel cylinder, 3 cm in length and 0.75 cm in diameter, closed at one end acts as both the electrochemical cell and counter electrode in the electrochemical setup. The photoresist is electrodeposited for 60s at -3.25 V onto the carbon fiber microelectrode using Controlled Potential Electrolysis (CPE with a BASi Epsilon-EC). The photoresist is then cured at 120 °C for 1 hour. A second application of the photoresist at the same potential for 30 seconds is administered to fill any defects in the insulating coating, and is cured identically to the first coating. The insulation is tested for defects using cyclic voltammetry. A peak current > 50 pA indicates a defective coating. The microelectrodes with a defective coating are coated and cured for a third time, using the identical treatment as the first two, and retested. Microlectrodes appearing defective after this third coating are discarded.

There is a correlation between the shape of the current-time transient during electrodeposition for the first coating and the appearance of the coating. Figure 29 shows a sample current versus time plot, which is characteristic of a carbon fiber microelectrode that was soaked in acetone to remove the sizing compound, and an image of the microelectrode produced.

Electrodeposition of Photoresist
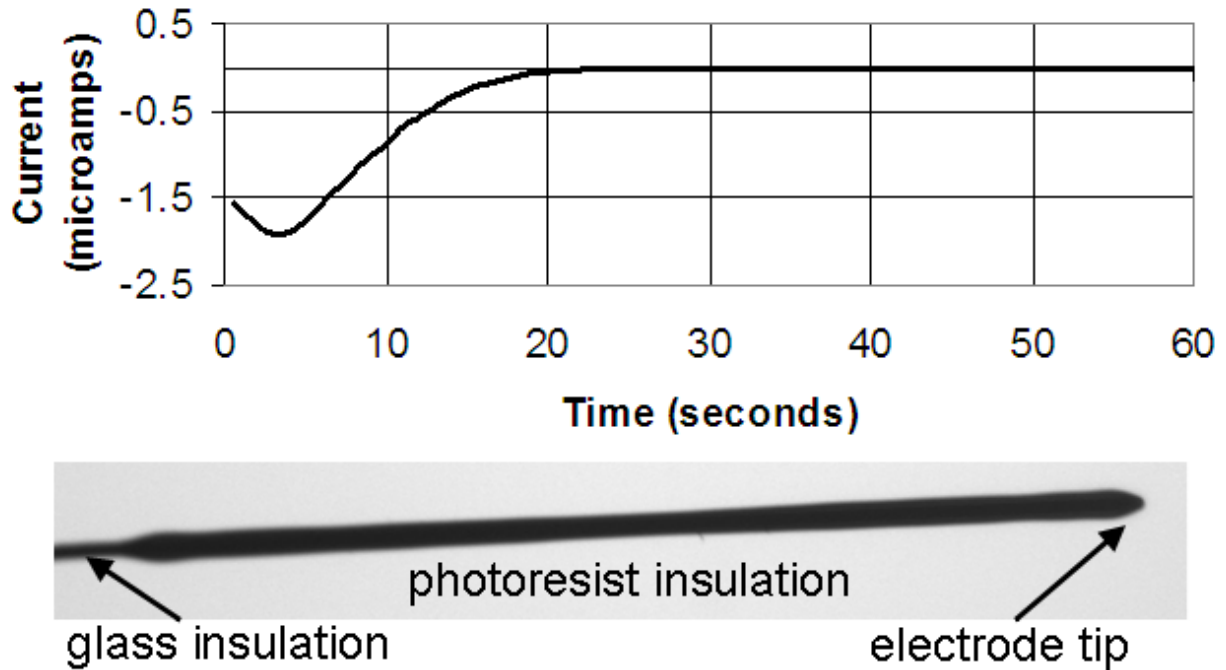
Figure 29. A sample graph of the electrodeposition of photoresist onto a carbon that has been soaked in acetone and its resulting microelectrode.

A current versus time plot that produces an irregular electrode coating, which is characteristic of a carbon fiber microelectrode that was not soaked in acetone to remove the sizing compound, and an image of the microelectrode produced, is shown in figure 30.

Electrodeposition of Photoresist
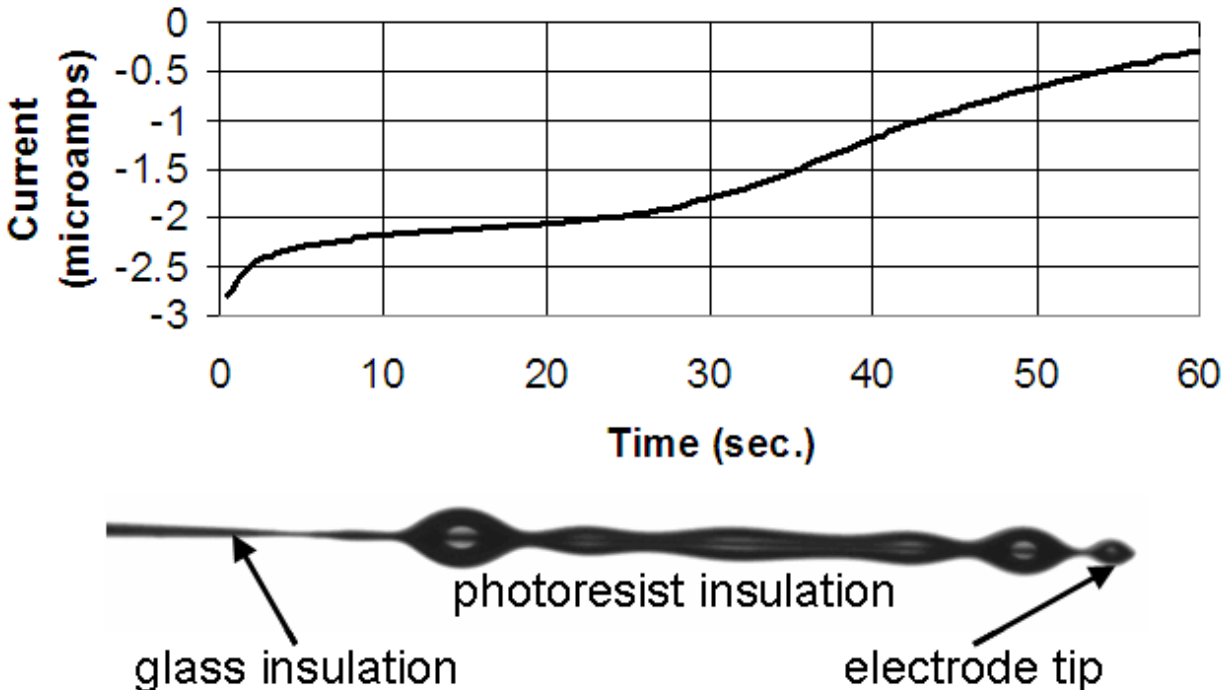
Figure 30 A sample graph of the electrodeposition of photoresist onto a carbon that has not been soaked in acetone and its resulting microelectrode.

The thickness of the coating put on the carbon fiber microelectrode can be controlled by varying the temperature of the photoresist solution during the electrodeposition process. Though only two different temperatures have been probed, these results coincide with what the photoresist's manufacture has observed with a metal substrate.   Electrodeposition of the photoresist solution at room temperature, 22° C ±2°, and 35° C ±1°, create coatings of two visually different thicknesses, figure 31. The coating thickness when electrodeposited at room temperature is approximately 5 μm, while it is approximately 2 μm at 35° C.
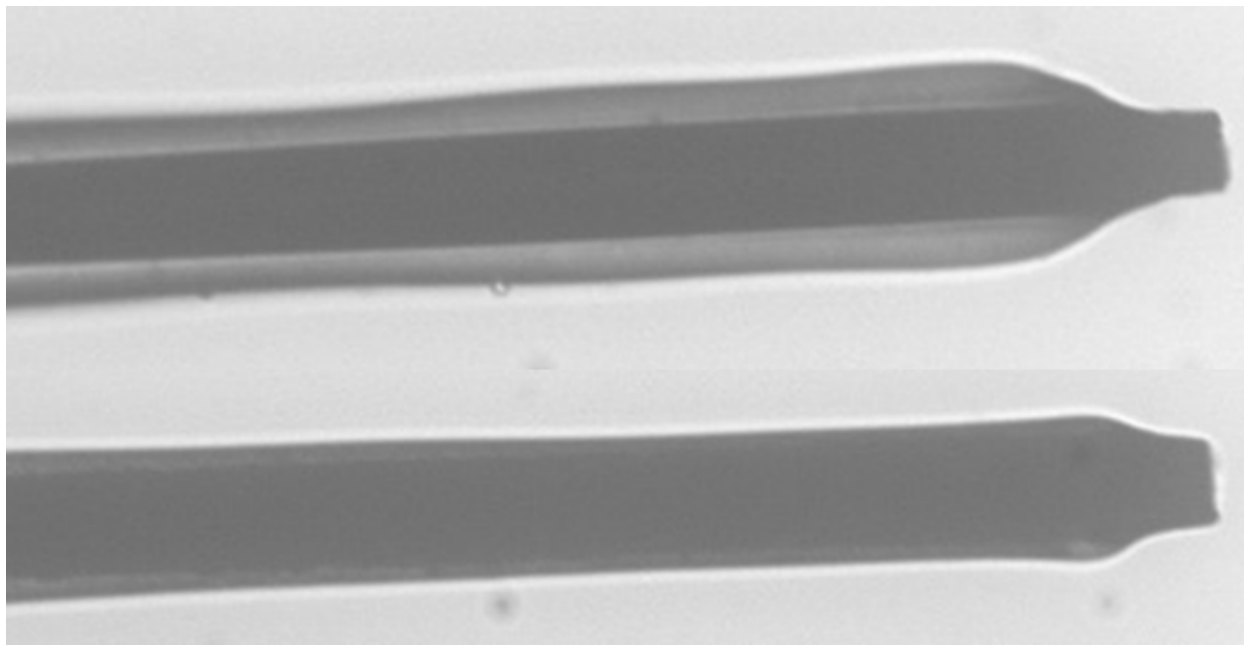
Figure 31. Images of the photoresict coating on microelectrode electrodeposited at two different temperature 22 °C ±2° (top) and 35 °C ±1° (bottom).

These images of the two microelectrodes were taken after part of the photoresist was removed, that is why the tips of the microelectrodes are not covered with photoresist. This trend was also evident when metals were used as the substrate for the photoresist in our laboratory.

4.3   REMOVAL OF PHOTORESIST

Carbon fiber microelectrodes after being coated in photoresist and tested are rinsed with Mill-Q water and allowed to dry prior to light exposure. A mercury-doped xenon arc lamp (Oriel, Stratford, CT) was used as the light source due to its high output in the UV wavelength range, 320 nm – 380 nm, that is required to remove the photoresist. The directions of the photon flux and the long axis of the microelectrode are aligned parallel to each other, as shown in figure 32.

This arrangement was used so that only the tip of the microelectrode is exposed. Exposure times varied.
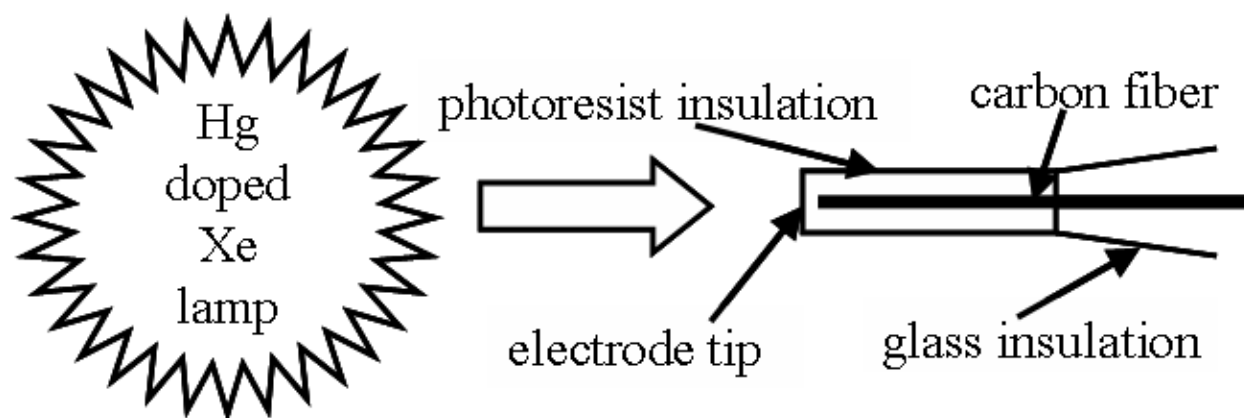
Figure 32. The parallel alignment of the light source, Hg doped Xe lamp, and the tip of the coated microelectrode permits one to selectively expose the tip of the microelectrode with little or no light exposure to the sides of it.

Following the exposure of the microelectrode to light, it is placed in the developing solution, an aqueous solution of 2-butoxyethanol and lactic acid, for 30 seconds. Unless otherwise stated, the respective concentrations were 8 vol% and 10 vol%. Microlectrodes are rinsed in two different baths of Milli-Q water and allowed to dry before repeating the exposure and development steps if desired. After the carbon fiber microelectrodes dry from their final rinse in the Milli-Q water, the amount of the carbon fiber exposed is estimated using cyclic voltammetry (CV) and optical images.

After the coated carbon fiber microelectrode is exposed to light it has to be immersed in an aqueous solution of 2-butoxyethanol and lactic acid, known as the developing solution, to remove the photoresist from the microelectrode. The manufacturer's suggested concentrations, 2% 2-butoxyethanol and 1% lactic acid, were tried first, but these conditions were "too weak" to remove the photoresist. This could have been due to the difference in substrate, metal versus carbon, or the difference in curing time, 5 versus 60 minutes. After these initial trials, higher

concentrations, up to 12 %, of the two components were tested. High concentrations of the two components cause removal of the non-exposed photoresist. We assessed the developing solution's nature using voltammetry. Following exposure and development of microelectrodes, they were photographed and subjected to CV in a 1 mM $K_4Fe(CN)_6$ / 0.1 M KCl aqueous solution (testing solution). Theoretical steady state currents could be estimated from the dimensions of the exposed electroactive area based on the optical images. Results from CV were compared to these theoretical currents. The developing conditions were classified as being "too weak" if the experimental current was less than half of the corresponding theoretical current. They were classified as "too aggressive" if the experimental current was more than twice the theoretical current. Microelectrodes that had an experimental current that was more than half but less than twice the theoretical current were classified as having had "normal" developing conditions (the Goldilocks conditions). Results for various developers are compared in table 5. A developing solution of 8% 2-butoxyethanol and 10% lactic acid was chosen because it gave the highest percentage of microelectrodes that fell into the "normal" classification.

Table 5. Summary of several different developing solution concentrations tested on microelectrodes. Microelectrodes were exposed for 7.5 minutes, immersed in the developing solution for 30 seconds, and then exposed and developed for a second time. Conditions too weak indicates little or no photoresist was removed (signal in 1 mM ferocyanide is < 0.5 nA). Conditions normal indicates exposed photoresist was removed, signal 0.5 – 2 nA. Conditions too aggressive indicates exposed and non-exposed photoresist was removed, signal >2 nA. Optical microscopy was used to confirm removal of non-exposed photoresist.

% 2-butoxyethanol / % lactic acid (number of microelectrodes)	Conditions too weak	Conditions normal	Conditions too aggressive
4/6 (6)	100%	0%	0%
5/5 (6)	100%	0%	0%
6/4 (6)	75%	25%	0%
6/8 (8)	75%	25%	0%
8/6 (6)	66.7%	33.3%	0%
6/10 (14)	85.7%	14.3%	0%
8/10 (15)	13.3%	80%	6.7%
8/8 (8)	37.5%	50%	12.5%
10/10 (8)	0%	50%	50%
10/6 (6)	33.3%	33.3%	33.3%
10/8 (8)	12.5%	37.5%	50%
12/10 (6)	0%	33.3%	66.7%

The photoresist used is a negative photoresist. Light exposure in the 320 nm - 380 nm range causes the coating to be susceptible to etching in the exposed area. Carbon fiber microelectrodes were exposed to the light for several different lengths of time. The relationship between the time the microelectrode is exposed to the light source and the area of the coating removed from the carbon fiber is not linear. This is attributed to the fact that the coating is not removed as it is exposed to light, but it is removed when immersed in the developing solution after light exposure. Many different exposure times were tested, ranging from 5 to 45 minutes per trial. Through trial and error type experiments on over 300 different carbon fiber microelectrodes a light exposure regimen was established. Two light exposures of 7.5 minutes each (followed by immersion in the developing solution) produced microelectrodes that

reproducibly gave a CV signal in ferrocyanide slightly below what is theoretically predicted for a hemispherical carbon fiber microelectrode (r = 5 μm) in the same solution.

4.4   RESULTING CARBON FIBER MICROELECTRODES

This method of carbon fiber microelectrode production is fairly reproducible. Figure 33 shows the average CV in ferrocyanide of 48 microelectrodes, that have all undergone two 7.5 minute light exposures each followed by immersion in a 10% 2-butoxyethanol / 8% lactic acid aqueous solution. Unfortunately, the production of two identical microelectrodes would be quite difficult because of slight microelectrode to microelectrode variations throughout this process. We hypothesized that the photoresist would be removed from the tip of the microelectrode before being removed from its sides, because of the difference in the angle of incidence of the light on the photoresist's surface. The light source is aligned parallel to the long axis of the microelectrode creating an angle of incidence that is 0° with respect to the normal to the tip surface and ~90° with respect to the normal to the sides of the microelectrode, figure 32. Our hypothesis is supported by the peak current of the average CV in ferrocyanide created by microelectrodes that have undergone two 7.5 minute exposures each followed by immersion in the developing solution for 30 seconds, in figure 33. It is slightly below what is predicted for the steady-state current for a hemispherical microelectrode with a radius of 5 μm in the same solution.   This steady-state current will be displayed with the CVs in ferrocyanide of microelectrodes that have underwent two, four, and six exposure/development trials, so that a quick and accurate comparison between these three sets of data can be made. The optical image in figure 33 also reinforces our hypothesis that the photoresist is predominately removed from

the tip of the microelectrode with very little, if any, being removed from the sides of the microelectrode.
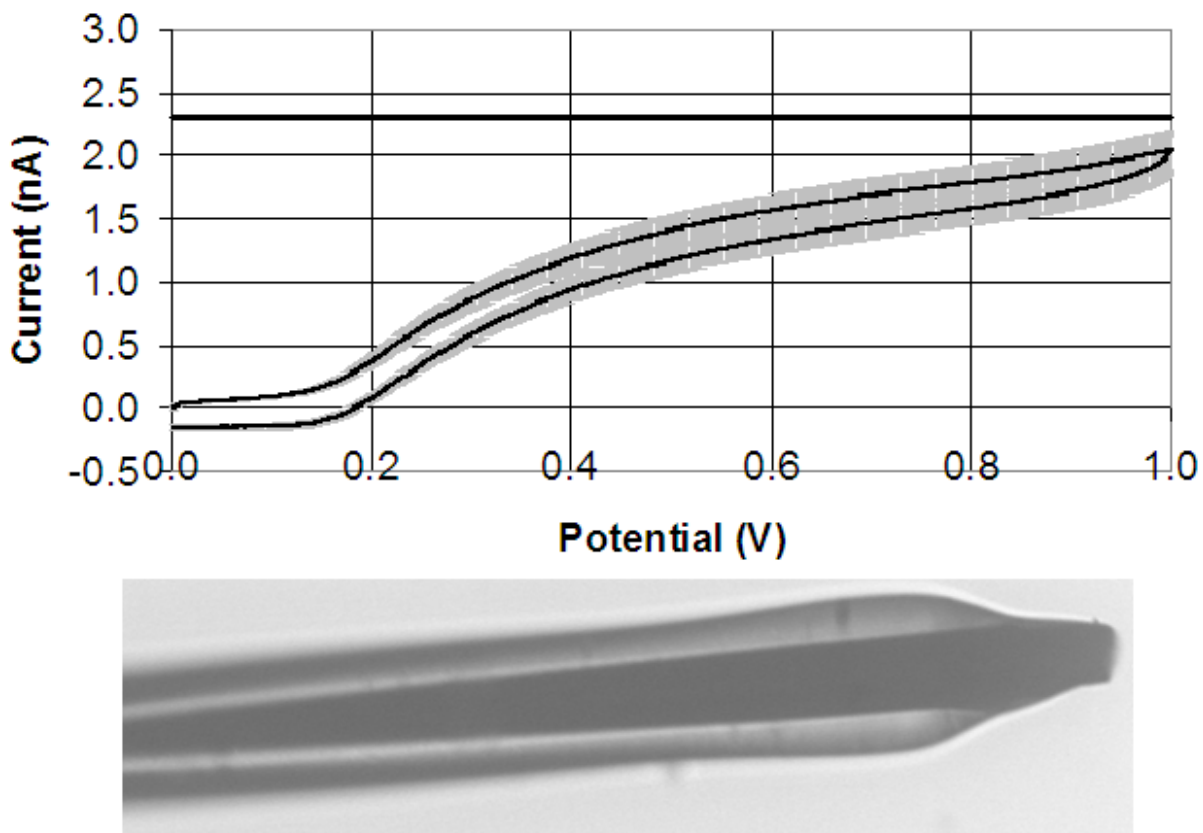
Figure 33. The average CV and standard deviation of the mean of 48 microelectrodes (top) that were exposed for 7.5 minutes twice and developed in a 10% 2-butoxyethanol and 8% lactic acid aqueous solution after each exposure. The straight line across the graph at ~ 2.3 nA is the steady state current predicted for a hemispherical microelectrode (r = 5 μm) in the testing solution. An optical image (bottom) of a microelectrode that has undergone the above treatment.

The photoresist on the sides of the microelectrode can be partially removed from multiple exposure/development trials. The peak current of the average CV in ferrocyanide in figure 34 is noticeably and statistically greater than that in figure 33.
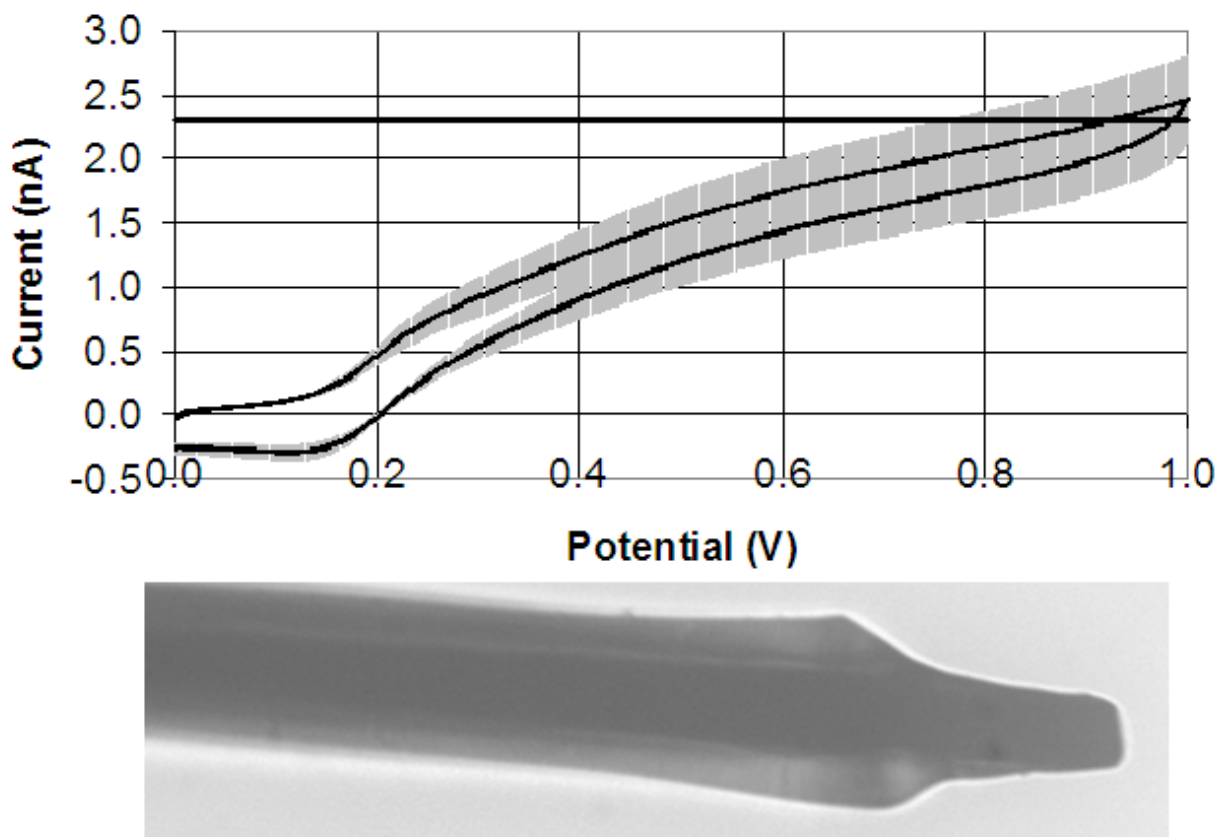
Figure 34. The average CV and standard deviation of the mean of 20 microelectrodes (top) that were exposed for 7.5 minutes four times and developed in a 10% 2-butoxyethanol and 8% lactic acid aqueous solution after each exposure. The straight line across the graph at ~ 2.3 nA is the steady state current predicted for the hemispherical microelectrode (r = 5 μm) in the testing solution. An optical image (bottom) of a microelectrode that has undergone the above treatment.

These carbon fiber microelectrodes have undergone four 7.5 minute exposures each followed by immersion in the developing solution. The increase in the average peak current led to the hypothesis that the photoresist on the sides of the microelectrode near its tip was being removed. Reinforcement of this hypothesis can be seen in figure 34, where the average peak current is now greater than that predicted for a hemispherical microelectrode of the same radius, 5 μm. The optical image in figure 34, is of the same microelectrode in figure 33 only it has now undergone two additional exposure/development trials (for a total of four). These optical images also

reinforce this hypothesis. One can clearly see that the photoresist on the sides of the microelectrode in figure 34 has receded when it is compared to the image in figure 33.

The next hypothesis we formulated is that more of the photoresist would be removed from the sides of the microelectrodes if additional exposure/development trials were performed. Unfortunately, the peak current of the average CV in ferrocyanide after six trials decreased in comparison to that after four trials. This does not necessarily mean that the coating was not being removed, as the difference is well within the standard deviation of the means. However, the optical image in figure 35, which is the same microelectrode as the one in the two previous figures, reinforces this hypothesis.
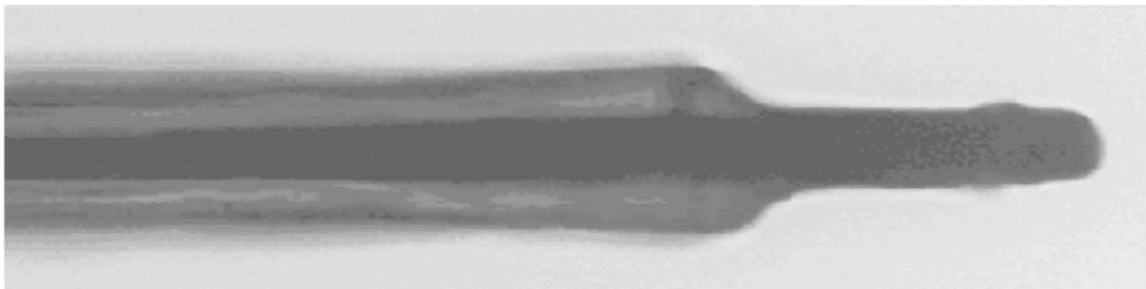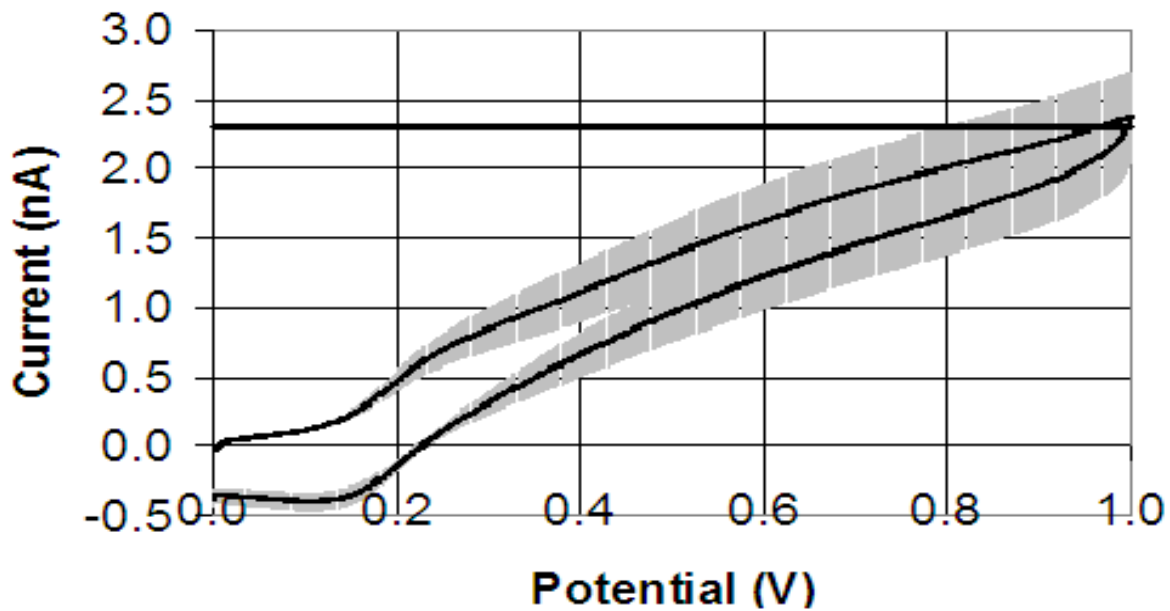
Figure 35. The average CV and standard deviation of the mean of 15 microelectrodes (top) that were exposed for 7.5 minutes six times and developed in a 10% 2-butoxyethanol and 8% lactic acid aqueous solution after each exposure. The straight line across the graph at ~ 2.3 nA is the steady state current predicted for a hemispherical microelectrode (r = 5 μm) in the testing solution. An optical image (bottom) of a microelectrode that has undergone the above treatment.

One can clearly see that the photoresist on the sides of the microelectrode in figure 35 has receded when compare to the image in figure 34. The steady-state current is not very sensitive to the area for geometries like those shown in figures 33-35, but the capacitive current is. The capacitive current at 0.1 volts of the average CVs in ferricyanide (table 6) indicates a greater electrochemically active surface area. The capacitive current and the optical images portray the

same picture. We conclude that photoresist can be removed in a programmed fashion from the surface.

Table 6.   The information for ferricyanide was taken from the average CV and their standard deviations in figures 33-35.   The values for hydroquinone (HQ) and ruthenium hexamine trichloride (Ru hex) are the average of two randomly selected microelectrodes that had the specified light exposure.

Light exposure	2 x 7.5 min.	4 x 7.5 min.	6 x 7.5 min.
Current at 1 volt in ferrocyanide	2.04 nA ± 0.154 nA	2.45 nA ± 0.356 nA	2.37 nA ± 0.341 nA
Capacitive current at 0.1 volts in ferrocyanide	0.234 nA ± 0.033 nA	0.382 nA ± 0.083 nA	0.509 nA ± 0.093 nA
Current at 1.2 volts in HQ	7.57 nA ± 1.13 nA	12.75 nA ± 4.68 nA	13.65 nA ± 5.40 nA
Current at -0.5 volts in Ru hex	-4.3 nA ± -.64 nA	-8.4 nA ± -3.08 nA	-10.75 nA ± -4.25 nA

While the photoresist seems to be removed, the voltammetry of ferrocyanide is not ideal. We assumed that there was some residue on the surface from the treatment. A variety of treatments including sonication in water and isopropanol and electrochemical treatments in HCl and NaOH were used to try to improve the voltammetric shape, to no avail. We had hoped that ten minutes of sonication in water would help with the removal of any residue. Sonication in water did not have any apparent effect on the CVs in ferrocyanide of the microelectrodes, but when isopropanol was used the shape of the CVs worsened. The 50 % HCl electrochemical treatment performed on the microelectrodes came from a paper by Frysz[72]. In this paper they reported an improvement in the detection of ferricyanide, but this treatment did not show any improvement or degradation in our CVs in ferrocyanide. The NaOH electrochemical treatment used in our laboratory was very similar to that described in a paper by Schulte with a few minor modifications[52]. This treatment etches the carbon fiber exposing a fresh carbon surface and makes the microelectrode slightly smaller in size. Etching times of 1, 2, 5, 10, and 20 seconds

were used in our trials. Only slightly smaller CV signals in the 10 and 20 second etching times were noticeable with no improvement in shape of the CVs for any of the etching times.

Dopamine detection at carbon fibers is known to be surface sensitive, so it is a severe test of the microelectrode's capabilities[73, 74]. Several microelectrodes that were exposed for 7.5 minutes two times and developed in a 10% 2-butoxyethanol and 8% lactic acid aqueous solution after each exposure were used in the *in vitro* detection of dopamine using fast-scan cyclic voltammetry. For the fast-scan cyclic voltammetry, a computer-controlled potentiostat was linearly ramped at 300 V/s from an initial potential of 0 V to +1 V, then to -0.5 V and back to 0 V versus a Ag/AgCl reference electrode. These CVs were performed using a flow cell in a phosphate-buffered saline (PBS) solution and a 5 μM dopamine spiked PBS solution. Before the initial CV, the microelectrodes were electrochemically pretreated, which is commonly done in preparation for the in vivo determination of dopamine with carbon fiber microelectrodes. The electrochemical pretreatment, which is a 50 Hz, 0 V to +2 V triangle wave applied for 1.5 seconds, was performed in a flow cell in a PBS solution. The fast-scan CVs and pretreatment of the carbon fiber microelectrodes were carried out at room temperature. The background subtracted CV of a sample microelectrode is shown in figure 36. The characteristic shape of the dopamine wave is evident in the CV. Thus, we conclude that the coating and selective removal processes illustrated here do not detrimentally change the carbon fiber surface.
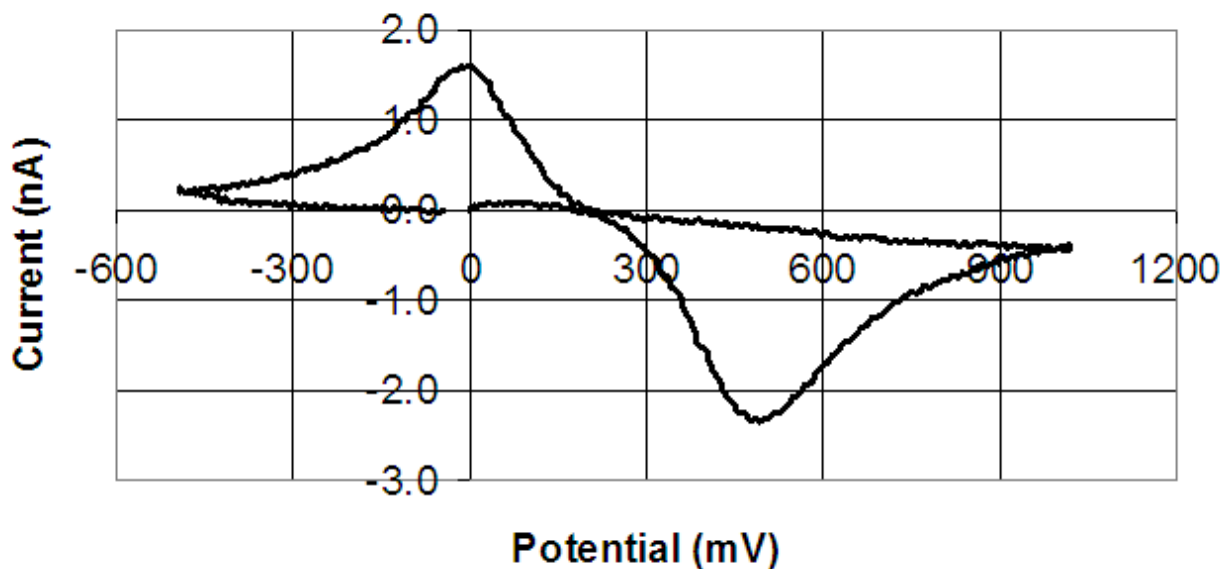
Figure 36. The average of six CVs of an electrode that was exposed for 7.5 minutes two times and developed in a 10% 2-butoxyethanol and 8% lactic acid aqueous solution after each exposure, in 5 µM dopamine spiked PBS solution. The microelectrode was electrochemically pretreated, which is commonly done in prepartation for the in vivo determination of dopamine with carbon fiber microelectrodes.

Now that we have concluded the carbon fiber surface has not been changed due to the evidence stated above, we hypothesized that non-ideal CVs were caused by the electroactive species (ferrocyanide) used in the experiments. Microelectrodes after two, four, and six 7.5 minute exposures were then used to detect several different electrochemically active species using CV. The first of these species was ferricyanide. The CVs of ferricyanide had a similar non-ideal shape as the ferrocyanide CVs (data not shown). This outcome was not surprising, seeing that the same microelectroactive molecules of the redox couples are present, the only major change was in the potential sweep of the CV. The next electrochemically active species tested with the microelectrodes was hydroquinone (HQ). The shapes of the CVs for HQ were normal; the CV of a sample microelectrode exposed two times for 7.5 minutes is shown in figure 37.
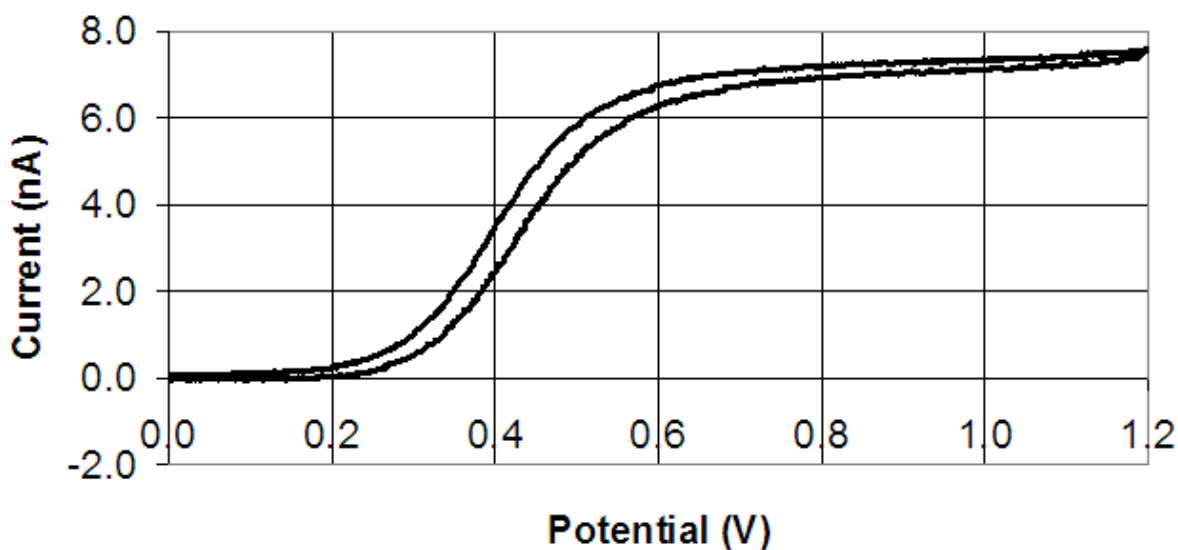
Figure 37. A CV in HQ of a sample microelectrode that had been exposed two times for 7.5 minutes and developed in a 10% 2-butoxyethanol and 8% lactic acid aqueous solution after each exposure.

The signals of the CVs in HQ increased as the number of exposures increased supporting our hypothesis that more electroactive surface area is exposed, table 6 above. The last electrochemically active species tested with the microelectrodes was ruthenium hexamine trichloride (Ru hex). The shapes of the CVs for Ru hex were also normal; the CV of a sample microelectrode exposed two times for 7.5 minutes is shown in figure 38. The signals of the CVs in Ru hex again increased as the number of exposures increased supporting our hypothesis that more electroactive surface area is exposed, table 6 above.
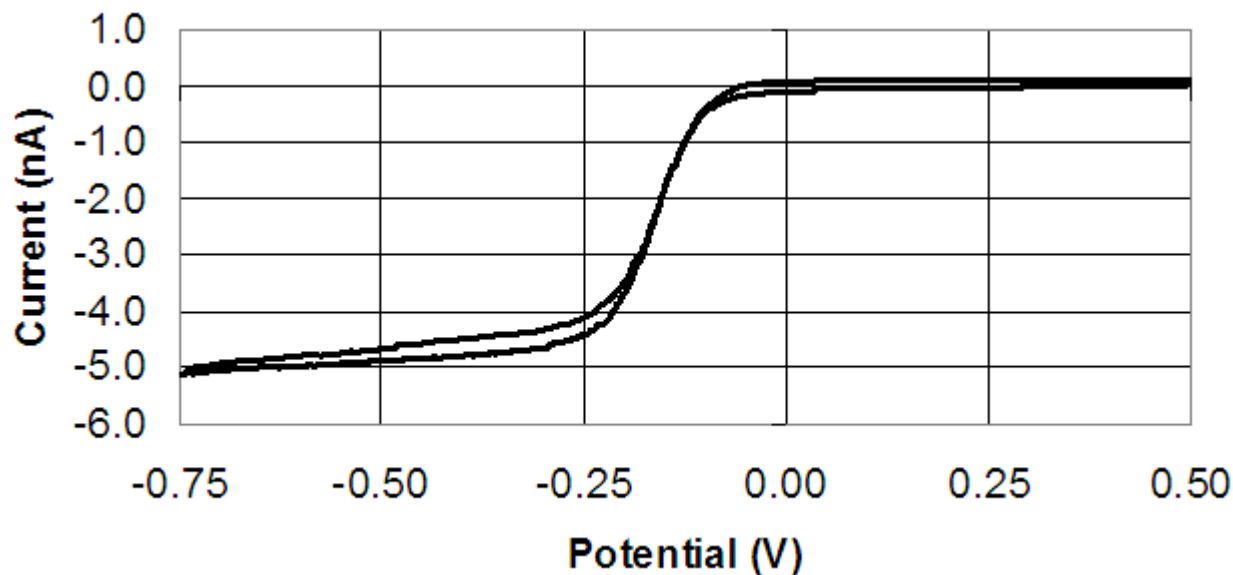
Figure 38. A CV in Ru hex of a sample microelectrode that had been exposed two times for 7.5 minutes and developed in a 10% 2-butoxyethanol and 8% lactic acid aqueous solution after each exposure.

One final attempt was made to clean the microelectrode surface with plasma cleaner. We were hesitant to use plasma cleaning because of possible damage to the electrically insulating property of the non-exposed photoresist. The microelectrodes were cleaned for one minute on the medium setting with air as the plasma cleaner's supply gas. Fortunately for us, the electrically insulating property of the non-exposed photoresist was not affected under these conditions and the CVs of ferrocyanide were more ideal in shape, figure 39.
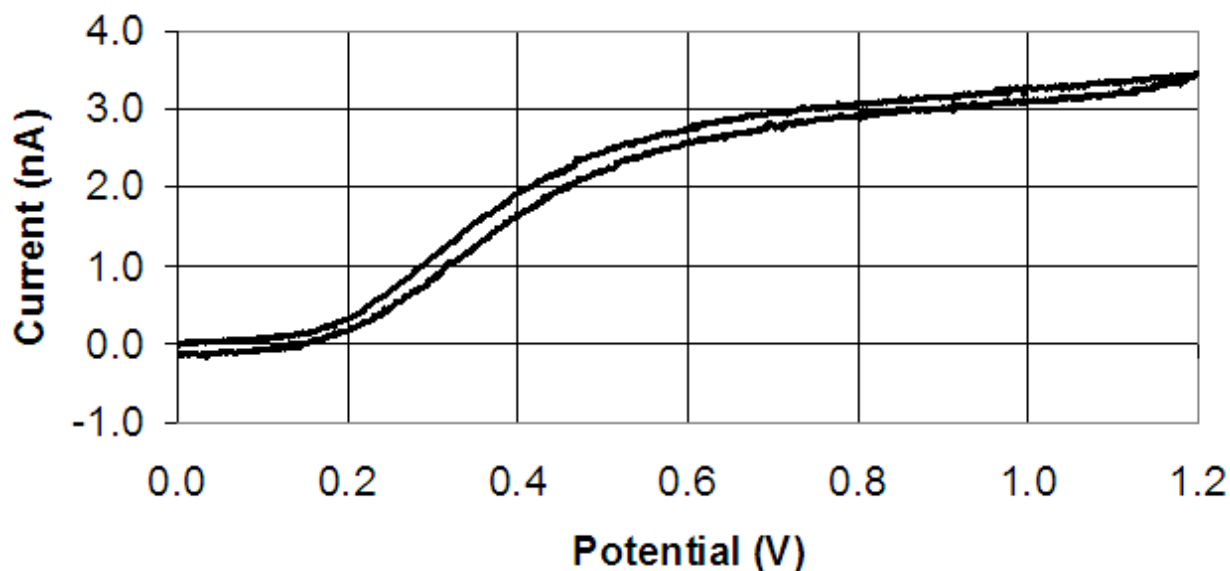
Figure 39. A sample CV in ferrocyanide of a plasma cleaned microelectrode that has had two 7.5 minute exposures each followed by development in a 10% 2-butoxyethanol and 8% lactic acid aqueous solution.

The shape of the CVs for Ru Hex and HQ were not affected (data not shown). The plasma cleaning did significantly increase the current for all three analytes, but the relative standard deviation from the mean stayed approximately the same, table 7.

Table 7. The average current and the standard deviation of the mean for the three analytes before and after plasma cleaning.

Exposure	Ferrocyanide (nA)	Hydroquinone (nA)	Ruthenium hexamine (nA)
2 x 7.5 minutes	1.93 (± 0.27)	5.60 (± 0.78)	-3.25 (± -0.45)
After	4.13 (± 0.52)	7.35 (± 0.92)	-5.35 (± -0.67)
4 x 7.5 minutes	2.15 (± 0.30)	5.95 (± 0.83)	-3.87 (± -0.54)
After	4.23 (± 0.53)	7.50 (± 0.94)	-5.70 (± -0.72)
6 x 7.5 minutes	4.30 (± 0.60)	10.65 (± 1.48)	-9.75 (± -1.36)
After	7.50 (± 0.94)	13.70 (± 1.72)	-13.20 (± -1.66)

With this method of carbon fiber microelectrode fabrication one can control how much of the photoresist coating is removed from the carbon fiber microelectrodes by controlling the

duration and number of cycles of exposure to light.   This allows the production of microelectrodes that have a specific electrochemically active surface area, within a small range.

5.0 SINGLE-CELL ELECTROPORATION WITH CARBON FIBER MICROELECTRODES

To electroporate a single-cell with a carbon fiber microelectrode, the current needed to do so must be calculated. In order to calculate this current several things must be known first 1) the length of the microelectrode being used, 2) the conductivity of the cell bath solution, 3) the current needed to get a potential drop of 1 volt in solution, 4) the values of the potential along the x-axis (y and z = 0) from the computer simulation, 5) the distance between the cell and microelectrode, 6) the length of the cell , and 7) the transmembrane potential needed to electroporate.

5.1 NEW SIMULATIONS: EXPERIMENTAL SET-UP

As demonstrated in a section above and seen in figure 23, the experimental solution resistance values and thus the cell constants for short microelectrodes in the Iso-osmolar buffer do not agree well with the calculated values. One of the reasons stated earlier for the discrepancies in the experimental and calculated solution resistances is the difference in the simulated geometry (vertical geometry) and the actual experimental geometry. Current interruption experiments were preformed on a few microelectrodes in vertical and experimental geometries. Simulations

were also done for these two geometries, for microelectrodes of various lengths. The solution resistances for the vertical and experimental geometries from the current interruption experiments and simulations are shown below in Table 8.

Table 8. The solution resistances for the vertical and experimental geometries from the current interruption experiments and simulations are shown. The % increase is calculated by taking the difference between the experimental and vertical and dividing that by the vertical and multiplying by 100%.

Current Interruption Experiments			
Electrode Length (μm)	Vertical (kΩ)	Experimental (kΩ)	% Increase
13.3	27.5	38.1	37.7
14.3	21.9	29.6	35.1
15.6	21.2	27.4	29.2
16.5	20.4	25.7	25.5
55.8	18.6	23.3	25.2
74.4	15.2	18.7	23.1
93.5	14.0	16.9	20.8
119.4	12.3	14.9	20.9
125.9	10.9	12.9	18.3
129.4	10.9	12.6	15.9
140.3	11.0	12.2	11.3
Simulations			
Electrode Length (μm)	Vertical (kΩ)	Experimental (kΩ)	% increase
100.0	13.3	16.2	21.5
200.0	8.9	9.7	9.2
300.0	6.5	7.0	7.2
400.0	5.1	5.3	4.3
500.0	4.2	4.4	3.8
1,000.0	2.3	2.4	3.5

As seen by the % increase in table 8, as the microelectrode becomes shorter the greater the impact on the solution resistance, and thus the cell constant. It should also be noted that there is good agreement between the experimental and simulated results for the two geometries, which can be seen in figure 40 below.
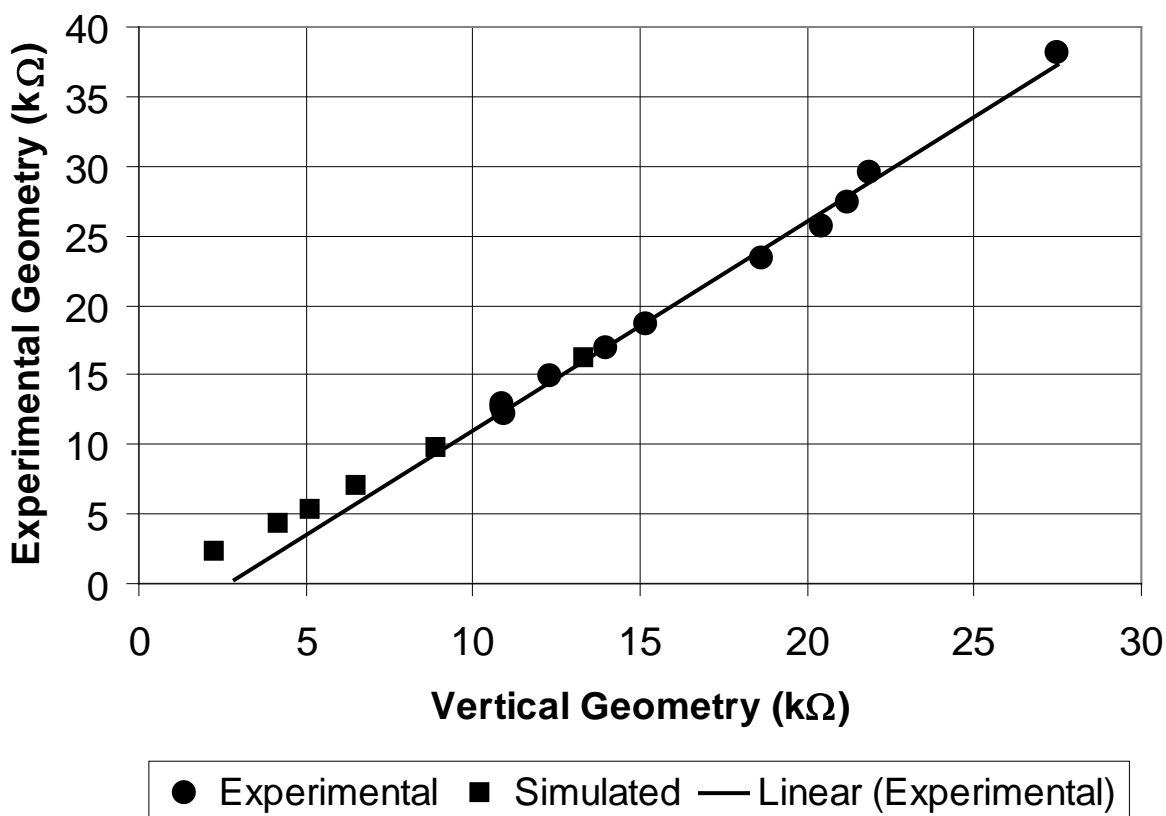
Figure 40. **A plot of the experimental and simulated solution resistances for the vertical and experimental geometries. The linear regression is based on the experimental geometry results only.**

A representation of the experimental set-up can be seen in figure 40 and how the new simulations were preformed is discussed below.
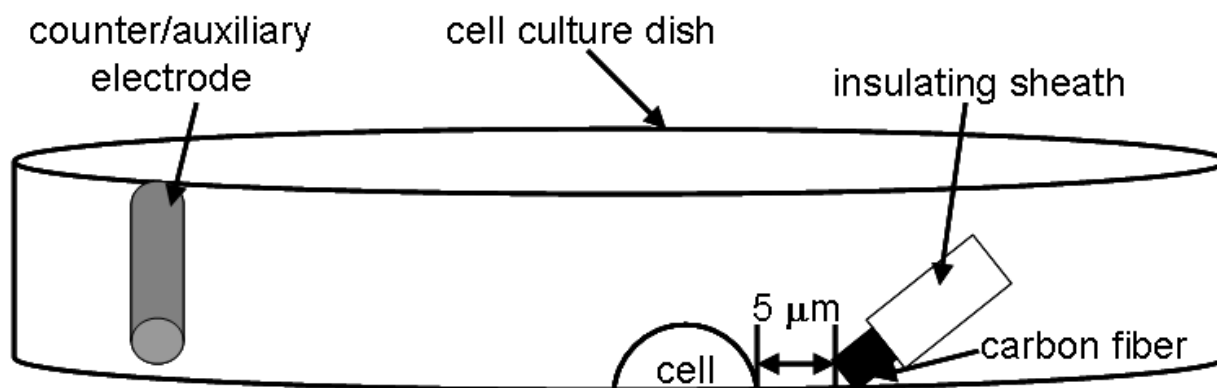
Figure 41. **Graphical representation of the experimental set-up with a 5 μm distance between the microelectrode and cell. Not to scale to show detail.**

These new simulation were completed in the same computer simulation program, FEMLAB now Comsol Multiphysics, as those for the electric field and cell constants. The experimental set-up simulations were performed in the 3D Conductive Media DC model but they were solved for the same equation #4 as the other simulations. The geometric shape was identical to that of the experimental set-up shown above, except no cell was present. The boundary conditions were set to the following: ground for the counter/auxiliary electrode, insulating for the walls of the cell dish, including the top, continuity for the outer edges of the carbon fiber and the insulating sheath, and current source for the end of the carbon fiber against the insulating sheath. The dimensions of the simulations were as follows: the cell dish was 3.5 cm in diameter and 0.75 cm in height, the counter/auxiliary electrode was 1 mm in diameter and 2.0 cm long, the insulating sheath was 15 μm in diameter and 50 μm long, and the carbon fiber was 10 μm in diameter and was the actual length to the closest 0.1 μm. These simulations unlike the other two sets had more than one subdomain, excluding ones created just to help refine the mesh. The subdomain settings were as follows: the interior of the cell dish had a conductivity of 0.35 S/m (Iso-osmolar buffer), the interior of the carbon fiber had a conductivity of 6.959×10^5 S/m (measured) and the insulating sheath had a conductivity of 1×10^{-9} S/m. The global mesh parameters for these simulations were also set to the predefined mesh size of 'finer'. A subdomain was created around the microelectrode to help with the refining the mesh and its dimensions were 0.35 mm by 0.35 mm by 0.35 mm. Its boundary conditions were continuity, except where it acted as the bottom of the cell dish, it was set to insulating and the subdomain setting was the same as the cell dish, 0.35 S/m. The maximum element sizes for the subdomains were as follows: the cell dish was 1×10^{-3} m, the cube around the microelectrode was $10 - 14 \times 10^{-6}$ m, the insulating sheath was 2.5×10^{-6} m and the carbon fiber was 0.75×10^{-6} m. These simulations had between

400,000 – 700,000 elements depending on the length of the carbon fiber and the minimum meshable maximum element size for the cube around the microelectrode subdomain. The information exported from these simulations were the values for the potential every 1 μm for the first 100 μm with 0 μm being directly below the top of the microelectrode tip.

5.2 EXPERIMENTAL SET-UP

5.2.1 Cell Cultures

Human lung cancer A549 cells were cultured in basal medium Eagle, supplemented with 10 % fetal bovine serum, and 1 % antibiotic. The A549 cells were chosen due to their high glutathione content, which were stained using the procedure below. Cells were grown in 75 ml cell culture flasks in a CO_2 cell culture incubator (HERA cell incubator, Newtown, CT) at 37° C and 5 % CO_2 to about 80 % confluency. Before the experiments, cells were plated on 35 mm glass bottom cell-culture dishes (MatTek Corporation, Ashland, MA) and were grown for 1-3 days. Experiments were performed on the 2nd and 3rd day following the cell plating.

5.2.2 Cell Staining

Prior to the experiments, the cells were stained with the dye Thioglo-1 (2 μM in Iso) for 60 seconds at room temperature or calcein AM (2.5 μM in Iso) for 30 min in the incubator. Thioglo-

1 is a cell permeable maleimide-based reagent which gives a highly fluorescent, cell-impermeant product upon its reaction with active –SH groups in proteins, enzymes, and small peptides. To remove excess uncaptured dye, the cells were washed in Iso twice. Cells were bathed in the Iso solution and mounted on the cell chamber (DH 35i culture dish incubator, Warner Instruments, Holliston, MA) and transferred to the stage of the microscope.

5.2.3   Fluorescence Imaging

Cells were observed using an inverted microscope (Olympus, IX 71, Melville, NY) with an Olympus UPlanApo 20X 0.7 NA objective or occasionally an Olympus UPlanFl 40X 1.3 NA oil immersion objective. The HBO 100 W mercury lamp in the microscope was used as the excitation source. For Thioglo-1, an Omega fluorescence cube (specially built, Omega, Brattleboro, VT) was used with filters for excitation: $\lambda_{ex} = 378$ nm and emission: $\lambda_{em} = 480$ nm. For calcein we used excitation: $\lambda_{ex} = 494$ nm and emission: $\lambda_{em} = 530$ nm. A 12 bit digital output charged couple device (CCD) camera (Hamamatsu, ORCA-285, Bridgewater, NJ) imaged cells. The image collection frequency varied. The gain and exposure times were set manually. Image processing was performed by the image acquisition software from Compix (Simple PCI).

5.3   PREDICTING THE CURRENT NEEDED TO ELECTROPORATE

5.3.1   Shape and Length of the Microelectrode

The length and shape of the microelectrode was determined with the use of the microscope, camera, and computer software. As shown in section 2.2.2, the shape of the microelectrode is not as important as the length of the microelectrode, except for the conical geometry. This is why microelectrodes with a conical shape are not desired and thus not used for my electroporation experiments.   The microelectrodes used in the experiments generally have the shape most like that of the thin-insulated geometry. It was noticed though that the more a microelectrode was used the less sharp the edges of the tip became, looking more like the rounded (hemispherical) geometry. This is attributed to the high current density seen at sharp edges and this high current density causing the carbon fiber to etch slowly in the cell bath solution.

The potential drop in solution of the thin-insulating layer geometry microelectrodes did not vary significantly for the different shapes of the microelectrode's tip that were simulated, except for the conical shape. The length, on the other hand, does have a large effect on the potential drop in solution. For the results discussed below the length of the microelectrode simulated was within ±0.1 μm of that measured for the actual microelectrode being used at the time.

5.3.2 Solution Conductivity and Distance between the Cell and Carbon Fiber Microlectrode

As discussed at the beginning of section 4.0, in order for the calculated current to be low enough to insure that the microelectrode will not be damaged, the solution must have a low conductivity. This is why the Iso solution was used as the cell bath solution for the experiments and results discussed below.

The distance between the cell and microelectrode were determined during the experimental process. The way this is done is by looking through the microscope or at real time images with the use of the attached camera of microelectrode tip and the cell to be electroporated, figure 42.
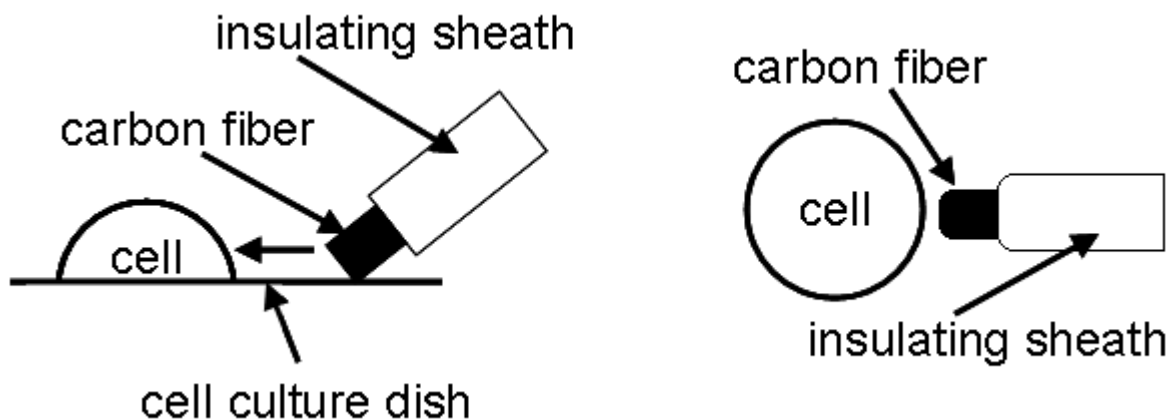
Figure 42. Side view of how the microelectrode approaches the cell (left) and the view through the microscope and camera (right).

The microelectrode tip is moved toward the cell with the micromanipulator until it and the outside of the cell membrane over lap. If the distance between the cell and microelectrode is going to be 0 the microelectrode is left here. If the distance is going to be some positive number the microelectrode is retracted to that distance with the micromanipulator. The desired distance

between the cell and microelectrode is estimated from the micromanipulator display and then measured with the used of the microscope, camera, and computer software.

5.3.3   Current Need for a 1 Volt in Potential

Using the set-up discussed in section 5.0 two different types of simulations was conducted. The first type had the outer boundaries of the carbon fiber set to a potential of 1 volt. The other had the current applied to the back of the microelectrode adjusted until the maximum potential in the simulation was 1 volt, which was on the carbon fiber surface. When the potential at z-axis = 0, y-axis = 0, and x-axis ranging from 1 μm to 100 μm was exported from these two different types of simulations the potential was almost identical for each micrometer of the x-axis. A few examples of these two types of calculations for actual microelectrode lengths can be seen in Appendix D. Computer simulations of microelectrodes of various lengths where there was a 1 volt drop of potential in solution were performed; the results of several of these simulations are plotted in figure 43.
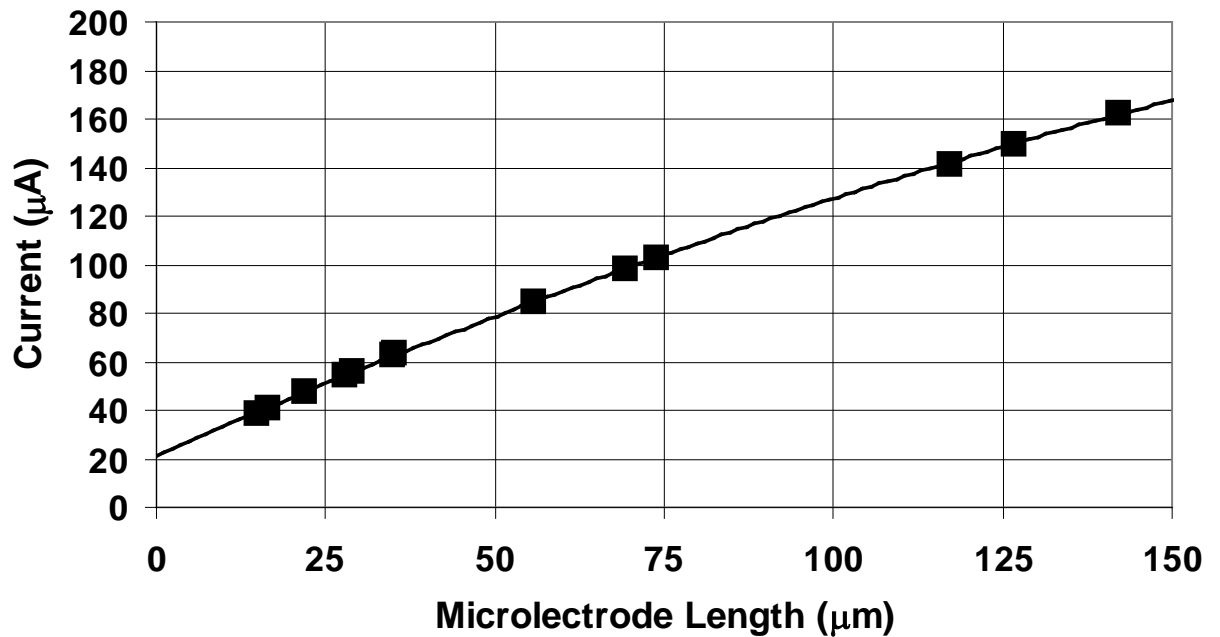
Figure 43. The length of microelectrodes versus the current needed to get a 1 volt drop in potential in a computer simulation.

Below, Equation 11, is the equation generated by plotting the microelectrode length and the current needed to get a 1 volt of potential drop in solution.

$$y = -0.0017x^2 + 1.2263x + 21.391 \qquad (11)$$

The values of the potential along the x-axis, with the y-axis and z-axis both being 0, from these simulations, the type discussed in section 5.0, were exported.

5.3.4   Calculating the Estimated Current

To predict the current needed to electroporate the experiments had the following conditions: 1) the length of the microelectrode being used was measured, 2) the conductivity of the cell bath solution, Iso solution ~ 350 µS/cm, used in the experiments and simulations 3) the current

needed to get a potential drop of 1 volt in solution, equation 11, 4) the values of the potential along the x-axis (y and z = 0) exported from the simulation, 5) the measured distance between the cell and microelectrode, 6) the measured length of the cell , and 7) the transmembrane potential needed to electroporate (250 mV).

Example calculations are shown in Appendix E, an explanation of the values and calculations in the spreadsheet are as follows. The exported potential values from the computer simulations are put into a spreadsheet with distance in meters from the microelectrode tip toward the counter/auxiliary electrode (x-axis) is put in column A and the value of the potential in volts in column B. The potential drop in solution per micrometer of length along the x-axis can be determined by taking the potential at the distance the cell will be from the microelectrode, 5 μm in the examples (B8), and subtract each consecutive value for the potential to get what the potential drop would be across that distance [1 (B9), 2 (B10), 3 μm (B11), etc.] in the solution column E. The distance which the potential is dropping across is in Column C, this would also be the length of the cell along the x-axis. The transmembrane potential needed to electroporate is 0.250 volts in these examples. The 0.250 volts is divided by the potential drop across the distance in solution (column E) and multiplied by the current needed to get a 1 volt drop in solution. This is the estimated current needed to electroporate a cell of a given length along the x-axis (column D).

5.4   RESULTS

The results of experiments using the above calculation with 5 different 10 μm carbon fiber microelectrodes (6.8, 11.5, 14.5, 14.9, and 16.5 μm long) and two distances between the cell and

microelectrode (0 and 5 μm) are that only 5.7% of cells electroporate when 0-85% of the predicted current is applied, 75.0% when 85-100%, and 90.9% when 100+%. The results are shown further broken down into 10% ranges with the number of experiments per range in figure 44.
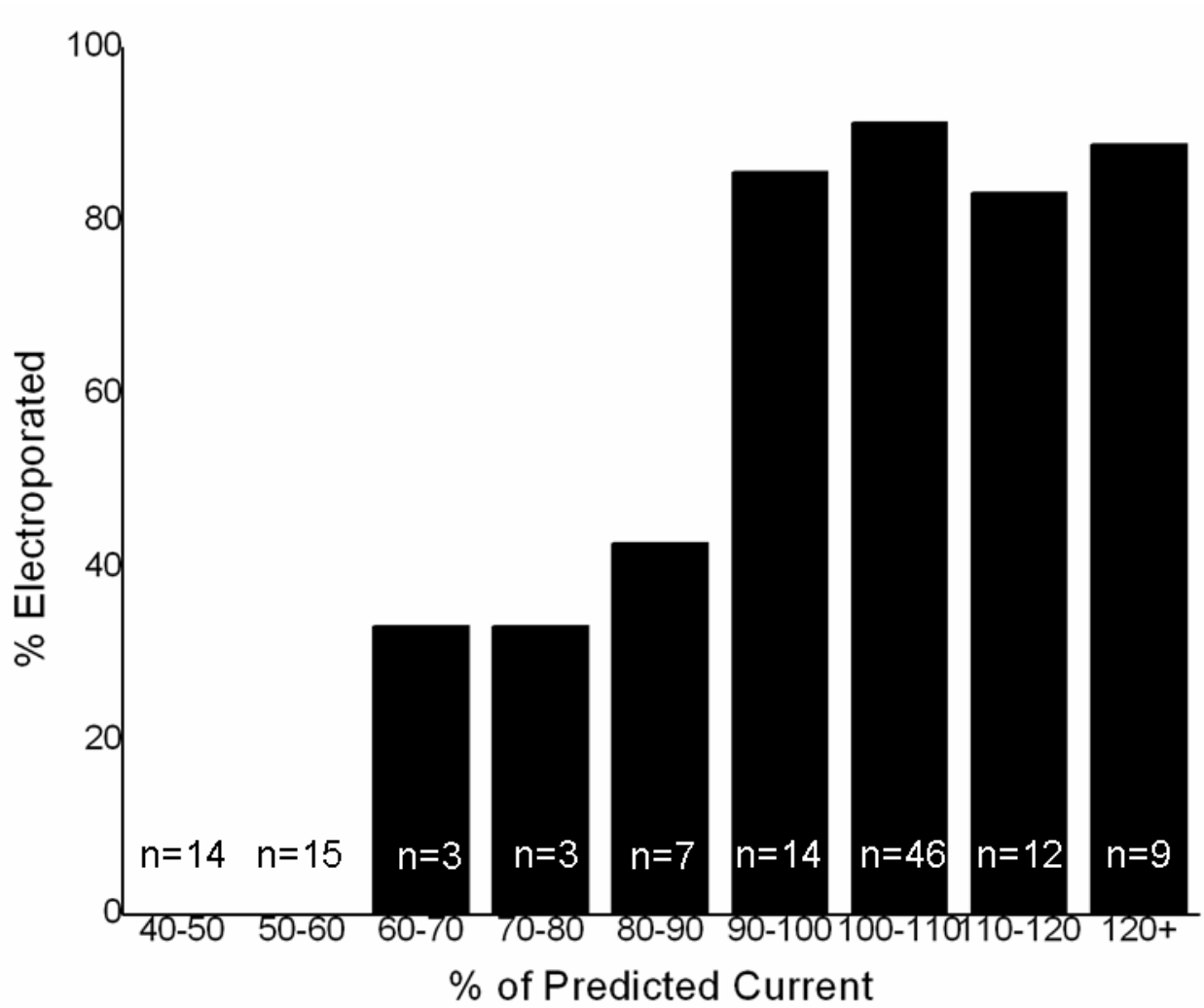
Figure 44. The percent of cells that electroporate versus the percent of the predicted current applied bar graph with n = being the number of experiments conducted in that percent current range.

Unfortunately the cells that were electroporated did not have a high rate a survival, approximately 74% died. Cell viability test were done in the Iso solution versus growth media to insure that exposure to the Iso solution did not cause a large increase in mortality rate. Two cell

dishes that were plated on the same day from the same culture flask were removed from the incubator. One of the cell dishes had the growth media removed, via a plastic transfer pipette, and was washed twice with Iso solution before being filled with Iso solution. After 3 hours, the Iso buffer was replaced with fresh growth media and placed back into the incubator. The other cell dish sat on the bench top next to the Iso solution filled cell dish, had its growth media replaced at the same time and was placed back into the incubator also. The cell culture of the previous day's experiment had what is known as a "live/dead" assay preformed on them. Calcein AM (the "live" dye) and propidium iodide (the "dead" dye) were administered at concentrations of 2.5 μM in growth media and placed back in the incubator for at least 30 minutes. The same microscope, light source, camera and software were used for imaging, but the objective was an Olympus UPlanApo 4X 0.16 NA objective. The excitation and emission filters for calcien were the same as above. For propidium iodide (PI) I used a Triple-band "Pinkel" filter set, Semrock (Rochester, NY) DA/Fl/TA-3X-A, (exciter 1 387 nm, exciter 2 494 nm, exciter 3 575 nm, dichromatic mirror: 394–414 nm, 484–504 nm, 566–586 nm, emitter: 457, 530, 628 nm). This caused the live cells to fluoresce green and the nuclei of the dead cell to fluoresce red, 628 nm emission. Five images were taken of each cell dish and the number of green and red cells were counted in each image with the help of the Simple PCI software. Two other possible factors for cell death were also tested, light exposure and Thioglo-1 exposure. The results of these experiments can be seen below in table 9. In table 9, the meaning of the following terms are as follows; Growth Media (Control) and Iso Solution are explained above; Light Exposure: indicates the cells were exposed to light similar to that during electroporation experiments for 3 hours; Thioglo-1: indicates the dishes had Thioglo-1 added to the cell dish which sat next to the microscope for 3 hours. After all experiments, the solution that was in the

cell dish was replaced with fresh growth medium and was placed back into the incubator overnight

Table 9. The total number of live and dead cells and the % of dead cells for the different conditions tested.

Conditions	Total Number of Cells	% of Dead Cells
Growth Media (Control)	5,237	0.79%
Iso Solution	6,575	1.18%
Light Exposure	3,820	0.90%
Thioglo-1	3,359	1.18%
Light Exposure + Thioglo-1	2,492	0.84%
Iso Solution + Thioglo-1	2,863	2.43%
Iso Solution + Light Exposure	2,880	2.31%
Iso Solution + Light Exposure + Thioglo-1	2,471	2.22%

ANOVA analysis was performed on the results in table 9 and the details of this analysis can be seen in appendix F. The conditions that showed a statistically greater % of dead cells were; Iso Solution + Thioglo-1, Iso Solution + Light Exposure, and Iso Solution + Light Exposure + Thioglo-1. This high death rate could in part be caused by Thioglo-1 reaction with the cell's cytoplasmic glutathione, which is part of the cell's major redox couple leaving the cell more vulnerable to oxidative stress.

APPENDIX A

MICROELECTRODE ETCHING STATISTICS

Table 10. Statistics on carbon fiber microelectrode etching.

Statistics				
NaOH concetnration	n=	Mean Current (μA)	Standard Deviation	Standard Error of Mean
0.1 M	8	-728.125	43.172	15.264
0.075 M	10	-555.000	70.514	22.298
0.05 M	8	-326.250	66.641	23.561

Individual Results: Current (μA)		
0.1 M	0.075 M	0.05 M
-775	-700	-425
-750	-600	-400
-750	-600	-375
-750	-550	-325
-750	-550	-300
-725	-550	-275
-675	-525	-260
-650	-525	-250
	-525	
	-425	

Anova: Single Factor
SUMMARY

Groups	Count	Sum	Average	Variance
0.1 M	8	-5825	-728.125	1863.839
0.075 M	10	-5550	-555	4972.222
0.05 M	8	-2610	-326.25	4441.071

ANOVA

Source of Variation	SS	df	MS	F	P-value	F crit
Between Groups	650774.3	2	325387.1	84.1982	2.62E-11	3.422132
Within Groups	88884.38	23	3864.538			
Total	739658.7	25				

Anova: Single Factor
SUMMARY

Groups	Count	Sum	Average	Variance
0.1 M	8	-5825	-728.125	1863.839
0.075 M	10	-5550	-555	4972.222

ANOVA

Source of Variation	SS	df	MS	F	P-value	F crit
Between Groups	133210.1	1	133210.1	36.87675	1.62E-05	4.493998
Within Groups	57796.88	16	3612.305			
Total	191006.9	17				

Anova: Single Factor
  SUMMARY

Groups	Count	Sum	Average	Variance			
0.075 M	10	-5550	-555	4972.222			
0.05 M	8	-2610	-326.25	4441.071			

  ANOVA

Source of Variation	SS	df	MS	F	P-value	F crit
Between Groups	232562.5	1	232562.5	49.06544	2.97E-06	4.493998
Within Groups	75837.5	16	4739.844			
Total	308400	17				

Anova: Single Factor
  SUMMARY

Groups	Count	Sum	Average	Variance			
0.1 M	8	-5825	-728.125	1863.839			
0.05 M	8	-2610	-326.25	4441.071			

  ANOVA

Source of Variation	SS	df	MS	F	P-value	F crit
Between Groups	646014.1	1	646014.1	204.9241	9.43E-10	4.60011
Within Groups	44134.38	14	3152.455			
Total	690148.4	15				

APPENDIX B

ELECTRIC POTENTIAL IN SOLUTION

Table 11.   Electric Pontential for 10 μm diameter microelectrodes of various lengths for three geometries (cylindrical, conical, and hemispherical) with an infinite and 5 μm insulating plane.

μm away	Infinite Insulating Plane (Cylindrical)							
	5 μm	10 μm	15 μm	25 μm	50 μm	100 μm	500 μm	1,000 μm
0	1.0000	1.0000	1.0000	1.0000	1.0000	1.0000	1.0000	1.0000
1	0.9036	0.9106	0.9145	0.9191	0.9248	0.9298	0.9391	0.9424
2	0.8127	0.8261	0.8337	0.8426	0.8537	0.8635	0.8815	0.8879
3	0.7310	0.7500	0.7608	0.7736	0.7895	0.8034	0.8294	0.8387
4	0.6598	0.6834	0.6969	0.7130	0.7330	0.7507	0.7835	0.7953
5	0.5988	0.6260	0.6417	0.6606	0.6841	0.7049	0.7438	0.7577
6	0.5467	0.5768	0.5942	0.6153	0.6418	0.6653	0.7093	0.7252
7	0.5021	0.5344	0.5532	0.5762	0.6052	0.6310	0.6795	0.6969
8	0.4639	0.4977	0.5177	0.5422	0.5733	0.6010	0.6534	0.6723
9	0.4308	0.4658	0.4867	0.5124	0.5453	0.5747	0.6304	0.6506
10	0.4020	0.4378	0.4594	0.4861	0.5205	0.5514	0.6101	0.6313
11	0.3767	0.4130	0.4352	0.4628	0.4984	0.5305	0.5919	0.6141
12	0.3544	0.3910	0.4135	0.4418	0.4785	0.5118	0.5755	0.5986
13	0.3345	0.3713	0.3941	0.4230	0.4606	0.4948	0.5606	0.5845
14	0.3167	0.3536	0.3766	0.4059	0.4442	0.4794	0.5471	0.5717
15	0.3007	0.3375	0.3607	0.3903	0.4293	0.4653	0.5347	0.5599
16	0.2863	0.3229	0.3461	0.3760	0.4156	0.4522	0.5232	0.5491
17	0.2732	0.3095	0.3328	0.3629	0.4030	0.4402	0.5126	0.5391
18	0.2612	0.2973	0.3205	0.3508	0.3913	0.4290	0.5028	0.5298
19	0.2502	0.2860	0.3092	0.3395	0.3804	0.4186	0.4936	0.5211
20	0.2401	0.2756	0.2987	0.3291	0.3702	0.4089	0.4850	0.5129
21	0.2308	0.2659	0.2889	0.3193	0.3607	0.3998	0.4769	0.5053
22	0.2222	0.2569	0.2798	0.3102	0.3518	0.3912	0.4693	0.4980
23	0.2142	0.2485	0.2713	0.3016	0.3434	0.3832	0.4621	0.4912
24	0.2068	0.2407	0.2633	0.2936	0.3355	0.3755	0.4553	0.4848

μm away	Infinite Insulating Plane (Cylindrical)							
	5 μm	10 μm	15 μm	25 μm	50 μm	100 μm	500 μm	1,000 μm
25	0.1999	0.2333	0.2558	0.2860	0.3280	0.3683	0.4489	0.4787
26	0.1934	0.2264	0.2487	0.2788	0.3209	0.3614	0.4428	0.4729
27	0.1873	0.2199	0.2421	0.2721	0.3141	0.3549	0.4369	0.4673
28	0.1816	0.2138	0.2358	0.2656	0.3077	0.3487	0.4313	0.4620
29	0.1763	0.2080	0.2298	0.2595	0.3017	0.3427	0.4260	0.4570
30	0.1712	0.2025	0.2241	0.2538	0.2958	0.3371	0.4209	0.4521
31	0.1664	0.1974	0.2188	0.2482	0.2903	0.3316	0.4160	0.4475
32	0.1619	0.1924	0.2137	0.2430	0.2850	0.3264	0.4113	0.4430
33	0.1576	0.1878	0.2088	0.2379	0.2799	0.3214	0.4068	0.4387
34	0.1536	0.1833	0.2041	0.2331	0.2750	0.3166	0.4025	0.4346
35	0.1498	0.1791	0.1997	0.2285	0.2703	0.3120	0.3983	0.4306
36	0.1461	0.1750	0.1955	0.2241	0.2658	0.3076	0.3942	0.4268
37	0.1426	0.1712	0.1914	0.2199	0.2615	0.3033	0.3903	0.4231
38	0.1393	0.1675	0.1875	0.2158	0.2573	0.2992	0.3866	0.4195
39	0.1361	0.1640	0.1838	0.2119	0.2533	0.2952	0.3829	0.4160
40	0.1331	0.1606	0.1803	0.2082	0.2494	0.2913	0.3794	0.4127
41	0.1302	0.1573	0.1768	0.2045	0.2457	0.2876	0.3760	0.4094
42	0.1274	0.1542	0.1735	0.2011	0.2421	0.2840	0.3726	0.4062
43	0.1248	0.1512	0.1704	0.1977	0.2386	0.2805	0.3694	0.4032
44	0.1222	0.1484	0.1673	0.1945	0.2352	0.2771	0.3663	0.4002
45	0.1198	0.1456	0.1644	0.1913	0.2319	0.2738	0.3633	0.3973
46	0.1174	0.1429	0.1615	0.1883	0.2287	0.2706	0.3603	0.3945
47	0.1152	0.1404	0.1588	0.1854	0.2257	0.2675	0.3574	0.3917
48	0.1130	0.1379	0.1561	0.1825	0.2227	0.2645	0.3546	0.3891
49	0.1109	0.1355	0.1536	0.1798	0.2198	0.2616	0.3519	0.3865
50	0.1089	0.1332	0.1511	0.1771	0.2170	0.2587	0.3492	0.3839
51	0.1070	0.1310	0.1487	0.1746	0.2142	0.2559	0.3466	0.3814
52	0.1051	0.1288	0.1464	0.1721	0.2116	0.2532	0.3441	0.3790
53	0.1033	0.1268	0.1442	0.1696	0.2090	0.2506	0.3416	0.3767
54	0.1015	0.1247	0.1420	0.1673	0.2065	0.2480	0.3392	0.3744
55	0.0998	0.1228	0.1399	0.1650	0.2040	0.2455	0.3369	0.3721
56	0.0982	0.1209	0.1378	0.1628	0.2016	0.2431	0.3345	0.3699
57	0.0966	0.1191	0.1358	0.1606	0.1993	0.2407	0.3323	0.3677
58	0.0951	0.1173	0.1339	0.1585	0.1970	0.2384	0.3301	0.3656
59	0.0936	0.1156	0.1320	0.1565	0.1948	0.2361	0.3279	0.3636
60	0.0922	0.1139	0.1302	0.1545	0.1927	0.2339	0.3258	0.3616
61	0.0908	0.1123	0.1285	0.1526	0.1906	0.2317	0.3237	0.3596
62	0.0894	0.1107	0.1267	0.1507	0.1885	0.2296	0.3217	0.3576
63	0.0881	0.1092	0.1251	0.1488	0.1865	0.2275	0.3197	0.3557
64	0.0869	0.1077	0.1234	0.1470	0.1846	0.2255	0.3178	0.3539
65	0.0856	0.1062	0.1219	0.1453	0.1826	0.2235	0.3158	0.3520
66	0.0844	0.1048	0.1203	0.1436	0.1808	0.2215	0.3140	0.3502
67	0.0832	0.1034	0.1188	0.1419	0.1789	0.2196	0.3121	0.3485
68	0.0821	0.1021	0.1173	0.1403	0.1771	0.2177	0.3103	0.3467
69	0.0810	0.1008	0.1159	0.1387	0.1754	0.2159	0.3085	0.3450

μm away	Infinite Insulating Plane (Cylindrical)							
	5 μm	10 μm	15 μm	25 μm	50 μm	100 μm	500 μm	1,000 μm
70	0.0799	0.0995	0.1145	0.1372	0.1737	0.2141	0.3068	0.3434
71	0.0789	0.0983	0.1132	0.1357	0.1720	0.2123	0.3051	0.3417
72	0.0779	0.0971	0.1118	0.1342	0.1704	0.2106	0.3034	0.3401
73	0.0769	0.0959	0.1105	0.1327	0.1687	0.2089	0.3018	0.3385
74	0.0759	0.0948	0.1093	0.1313	0.1672	0.2072	0.3001	0.3370
75	0.0750	0.0936	0.1080	0.1299	0.1656	0.2056	0.2985	0.3354
76	0.0740	0.0925	0.1068	0.1286	0.1641	0.2040	0.2970	0.3339
77	0.0731	0.0915	0.1056	0.1273	0.1626	0.2024	0.2954	0.3324
78	0.0723	0.0904	0.1045	0.1260	0.1612	0.2009	0.2939	0.3310
79	0.0714	0.0894	0.1033	0.1247	0.1597	0.1994	0.2924	0.3295
80	0.0706	0.0884	0.1022	0.1234	0.1583	0.1979	0.2909	0.3281
81	0.0697	0.0874	0.1012	0.1222	0.1570	0.1964	0.2895	0.3267
82	0.0689	0.0865	0.1001	0.1210	0.1556	0.1950	0.2880	0.3253
83	0.0682	0.0855	0.0991	0.1199	0.1543	0.1935	0.2866	0.3240
84	0.0674	0.0846	0.0980	0.1187	0.1530	0.1921	0.2852	0.3226
85	0.0667	0.0837	0.0970	0.1176	0.1517	0.1908	0.2839	0.3213
86	0.0659	0.0829	0.0961	0.1165	0.1505	0.1894	0.2825	0.3200
87	0.0652	0.0820	0.0951	0.1154	0.1492	0.1881	0.2812	0.3187
88	0.0645	0.0812	0.0942	0.1143	0.1480	0.1868	0.2799	0.3175
89	0.0638	0.0804	0.0933	0.1133	0.1468	0.1855	0.2786	0.3162
90	0.0632	0.0795	0.0924	0.1123	0.1456	0.1842	0.2773	0.3150
91	0.0625	0.0788	0.0915	0.1113	0.1445	0.1830	0.2760	0.3138
92	0.0619	0.0780	0.0906	0.1103	0.1434	0.1818	0.2748	0.3126
93	0.0613	0.0772	0.0898	0.1093	0.1422	0.1805	0.2736	0.3114
94	0.0606	0.0765	0.0889	0.1084	0.1412	0.1794	0.2724	0.3102
95	0.0600	0.0758	0.0881	0.1074	0.1401	0.1782	0.2712	0.3091
96	0.0594	0.0750	0.0873	0.1065	0.1390	0.1770	0.2700	0.3080
97	0.0589	0.0743	0.0865	0.1056	0.1380	0.1759	0.2688	0.3068
98	0.0583	0.0737	0.0858	0.1047	0.1369	0.1748	0.2677	0.3057
99	0.0577	0.0730	0.0850	0.1039	0.1359	0.1737	0.2666	0.3046
100	0.0572	0.0723	0.0843	0.1030	0.1349	0.1726	0.2655	0.3036

μm away	5 μm Insulating Plane (Cylindrical)							
	5 μm	10 μm	15 μm	25 μm	50 μm	100 μm	500 μm	1,000 μm
0	1.0000	1.0000	1.0000	1.0000	1.0000	1.0000	1.0000	1.0000
1	0.8915	0.9001	0.9052	0.9113	0.9187	0.9251	0.9369	0.9411
2	0.7895	0.8060	0.8158	0.8276	0.8419	0.8543	0.8772	0.8853
3	0.6983	0.7216	0.7354	0.7521	0.7726	0.7903	0.8233	0.8349
4	0.6195	0.6481	0.6652	0.6860	0.7117	0.7341	0.7758	0.7906
5	0.5526	0.5852	0.6049	0.6290	0.6591	0.6854	0.7346	0.7521
6	0.4961	0.5316	0.5533	0.5801	0.6137	0.6433	0.6990	0.7189
7	0.4485	0.4860	0.5091	0.5380	0.5745	0.6069	0.6681	0.6900
8	0.4080	0.4469	0.4711	0.5015	0.5404	0.5751	0.6411	0.6647
9	0.3735	0.4132	0.4382	0.4698	0.5105	0.5472	0.6174	0.6425
10	0.3439	0.3839	0.4094	0.4419	0.4842	0.5225	0.5963	0.6228
11	0.3182	0.3583	0.3841	0.4173	0.4608	0.5005	0.5775	0.6052
12	0.2958	0.3358	0.3618	0.3953	0.4398	0.4808	0.5605	0.5894
13	0.2761	0.3159	0.3418	0.3757	0.4209	0.4629	0.5452	0.5750
14	0.2588	0.2981	0.3240	0.3580	0.4038	0.4467	0.5312	0.5619
15	0.2434	0.2821	0.3079	0.3420	0.3883	0.4318	0.5184	0.5499
16	0.2296	0.2678	0.2933	0.3274	0.3740	0.4182	0.5065	0.5388
17	0.2172	0.2548	0.2801	0.3140	0.3609	0.4057	0.4956	0.5286
18	0.2060	0.2429	0.2680	0.3018	0.3488	0.3940	0.4854	0.5191
19	0.1959	0.2321	0.2569	0.2905	0.3376	0.3832	0.4760	0.5102
20	0.1867	0.2222	0.2467	0.2801	0.3272	0.3731	0.4671	0.5019
21	0.1783	0.2132	0.2373	0.2704	0.3174	0.3637	0.4588	0.4941
22	0.1706	0.2048	0.2286	0.2614	0.3083	0.3548	0.4509	0.4867
23	0.1635	0.1970	0.2205	0.2530	0.2998	0.3464	0.4435	0.4797
24	0.1570	0.1898	0.2129	0.2451	0.2918	0.3386	0.4365	0.4732
25	0.1509	0.1831	0.2059	0.2378	0.2843	0.3311	0.4299	0.4669
26	0.1453	0.1769	0.1993	0.2308	0.2772	0.3241	0.4236	0.4610
27	0.1401	0.1710	0.1931	0.2243	0.2704	0.3174	0.4176	0.4553
28	0.1352	0.1656	0.1873	0.2182	0.2641	0.3111	0.4119	0.4499
29	0.1307	0.1605	0.1819	0.2124	0.2580	0.3050	0.4064	0.4448
30	0.1264	0.1556	0.1767	0.2069	0.2522	0.2992	0.4011	0.4398
31	0.1225	0.1511	0.1719	0.2017	0.2468	0.2937	0.3961	0.4351
32	0.1187	0.1468	0.1673	0.1968	0.2416	0.2885	0.3913	0.4306
33	0.1152	0.1428	0.1629	0.1921	0.2366	0.2834	0.3867	0.4262
34	0.1119	0.1390	0.1588	0.1876	0.2318	0.2786	0.3822	0.4220
35	0.1087	0.1353	0.1549	0.1834	0.2273	0.2739	0.3779	0.4179
36	0.1058	0.1319	0.1512	0.1793	0.2229	0.2695	0.3738	0.4140
37	0.1029	0.1286	0.1476	0.1755	0.2187	0.2652	0.3698	0.4102
38	0.1003	0.1255	0.1442	0.1718	0.2147	0.2611	0.3659	0.4066
39	0.0978	0.1226	0.1410	0.1682	0.2108	0.2571	0.3622	0.4031
40	0.0953	0.1197	0.1379	0.1648	0.2071	0.2532	0.3586	0.3996
41	0.0931	0.1170	0.1350	0.1616	0.2036	0.2495	0.3551	0.3963
42	0.0909	0.1145	0.1321	0.1584	0.2001	0.2459	0.3517	0.3931

μm away	5 μm Insulating Plane (Cylindrical)							
	5 μm	10 μm	15 μm	25 μm	50 μm	100 μm	500 μm	1,000 μm
43	0.0888	0.1120	0.1294	0.1554	0.1968	0.2425	0.3484	0.3900
44	0.0868	0.1096	0.1268	0.1525	0.1936	0.2391	0.3452	0.3870
45	0.0849	0.1074	0.1244	0.1498	0.1905	0.2359	0.3421	0.3840
46	0.0831	0.1052	0.1220	0.1471	0.1875	0.2327	0.3391	0.3811
47	0.0813	0.1031	0.1197	0.1445	0.1847	0.2297	0.3361	0.3784
48	0.0797	0.1011	0.1174	0.1420	0.1819	0.2267	0.3333	0.3756
49	0.0781	0.0992	0.1153	0.1396	0.1792	0.2239	0.3305	0.3730
50	0.0765	0.0974	0.1133	0.1373	0.1766	0.2211	0.3278	0.3704
51	0.0751	0.0956	0.1113	0.1351	0.1740	0.2184	0.3251	0.3679
52	0.0736	0.0939	0.1094	0.1329	0.1716	0.2158	0.3226	0.3655
53	0.0723	0.0922	0.1075	0.1308	0.1692	0.2132	0.3201	0.3631
54	0.0710	0.0906	0.1057	0.1288	0.1669	0.2107	0.3176	0.3607
55	0.0697	0.0891	0.1040	0.1269	0.1646	0.2083	0.3152	0.3584
56	0.0685	0.0876	0.1024	0.1250	0.1625	0.2059	0.3129	0.3562
57	0.0673	0.0862	0.1007	0.1231	0.1603	0.2036	0.3106	0.3540
58	0.0661	0.0848	0.0992	0.1213	0.1583	0.2014	0.3083	0.3519
59	0.0650	0.0834	0.0977	0.1196	0.1563	0.1992	0.3061	0.3498
60	0.0640	0.0821	0.0962	0.1179	0.1543	0.1971	0.3040	0.3477
61	0.0629	0.0809	0.0948	0.1163	0.1524	0.1950	0.3019	0.3457
62	0.0620	0.0797	0.0934	0.1147	0.1506	0.1930	0.2998	0.3437
63	0.0610	0.0785	0.0921	0.1132	0.1488	0.1910	0.2978	0.3418
64	0.0601	0.0773	0.0908	0.1117	0.1470	0.1891	0.2958	0.3399
65	0.0591	0.0762	0.0895	0.1102	0.1453	0.1872	0.2939	0.3381
66	0.0583	0.0751	0.0883	0.1088	0.1437	0.1853	0.2920	0.3362
67	0.0574	0.0741	0.0871	0.1074	0.1420	0.1835	0.2902	0.3345
68	0.0566	0.0731	0.0860	0.1061	0.1404	0.1818	0.2883	0.3327
69	0.0558	0.0721	0.0848	0.1048	0.1389	0.1800	0.2865	0.3310
70	0.0550	0.0711	0.0837	0.1035	0.1374	0.1783	0.2848	0.3293
71	0.0543	0.0702	0.0827	0.1022	0.1359	0.1767	0.2830	0.3276
72	0.0535	0.0693	0.0816	0.1010	0.1345	0.1751	0.2814	0.3260
73	0.0528	0.0684	0.0806	0.0998	0.1330	0.1735	0.2797	0.3244
74	0.0521	0.0675	0.0796	0.0987	0.1317	0.1719	0.2780	0.3228
75	0.0514	0.0667	0.0787	0.0976	0.1303	0.1704	0.2764	0.3213
76	0.0508	0.0658	0.0777	0.0965	0.1290	0.1689	0.2749	0.3197
77	0.0501	0.0650	0.0768	0.0954	0.1277	0.1674	0.2733	0.3182
78	0.0495	0.0643	0.0759	0.0943	0.1264	0.1660	0.2718	0.3167
79	0.0489	0.0635	0.0751	0.0933	0.1252	0.1646	0.2703	0.3153
80	0.0483	0.0628	0.0742	0.0923	0.1240	0.1632	0.2688	0.3139
81	0.0477	0.0620	0.0734	0.0913	0.1228	0.1618	0.2673	0.3125
82	0.0472	0.0613	0.0726	0.0904	0.1216	0.1605	0.2659	0.3111
83	0.0466	0.0606	0.0718	0.0894	0.1205	0.1592	0.2645	0.3097
84	0.0461	0.0600	0.0710	0.0885	0.1194	0.1579	0.2631	0.3083
85	0.0455	0.0593	0.0702	0.0876	0.1183	0.1567	0.2617	0.3070
86	0.0450	0.0587	0.0695	0.0867	0.1172	0.1554	0.2604	0.3057
87	0.0445	0.0580	0.0688	0.0859	0.1162	0.1542	0.2590	0.3044

μm away	5 μm Insulating Plane (Cylindrical)							
	5 μm	10 μm	15 μm	25 μm	50 μm	100 μm	500 μm	1,000 μm
88	0.0440	0.0574	0.0681	0.0850	0.1151	0.1530	0.2577	0.3031
89	0.0436	0.0568	0.0674	0.0842	0.1141	0.1518	0.2564	0.3019
90	0.0431	0.0562	0.0667	0.0834	0.1131	0.1507	0.2552	0.3007
91	0.0426	0.0556	0.0660	0.0826	0.1121	0.1496	0.2539	0.2994
92	0.0422	0.0551	0.0654	0.0818	0.1112	0.1484	0.2527	0.2982
93	0.0417	0.0545	0.0647	0.0811	0.1102	0.1473	0.2514	0.2970
94	0.0413	0.0540	0.0641	0.0803	0.1093	0.1463	0.2502	0.2959
95	0.0409	0.0535	0.0635	0.0796	0.1084	0.1452	0.2490	0.2947
96	0.0405	0.0529	0.0629	0.0789	0.1075	0.1442	0.2479	0.2936
97	0.0401	0.0524	0.0623	0.0782	0.1066	0.1431	0.2467	0.2924
98	0.0397	0.0519	0.0617	0.0775	0.1058	0.1421	0.2456	0.2913
99	0.0393	0.0514	0.0612	0.0768	0.1049	0.1411	0.2445	0.2902
100	0.0389	0.0510	0.0606	0.0761	0.1041	0.1402	0.2433	0.2891

	Infinite Insulating Plane (Hemispherical)							
μm away	5 μm	10 μm	15 μm	25 μm	50 μm	100 μm	500 μm	1,000 μm
0	1.0000	1.0000	1.0000	1.0000	1.0000	1.0000	1.0000	1.0000
1	0.9818	0.9843	0.9859	0.9882	0.9921	0.8845	0.8999	0.9054
2	0.9640	0.9690	0.9721	0.9766	0.9844	0.8012	0.8277	0.8371
3	0.9467	0.9541	0.9586	0.9652	0.9768	0.7378	0.7727	0.7852
4	0.9299	0.9396	0.9455	0.9541	0.9693	0.6876	0.7291	0.7439
5	0.9136	0.9255	0.9327	0.9432	0.9619	0.6465	0.6935	0.7102
6	0.8977	0.9117	0.9202	0.9326	0.9546	0.6121	0.6636	0.6820
7	0.8824	0.8984	0.9081	0.9222	0.9475	0.5827	0.6380	0.6578
8	0.8675	0.8855	0.8963	0.9121	0.9404	0.5573	0.6159	0.6368
9	0.8531	0.8729	0.8848	0.9022	0.9335	0.5349	0.5964	0.6184
10	0.8392	0.8608	0.8737	0.8926	0.9267	0.5151	0.5790	0.6020
11	0.8257	0.8490	0.8629	0.8832	0.9200	0.4972	0.5634	0.5872
12	0.8128	0.8376	0.8524	0.8740	0.9135	0.4811	0.5494	0.5739
13	0.8003	0.8266	0.8423	0.8651	0.9070	0.4665	0.5365	0.5617
14	0.7883	0.8160	0.8325	0.8564	0.9007	0.4531	0.5247	0.5506
15	0.7768	0.8058	0.8230	0.8480	0.8944	0.4407	0.5139	0.5403
16	0.7657	0.7960	0.8139	0.8398	0.8883	0.4293	0.5038	0.5308
17	0.7550	0.7866	0.8051	0.8319	0.8824	0.4187	0.4944	0.5219
18	0.7444	0.7773	0.7966	0.8242	0.8765	0.4088	0.4857	0.5136
19	0.7341	0.7681	0.7882	0.8168	0.8707	0.3995	0.4775	0.5059
20	0.7240	0.7592	0.7799	0.8095	0.8651	0.3908	0.4698	0.4986
21	0.7141	0.7504	0.7718	0.8024	0.8596	0.3826	0.4625	0.4917
22	0.7045	0.7418	0.7639	0.7955	0.8542	0.3749	0.4556	0.4851
23	0.6950	0.7334	0.7561	0.7886	0.8489	0.3676	0.4491	0.4790
24	0.6858	0.7252	0.7485	0.7818	0.8437	0.3606	0.4429	0.4731
25	0.6769	0.7172	0.7411	0.7752	0.8387	0.3541	0.4370	0.4675
26	0.6682	0.7094	0.7338	0.7687	0.8338	0.3478	0.4314	0.4622
27	0.6597	0.7017	0.7266	0.7623	0.8289	0.3418	0.4261	0.4571
28	0.6514	0.6943	0.7197	0.7560	0.8242	0.3361	0.4209	0.4522
29	0.6434	0.6870	0.7128	0.7499	0.8196	0.3306	0.4160	0.4476
30	0.6355	0.6799	0.7062	0.7438	0.8150	0.3254	0.4113	0.4431
31	0.6280	0.6730	0.6997	0.7379	0.8104	0.3204	0.4068	0.4388
32	0.6206	0.6663	0.6933	0.7321	0.8059	0.3156	0.4024	0.4346
33	0.6135	0.6598	0.6871	0.7264	0.8014	0.3109	0.3982	0.4306
34	0.6065	0.6535	0.6811	0.7209	0.7970	0.3065	0.3941	0.4268
35	0.5996	0.6472	0.6752	0.7154	0.7927	0.3022	0.3902	0.4230
36	0.5928	0.6411	0.6695	0.7101	0.7884	0.2980	0.3864	0.4195
37	0.5862	0.6351	0.6639	0.7049	0.7841	0.2940	0.3828	0.4160
38	0.5797	0.6291	0.6583	0.6998	0.7799	0.2901	0.3792	0.4126
39	0.5733	0.6233	0.6529	0.6948	0.7758	0.2864	0.3758	0.4093
40	0.5671	0.6176	0.6475	0.6900	0.7717	0.2828	0.3725	0.4062
41	0.5610	0.6120	0.6422	0.6852	0.7677	0.2793	0.3692	0.4031
42	0.5550	0.6065	0.6370	0.6805	0.7637	0.2759	0.3661	0.4001

μm away	Infinite Insulating Plane (Hemispherical)							
	5 μm	10 μm	15 μm	25 μm	50 μm	100 μm	500 μm	1,000 μm
43	0.5491	0.6011	0.6319	0.6758	0.7598	0.2726	0.3631	0.3972
44	0.5434	0.5958	0.6269	0.6712	0.7559	0.2694	0.3601	0.3944
45	0.5378	0.5906	0.6220	0.6667	0.7521	0.2663	0.3572	0.3916
46	0.5323	0.5855	0.6171	0.6622	0.7484	0.2633	0.3544	0.3890
47	0.5270	0.5805	0.6124	0.6578	0.7447	0.2603	0.3517	0.3864
48	0.5218	0.5756	0.6077	0.6535	0.7410	0.2575	0.3490	0.3838
49	0.5167	0.5709	0.6031	0.6493	0.7374	0.2547	0.3464	0.3813
50	0.5117	0.5662	0.5986	0.6451	0.7339	0.2520	0.3439	0.3789
51	0.5068	0.5616	0.5942	0.6409	0.7304	0.2493	0.3414	0.3766
52	0.5019	0.5571	0.5899	0.6369	0.7270	0.2468	0.3390	0.3742
53	0.4972	0.5527	0.5857	0.6329	0.7236	0.2443	0.3366	0.3720
54	0.4925	0.5483	0.5815	0.6290	0.7203	0.2418	0.3343	0.3698
55	0.4879	0.5440	0.5774	0.6251	0.7170	0.2394	0.3320	0.3676
56	0.4834	0.5398	0.5734	0.6213	0.7138	0.2371	0.3298	0.3655
57	0.4790	0.5356	0.5694	0.6176	0.7107	0.2348	0.3277	0.3634
58	0.4746	0.5315	0.5655	0.6139	0.7075	0.2326	0.3256	0.3614
59	0.4703	0.5274	0.5617	0.6103	0.7044	0.2304	0.3235	0.3594
60	0.4661	0.5234	0.5579	0.6068	0.7014	0.2283	0.3215	0.3575
61	0.4620	0.5195	0.5541	0.6033	0.6983	0.2262	0.3195	0.3556
62	0.4579	0.5157	0.5504	0.5998	0.6953	0.2242	0.3175	0.3537
63	0.4540	0.5119	0.5467	0.5964	0.6923	0.2222	0.3156	0.3519
64	0.4501	0.5082	0.5432	0.5931	0.6894	0.2202	0.3137	0.3501
65	0.4463	0.5045	0.5396	0.5897	0.6864	0.2183	0.3119	0.3483
66	0.4426	0.5009	0.5361	0.5865	0.6835	0.2165	0.3101	0.3466
67	0.4389	0.4974	0.5327	0.5832	0.6807	0.2146	0.3083	0.3449
68	0.4353	0.4940	0.5293	0.5800	0.6778	0.2128	0.3065	0.3432
69	0.4317	0.4905	0.5260	0.5769	0.6750	0.2111	0.3048	0.3416
70	0.4282	0.4872	0.5227	0.5737	0.6723	0.2093	0.3031	0.3400
71	0.4247	0.4838	0.5195	0.5707	0.6695	0.2076	0.3015	0.3384
72	0.4213	0.4806	0.5164	0.5676	0.6668	0.2060	0.2999	0.3368
73	0.4179	0.4773	0.5133	0.5646	0.6641	0.2043	0.2983	0.3353
74	0.4146	0.4741	0.5102	0.5617	0.6615	0.2027	0.2967	0.3338
75	0.4113	0.4710	0.5071	0.5587	0.6589	0.2012	0.2951	0.3323
76	0.4081	0.4678	0.5041	0.5559	0.6563	0.1996	0.2936	0.3308
77	0.4049	0.4648	0.5012	0.5530	0.6537	0.1981	0.2921	0.3294
78	0.4018	0.4617	0.4982	0.5502	0.6512	0.1966	0.2906	0.3280
79	0.3987	0.4588	0.4953	0.5475	0.6487	0.1951	0.2892	0.3266
80	0.3957	0.4558	0.4925	0.5448	0.6462	0.1937	0.2878	0.3252
81	0.3928	0.4529	0.4896	0.5421	0.6438	0.1923	0.2863	0.3238
82	0.3898	0.4500	0.4868	0.5395	0.6414	0.1909	0.2850	0.3225
83	0.3870	0.4472	0.4841	0.5368	0.6390	0.1895	0.2836	0.3212
84	0.3842	0.4444	0.4814	0.5343	0.6366	0.1882	0.2822	0.3199
85	0.3814	0.4417	0.4787	0.5317	0.6343	0.1868	0.2809	0.3186
86	0.3787	0.4390	0.4760	0.5291	0.6320	0.1855	0.2796	0.3173
87	0.3760	0.4364	0.4734	0.5266	0.6297	0.1843	0.2783	0.3161

100

	Infinite Insulating Plane (Hemispherical)							
μm away	5 μm	10 μm	15 μm	25 μm	50 μm	100 μm	500 μm	1,000 μm
88	0.3733	0.4338	0.4708	0.5241	0.6275	0.1830	0.2770	0.3149
89	0.3706	0.4312	0.4683	0.5217	0.6252	0.1817	0.2758	0.3136
90	0.3680	0.4286	0.4658	0.5193	0.6230	0.1805	0.2745	0.3124
91	0.3655	0.4261	0.4633	0.5169	0.6208	0.1793	0.2733	0.3113
92	0.3629	0.4236	0.4609	0.5145	0.6186	0.1781	0.2721	0.3101
93	0.3604	0.4211	0.4584	0.5121	0.6165	0.1769	0.2709	0.3090
94	0.3580	0.4186	0.4561	0.5098	0.6143	0.1758	0.2697	0.3078
95	0.3555	0.4162	0.4537	0.5075	0.6122	0.1747	0.2686	0.3067
96	0.3531	0.4138	0.4514	0.5052	0.6101	0.1735	0.2674	0.3056
97	0.3507	0.4115	0.4490	0.5030	0.6080	0.1724	0.2663	0.3045
98	0.3484	0.4091	0.4468	0.5008	0.6059	0.1713	0.2652	0.3034
99	0.3461	0.4068	0.4445	0.4986	0.6038	0.1703	0.2641	0.3023
100	0.3438	0.4045	0.4423	0.4964	0.6018	0.1692	0.2630	0.3013

μm away	5 μm Insulating Plane (Hemispherical)							
	5 μm	10 μm	15 μm	25 μm	50 μm	100 μm	500 μm	1,000 μm
0	1.0000	1.0000	1.0000	1.0000	1.0000	1.0000	1.0000	1.0000
1	0.8138	0.8323	0.8420	0.8531	0.8660	0.8768	0.8964	0.9032
2	0.6815	0.7124	0.7288	0.7476	0.7695	0.7880	0.8216	0.8334
3	0.5832	0.6224	0.6434	0.6677	0.6963	0.7205	0.7646	0.7802
4	0.5076	0.5522	0.5766	0.6048	0.6384	0.6670	0.7195	0.7381
5	0.4479	0.4961	0.5227	0.5538	0.5912	0.6233	0.6826	0.7036
6	0.3997	0.4501	0.4782	0.5115	0.5519	0.5868	0.6516	0.6747
7	0.3602	0.4118	0.4409	0.4758	0.5185	0.5557	0.6252	0.6500
8	0.3272	0.3793	0.4091	0.4451	0.4896	0.5287	0.6023	0.6285
9	0.2994	0.3515	0.3817	0.4185	0.4644	0.5051	0.5821	0.6097
10	0.2756	0.3274	0.3578	0.3951	0.4421	0.4841	0.5642	0.5929
11	0.2552	0.3063	0.3367	0.3743	0.4222	0.4654	0.5481	0.5778
12	0.2373	0.2878	0.3180	0.3558	0.4044	0.4484	0.5335	0.5642
13	0.2217	0.2713	0.3013	0.3391	0.3882	0.4331	0.5202	0.5518
14	0.2079	0.2565	0.2863	0.3240	0.3734	0.4190	0.5081	0.5404
15	0.1957	0.2433	0.2727	0.3103	0.3600	0.4061	0.4968	0.5299
16	0.1847	0.2313	0.2603	0.2977	0.3475	0.3942	0.4865	0.5201
17	0.1749	0.2205	0.2491	0.2862	0.3361	0.3831	0.4768	0.5111
18	0.1660	0.2105	0.2388	0.2756	0.3255	0.3728	0.4678	0.5026
19	0.1579	0.2015	0.2293	0.2657	0.3156	0.3632	0.4593	0.4947
20	0.1506	0.1932	0.2205	0.2566	0.3064	0.3542	0.4514	0.4872
21	0.1439	0.1855	0.2124	0.2481	0.2977	0.3458	0.4439	0.4802
22	0.1377	0.1784	0.2049	0.2402	0.2896	0.3378	0.4368	0.4735
23	0.1321	0.1718	0.1979	0.2328	0.2820	0.3303	0.4301	0.4672
24	0.1268	0.1657	0.1913	0.2259	0.2748	0.3232	0.4237	0.4612
25	0.1220	0.1600	0.1852	0.2194	0.2680	0.3164	0.4177	0.4555
26	0.1175	0.1547	0.1795	0.2132	0.2616	0.3100	0.4119	0.4501
27	0.1133	0.1497	0.1741	0.2074	0.2555	0.3039	0.4064	0.4449
28	0.1094	0.1451	0.1690	0.2019	0.2497	0.2981	0.4011	0.4399
29	0.1058	0.1407	0.1642	0.1968	0.2442	0.2926	0.3961	0.4352
30	0.1024	0.1366	0.1597	0.1918	0.2390	0.2873	0.3912	0.4306
31	0.0992	0.1327	0.1554	0.1872	0.2340	0.2822	0.3866	0.4262
32	0.0962	0.1290	0.1514	0.1827	0.2292	0.2773	0.3821	0.4220
33	0.0933	0.1255	0.1476	0.1785	0.2247	0.2727	0.3778	0.4179
34	0.0907	0.1222	0.1439	0.1745	0.2203	0.2682	0.3736	0.4140
35	0.0882	0.1191	0.1404	0.1706	0.2161	0.2639	0.3696	0.4102
36	0.0858	0.1161	0.1371	0.1670	0.2121	0.2597	0.3657	0.4065
37	0.0835	0.1133	0.1340	0.1635	0.2082	0.2558	0.3620	0.4030
38	0.0814	0.1106	0.1310	0.1601	0.2045	0.2519	0.3584	0.3996
39	0.0793	0.1080	0.1281	0.1569	0.2010	0.2482	0.3549	0.3963
40	0.0774	0.1056	0.1254	0.1538	0.1975	0.2446	0.3515	0.3930
41	0.0755	0.1033	0.1228	0.1508	0.1942	0.2411	0.3482	0.3899
42	0.0738	0.1010	0.1202	0.1480	0.1910	0.2378	0.3450	0.3869

μm away	5 μm Insulating Plane (Hemispherical)							
	5 μm	10 μm	15 μm	25 μm	50 μm	100 μm	500 μm	1,000 μm
43	0.0721	0.0989	0.1178	0.1452	0.1879	0.2345	0.3418	0.3839
44	0.0705	0.0968	0.1155	0.1426	0.1850	0.2314	0.3388	0.3810
45	0.0690	0.0949	0.1133	0.1401	0.1821	0.2283	0.3359	0.3782
46	0.0675	0.0930	0.1111	0.1376	0.1793	0.2254	0.3330	0.3755
47	0.0661	0.0912	0.1091	0.1353	0.1766	0.2225	0.3302	0.3729
48	0.0647	0.0894	0.1071	0.1330	0.1740	0.2197	0.3275	0.3703
49	0.0634	0.0878	0.1052	0.1308	0.1715	0.2170	0.3249	0.3678
50	0.0622	0.0862	0.1034	0.1287	0.1691	0.2144	0.3223	0.3653
51	0.0610	0.0846	0.1016	0.1266	0.1667	0.2118	0.3198	0.3629
52	0.0599	0.0831	0.0999	0.1246	0.1644	0.2094	0.3173	0.3606
53	0.0588	0.0817	0.0982	0.1227	0.1622	0.2069	0.3149	0.3583
54	0.0577	0.0803	0.0966	0.1208	0.1600	0.2046	0.3126	0.3561
55	0.0567	0.0789	0.0951	0.1190	0.1579	0.2023	0.3103	0.3539
56	0.0557	0.0776	0.0936	0.1173	0.1558	0.2000	0.3080	0.3517
57	0.0547	0.0764	0.0921	0.1156	0.1539	0.1979	0.3058	0.3496
58	0.0538	0.0751	0.0907	0.1139	0.1519	0.1957	0.3037	0.3476
59	0.0529	0.0740	0.0893	0.1124	0.1500	0.1937	0.3016	0.3456
60	0.0520	0.0728	0.0880	0.1108	0.1482	0.1916	0.2995	0.3436
61	0.0512	0.0717	0.0867	0.1093	0.1464	0.1897	0.2975	0.3417
62	0.0504	0.0707	0.0855	0.1078	0.1447	0.1877	0.2955	0.3398
63	0.0496	0.0696	0.0843	0.1064	0.1430	0.1858	0.2936	0.3379
64	0.0489	0.0686	0.0831	0.1050	0.1413	0.1840	0.2917	0.3361
65	0.0481	0.0676	0.0820	0.1037	0.1397	0.1822	0.2899	0.3343
66	0.0474	0.0667	0.0809	0.1024	0.1381	0.1804	0.2880	0.3325
67	0.0467	0.0658	0.0798	0.1011	0.1366	0.1787	0.2862	0.3308
68	0.0461	0.0649	0.0788	0.0998	0.1351	0.1770	0.2845	0.3291
69	0.0454	0.0640	0.0777	0.0986	0.1336	0.1754	0.2827	0.3275
70	0.0448	0.0632	0.0768	0.0974	0.1322	0.1737	0.2810	0.3258
71	0.0442	0.0623	0.0758	0.0963	0.1308	0.1722	0.2794	0.3242
72	0.0436	0.0615	0.0748	0.0952	0.1294	0.1706	0.2777	0.3226
73	0.0430	0.0607	0.0739	0.0941	0.1281	0.1691	0.2761	0.3211
74	0.0424	0.0600	0.0730	0.0930	0.1268	0.1676	0.2745	0.3196
75	0.0419	0.0592	0.0722	0.0919	0.1255	0.1661	0.2730	0.3181
76	0.0413	0.0585	0.0713	0.0909	0.1242	0.1647	0.2715	0.3166
77	0.0408	0.0578	0.0705	0.0899	0.1230	0.1633	0.2700	0.3151
78	0.0403	0.0571	0.0697	0.0889	0.1218	0.1619	0.2685	0.3137
79	0.0398	0.0565	0.0689	0.0880	0.1206	0.1606	0.2670	0.3123
80	0.0393	0.0558	0.0681	0.0870	0.1195	0.1592	0.2656	0.3109
81	0.0389	0.0552	0.0674	0.0861	0.1184	0.1579	0.2642	0.3095
82	0.0384	0.0545	0.0666	0.0852	0.1173	0.1567	0.2628	0.3082
83	0.0380	0.0539	0.0659	0.0844	0.1162	0.1554	0.2614	0.3069
84	0.0375	0.0533	0.0652	0.0835	0.1151	0.1542	0.2600	0.3055
85	0.0371	0.0528	0.0645	0.0827	0.1141	0.1530	0.2587	0.3042
86	0.0367	0.0522	0.0638	0.0819	0.1130	0.1518	0.2574	0.3030
87	0.0363	0.0516	0.0632	0.0811	0.1120	0.1506	0.2561	0.3017

	5 μm Insulating Plane (Hemispherical)							
μm away	5 μm	10 μm	15 μm	25 μm	50 μm	100 μm	500 μm	1,000 μm
88	0.0359	0.0511	0.0625	0.0803	0.1111	0.1494	0.2548	0.3005
89	0.0355	0.0505	0.0619	0.0795	0.1101	0.1483	0.2536	0.2993
90	0.0351	0.0500	0.0613	0.0787	0.1091	0.1472	0.2523	0.2981
91	0.0347	0.0495	0.0607	0.0780	0.1082	0.1461	0.2511	0.2969
92	0.0344	0.0490	0.0601	0.0773	0.1073	0.1450	0.2499	0.2957
93	0.0340	0.0485	0.0595	0.0766	0.1064	0.1440	0.2487	0.2945
94	0.0337	0.0481	0.0589	0.0759	0.1055	0.1429	0.2476	0.2934
95	0.0333	0.0476	0.0584	0.0752	0.1047	0.1419	0.2464	0.2923
96	0.0330	0.0471	0.0578	0.0745	0.1038	0.1409	0.2453	0.2912
97	0.0327	0.0467	0.0573	0.0739	0.1030	0.1399	0.2441	0.2901
98	0.0323	0.0462	0.0568	0.0732	0.1022	0.1389	0.2430	0.2890
99	0.0320	0.0458	0.0563	0.0726	0.1014	0.1380	0.2419	0.2879
100	0.0317	0.0454	0.0557	0.0720	0.1006	0.1370	0.2408	0.2868

	Infinite Insulating Plane (Conical)							
μm away	5 μm	10 μm	15 μm	25 μm	50 μm	100 μm	500 μm	1000 μm
0	1.0000	1.0000	1.0000	1.0000	1.0000	1.0000	0.9999	0.9998
1	0.6901	0.7305	0.7464	0.7629	0.7813	0.7966	0.8239	0.8335
2	0.5810	0.6349	0.6560	0.6782	0.7030	0.7236	0.7607	0.7738
3	0.5064	0.5679	0.5924	0.6183	0.6476	0.6719	0.7159	0.7315
4	0.4502	0.5161	0.5430	0.5716	0.6042	0.6314	0.6808	0.6982
5	0.4058	0.4742	0.5027	0.5334	0.5686	0.5981	0.6518	0.6709
6	0.3695	0.4392	0.4689	0.5012	0.5385	0.5699	0.6273	0.6477
7	0.3393	0.4094	0.4399	0.4735	0.5125	0.5456	0.6061	0.6277
8	0.3136	0.3837	0.4148	0.4493	0.4897	0.5242	0.5875	0.6100
9	0.2916	0.3612	0.3926	0.4279	0.4695	0.5052	0.5709	0.5944
10	0.2725	0.3413	0.3730	0.4088	0.4514	0.4881	0.5560	0.5802
11	0.2557	0.3236	0.3554	0.3916	0.4351	0.4727	0.5425	0.5675
12	0.2409	0.3077	0.3395	0.3760	0.4202	0.4586	0.5301	0.5558
13	0.2277	0.2933	0.3251	0.3618	0.4066	0.4457	0.5188	0.5451
14	0.2159	0.2803	0.3119	0.3488	0.3940	0.4338	0.5083	0.5351
15	0.2052	0.2684	0.2999	0.3368	0.3824	0.4227	0.4986	0.5259
16	0.1955	0.2575	0.2887	0.3257	0.3717	0.4125	0.4896	0.5174
17	0.1867	0.2475	0.2785	0.3154	0.3617	0.4029	0.4811	0.5094
18	0.1787	0.2382	0.2690	0.3058	0.3523	0.3939	0.4732	0.5018
19	0.1713	0.2297	0.2601	0.2969	0.3435	0.3855	0.4657	0.4947
20	0.1645	0.2217	0.2518	0.2885	0.3352	0.3775	0.4586	0.4880
21	0.1582	0.2143	0.2441	0.2806	0.3274	0.3700	0.4519	0.4817
22	0.1524	0.2074	0.2369	0.2732	0.3201	0.3629	0.4456	0.4757
23	0.1470	0.2009	0.2301	0.2662	0.3131	0.3561	0.4396	0.4700
24	0.1420	0.1948	0.2237	0.2596	0.3065	0.3497	0.4338	0.4645
25	0.1373	0.1891	0.2176	0.2533	0.3002	0.3436	0.4283	0.4593
26	0.1329	0.1837	0.2119	0.2474	0.2942	0.3377	0.4231	0.4543
27	0.1288	0.1786	0.2065	0.2417	0.2885	0.3322	0.4181	0.4496
28	0.1249	0.1738	0.2013	0.2363	0.2830	0.3268	0.4133	0.4450
29	0.1212	0.1693	0.1965	0.2312	0.2778	0.3217	0.4086	0.4406
30	0.1178	0.1649	0.1918	0.2263	0.2728	0.3168	0.4042	0.4364
31	0.1146	0.1608	0.1874	0.2216	0.2680	0.3121	0.3999	0.4323
32	0.1115	0.1569	0.1832	0.2171	0.2634	0.3075	0.3958	0.4284
33	0.1086	0.1532	0.1792	0.2129	0.2590	0.3031	0.3918	0.4246
34	0.1058	0.1497	0.1753	0.2088	0.2547	0.2989	0.3880	0.4210
35	0.1032	0.1463	0.1716	0.2048	0.2506	0.2948	0.3842	0.4174
36	0.1007	0.1431	0.1681	0.2010	0.2467	0.2909	0.3807	0.4140
37	0.0983	0.1400	0.1647	0.1974	0.2429	0.2871	0.3772	0.4107
38	0.0960	0.1371	0.1615	0.1939	0.2392	0.2834	0.3738	0.4075
39	0.0938	0.1342	0.1584	0.1905	0.2356	0.2799	0.3705	0.4044
40	0.0918	0.1315	0.1554	0.1873	0.2322	0.2764	0.3673	0.4014
41	0.0898	0.1289	0.1525	0.1841	0.2289	0.2731	0.3643	0.3984
42	0.0879	0.1264	0.1497	0.1811	0.2257	0.2698	0.3613	0.3956

μm away	Infinite Insulating Plane (Conical)							
	5 μm	10 μm	15 μm	25 μm	50 μm	100 μm	500 μm	1000 μm
43	0.0861	0.1240	0.1471	0.1782	0.2225	0.2667	0.3583	0.3928
44	0.0843	0.1217	0.1445	0.1753	0.2195	0.2636	0.3555	0.3901
45	0.0826	0.1194	0.1420	0.1726	0.2166	0.2607	0.3527	0.3874
46	0.0810	0.1173	0.1396	0.1699	0.2137	0.2578	0.3500	0.3849
47	0.0795	0.1152	0.1373	0.1674	0.2110	0.2550	0.3474	0.3824
48	0.0780	0.1132	0.1350	0.1649	0.2083	0.2522	0.3448	0.3799
49	0.0765	0.1113	0.1329	0.1625	0.2057	0.2496	0.3423	0.3775
50	0.0752	0.1094	0.1308	0.1602	0.2031	0.2470	0.3399	0.3752
51	0.0738	0.1076	0.1287	0.1579	0.2007	0.2444	0.3375	0.3729
52	0.0725	0.1059	0.1268	0.1557	0.1983	0.2419	0.3352	0.3707
53	0.0713	0.1042	0.1249	0.1536	0.1959	0.2395	0.3329	0.3685
54	0.0701	0.1026	0.1230	0.1515	0.1937	0.2372	0.3307	0.3664
55	0.0689	0.1010	0.1212	0.1495	0.1914	0.2349	0.3285	0.3643
56	0.0678	0.0994	0.1195	0.1475	0.1893	0.2326	0.3263	0.3622
57	0.0667	0.0980	0.1178	0.1456	0.1871	0.2304	0.3242	0.3602
58	0.0657	0.0965	0.1162	0.1437	0.1851	0.2283	0.3222	0.3583
59	0.0646	0.0951	0.1146	0.1419	0.1831	0.2262	0.3202	0.3563
60	0.0637	0.0937	0.1130	0.1401	0.1811	0.2241	0.3182	0.3545
61	0.0627	0.0924	0.1115	0.1384	0.1792	0.2221	0.3163	0.3526
62	0.0618	0.0911	0.1100	0.1367	0.1773	0.2202	0.3144	0.3508
63	0.0609	0.0899	0.1086	0.1351	0.1755	0.2182	0.3125	0.3490
64	0.0600	0.0887	0.1072	0.1335	0.1737	0.2163	0.3107	0.3473
65	0.0591	0.0875	0.1058	0.1319	0.1719	0.2145	0.3089	0.3456
66	0.0583	0.0863	0.1045	0.1304	0.1702	0.2127	0.3071	0.3439
67	0.0575	0.0852	0.1032	0.1289	0.1685	0.2109	0.3054	0.3422
68	0.0567	0.0841	0.1020	0.1275	0.1669	0.2092	0.3037	0.3406
69	0.0560	0.0831	0.1007	0.1261	0.1653	0.2074	0.3021	0.3390
70	0.0552	0.0820	0.0995	0.1247	0.1637	0.2058	0.3004	0.3374
71	0.0545	0.0810	0.0984	0.1233	0.1621	0.2041	0.2988	0.3359
72	0.0538	0.0800	0.0972	0.1220	0.1606	0.2025	0.2972	0.3343
73	0.0531	0.0790	0.0961	0.1207	0.1591	0.2009	0.2957	0.3328
74	0.0524	0.0781	0.0950	0.1195	0.1577	0.1994	0.2941	0.3314
75	0.0518	0.0772	0.0939	0.1182	0.1563	0.1978	0.2926	0.3299
76	0.0512	0.0763	0.0929	0.1170	0.1549	0.1963	0.2911	0.3285
77	0.0505	0.0754	0.0919	0.1158	0.1535	0.1949	0.2897	0.3271
78	0.0499	0.0746	0.0909	0.1146	0.1521	0.1934	0.2882	0.3257
79	0.0493	0.0737	0.0899	0.1135	0.1508	0.1920	0.2868	0.3243
80	0.0488	0.0729	0.0890	0.1124	0.1495	0.1906	0.2854	0.3230
81	0.0482	0.0721	0.0880	0.1113	0.1482	0.1892	0.2840	0.3217
82	0.0476	0.0713	0.0871	0.1102	0.1470	0.1878	0.2827	0.3204
83	0.0471	0.0706	0.0862	0.1092	0.1458	0.1865	0.2813	0.3191
84	0.0466	0.0698	0.0853	0.1081	0.1446	0.1852	0.2800	0.3178
85	0.0461	0.0691	0.0845	0.1071	0.1434	0.1839	0.2787	0.3165
86	0.0456	0.0684	0.0836	0.1061	0.1422	0.1826	0.2774	0.3153
87	0.0451	0.0677	0.0828	0.1052	0.1411	0.1814	0.2762	0.3141

μm away	Infinite Insulating Plane (Conical)							
	5 μm	10 μm	15 μm	25 μm	50 μm	100 μm	500 μm	1000 μm
88	0.0446	0.0670	0.0820	0.1042	0.1399	0.1801	0.2749	0.3129
89	0.0441	0.0663	0.0812	0.1033	0.1388	0.1789	0.2737	0.3117
90	0.0437	0.0656	0.0804	0.1023	0.1377	0.1777	0.2725	0.3105
91	0.0432	0.0650	0.0797	0.1014	0.1367	0.1765	0.2713	0.3094
92	0.0428	0.0644	0.0789	0.1006	0.1356	0.1754	0.2701	0.3082
93	0.0423	0.0637	0.0782	0.0997	0.1346	0.1742	0.2689	0.3071
94	0.0419	0.0631	0.0775	0.0988	0.1336	0.1731	0.2678	0.3060
95	0.0415	0.0625	0.0768	0.0980	0.1325	0.1720	0.2666	0.3049
96	0.0411	0.0619	0.0761	0.0972	0.1316	0.1709	0.2655	0.3038
97	0.0407	0.0614	0.0754	0.0963	0.1306	0.1698	0.2644	0.3027
98	0.0403	0.0608	0.0747	0.0955	0.1296	0.1688	0.2633	0.3017
99	0.0399	0.0602	0.0741	0.0948	0.1287	0.1677	0.2622	0.3006
100	0.0395	0.0597	0.0734	0.0940	0.1278	0.1667	0.2611	0.2996

	5 μm Insulating Plane (Conical)							
μm away	5 μm	10 μm	15 μm	25 μm	50 μm	100 μm	500 μm	1000 μm
0	1.0000	1.0000	0.9998	1.0000	0.9996	1.0000	1.0000	0.9998
1	0.6564	0.6998	0.7191	0.7401	0.7637	0.7830	0.8176	0.8297
2	0.5378	0.5943	0.6198	0.6477	0.6793	0.7053	0.7522	0.7686
3	0.4576	0.5212	0.5504	0.5827	0.6196	0.6503	0.7058	0.7253
4	0.3980	0.4654	0.4970	0.5323	0.5731	0.6072	0.6694	0.6913
5	0.3515	0.4207	0.4538	0.4912	0.5350	0.5719	0.6395	0.6634
6	0.3141	0.3840	0.4180	0.4569	0.5029	0.5420	0.6141	0.6397
7	0.2835	0.3531	0.3877	0.4276	0.4753	0.5162	0.5922	0.6191
8	0.2579	0.3268	0.3616	0.4022	0.4512	0.4936	0.5729	0.6011
9	0.2363	0.3041	0.3389	0.3798	0.4299	0.4736	0.5558	0.5851
10	0.2178	0.2843	0.3189	0.3600	0.4108	0.4556	0.5403	0.5707
11	0.2018	0.2668	0.3011	0.3423	0.3937	0.4394	0.5264	0.5576
12	0.1879	0.2513	0.2853	0.3264	0.3782	0.4246	0.5136	0.5457
13	0.1757	0.2375	0.2710	0.3120	0.3641	0.4111	0.5019	0.5347
14	0.1649	0.2251	0.2581	0.2988	0.3511	0.3987	0.4911	0.5246
15	0.1553	0.2139	0.2464	0.2868	0.3392	0.3872	0.4811	0.5152
16	0.1467	0.2037	0.2358	0.2758	0.3281	0.3765	0.4718	0.5064
17	0.1389	0.1945	0.2260	0.2656	0.3179	0.3666	0.4630	0.4982
18	0.1319	0.1860	0.2170	0.2562	0.3083	0.3573	0.4548	0.4905
19	0.1256	0.1782	0.2086	0.2474	0.2994	0.3486	0.4471	0.4833
20	0.1198	0.1711	0.2009	0.2393	0.2911	0.3404	0.4399	0.4765
21	0.1145	0.1645	0.1938	0.2317	0.2832	0.3326	0.4330	0.4700
22	0.1096	0.1584	0.1871	0.2246	0.2758	0.3253	0.4264	0.4639
23	0.1052	0.1527	0.1809	0.2179	0.2689	0.3184	0.4202	0.4580
24	0.1010	0.1474	0.1751	0.2116	0.2623	0.3118	0.4143	0.4525
25	0.0972	0.1424	0.1697	0.2057	0.2560	0.3056	0.4087	0.4472
26	0.0937	0.1378	0.1646	0.2001	0.2501	0.2997	0.4033	0.4421
27	0.0903	0.1335	0.1598	0.1948	0.2445	0.2940	0.3982	0.4372
28	0.0873	0.1294	0.1552	0.1898	0.2391	0.2886	0.3932	0.4326
29	0.0844	0.1256	0.1509	0.1851	0.2340	0.2834	0.3885	0.4281
30	0.0817	0.1219	0.1469	0.1806	0.2292	0.2784	0.3839	0.4238
31	0.0791	0.1185	0.1431	0.1763	0.2245	0.2737	0.3795	0.4197
32	0.0767	0.1153	0.1394	0.1722	0.2201	0.2691	0.3753	0.4157
33	0.0745	0.1123	0.1360	0.1684	0.2158	0.2647	0.3712	0.4118
34	0.0724	0.1094	0.1327	0.1647	0.2117	0.2605	0.3673	0.4081
35	0.0704	0.1066	0.1295	0.1611	0.2078	0.2565	0.3635	0.4045
36	0.0685	0.1040	0.1266	0.1577	0.2041	0.2525	0.3598	0.4010
37	0.0667	0.1015	0.1237	0.1545	0.2004	0.2488	0.3562	0.3976
38	0.0650	0.0991	0.1210	0.1514	0.1970	0.2451	0.3528	0.3944
39	0.0634	0.0969	0.1184	0.1484	0.1936	0.2416	0.3494	0.3912
40	0.0618	0.0947	0.1159	0.1455	0.1904	0.2382	0.3462	0.3881
41	0.0603	0.0926	0.1135	0.1428	0.1873	0.2349	0.3430	0.3851
42	0.0589	0.0907	0.1112	0.1401	0.1842	0.2317	0.3400	0.3822

μm away	5 μm	10 μm	15 μm	25 μm	50 μm	100 μm	500 μm	1000 μm
				5 μm Insulating Plane (Conical)				
43	0.0576	0.0888	0.1090	0.1376	0.1813	0.2286	0.3370	0.3794
44	0.0563	0.0870	0.1069	0.1352	0.1785	0.2256	0.3341	0.3766
45	0.0551	0.0852	0.1049	0.1328	0.1758	0.2227	0.3313	0.3740
46	0.0539	0.0835	0.1029	0.1305	0.1732	0.2199	0.3285	0.3713
47	0.0528	0.0819	0.1011	0.1283	0.1706	0.2172	0.3259	0.3688
48	0.0518	0.0804	0.0993	0.1262	0.1682	0.2145	0.3232	0.3663
49	0.0507	0.0789	0.0975	0.1241	0.1658	0.2119	0.3207	0.3639
50	0.0497	0.0775	0.0958	0.1222	0.1635	0.2094	0.3182	0.3615
51	0.0488	0.0761	0.0942	0.1202	0.1612	0.2070	0.3158	0.3592
52	0.0479	0.0748	0.0926	0.1184	0.1590	0.2046	0.3134	0.3569
53	0.0470	0.0735	0.0911	0.1166	0.1569	0.2023	0.3111	0.3547
54	0.0461	0.0722	0.0897	0.1148	0.1548	0.2000	0.3088	0.3526
55	0.0453	0.0710	0.0882	0.1132	0.1528	0.1978	0.3066	0.3505
56	0.0445	0.0699	0.0869	0.1115	0.1509	0.1956	0.3045	0.3484
57	0.0438	0.0688	0.0855	0.1099	0.1490	0.1935	0.3023	0.3464
58	0.0430	0.0677	0.0842	0.1084	0.1472	0.1915	0.3003	0.3444
59	0.0423	0.0666	0.0830	0.1069	0.1454	0.1895	0.2982	0.3424
60	0.0416	0.0656	0.0818	0.1054	0.1436	0.1876	0.2962	0.3405
61	0.0410	0.0646	0.0806	0.1040	0.1419	0.1857	0.2943	0.3386
62	0.0403	0.0637	0.0795	0.1026	0.1402	0.1838	0.2924	0.3368
63	0.0397	0.0627	0.0784	0.1013	0.1386	0.1820	0.2905	0.3350
64	0.0391	0.0618	0.0773	0.1000	0.1370	0.1802	0.2886	0.3332
65	0.0385	0.0610	0.0762	0.0987	0.1355	0.1785	0.2868	0.3315
66	0.0379	0.0601	0.0752	0.0975	0.1340	0.1768	0.2850	0.3298
67	0.0374	0.0593	0.0742	0.0963	0.1325	0.1751	0.2833	0.3281
68	0.0369	0.0585	0.0733	0.0951	0.1311	0.1735	0.2816	0.3265
69	0.0363	0.0577	0.0723	0.0940	0.1297	0.1719	0.2799	0.3248
70	0.0358	0.0570	0.0714	0.0929	0.1283	0.1703	0.2783	0.3232
71	0.0353	0.0562	0.0705	0.0918	0.1270	0.1688	0.2766	0.3217
72	0.0349	0.0555	0.0697	0.0907	0.1256	0.1673	0.2750	0.3201
73	0.0344	0.0548	0.0688	0.0897	0.1244	0.1658	0.2735	0.3186
74	0.0340	0.0541	0.0680	0.0887	0.1231	0.1644	0.2719	0.3171
75	0.0335	0.0535	0.0672	0.0877	0.1219	0.1629	0.2704	0.3157
76	0.0331	0.0528	0.0664	0.0867	0.1207	0.1615	0.2689	0.3142
77	0.0327	0.0522	0.0656	0.0858	0.1195	0.1602	0.2675	0.3128
78	0.0323	0.0516	0.0649	0.0848	0.1183	0.1589	0.2660	0.3114
79	0.0319	0.0510	0.0642	0.0839	0.1172	0.1575	0.2646	0.3100
80	0.0315	0.0504	0.0634	0.0831	0.1161	0.1563	0.2632	0.3087
81	0.0311	0.0498	0.0628	0.0822	0.1150	0.1550	0.2618	0.3073
82	0.0307	0.0492	0.0621	0.0814	0.1140	0.1538	0.2604	0.3060
83	0.0304	0.0487	0.0614	0.0805	0.1129	0.1525	0.2591	0.3047
84	0.0300	0.0482	0.0608	0.0797	0.1119	0.1513	0.2578	0.3034
85	0.0297	0.0476	0.0601	0.0789	0.1109	0.1502	0.2565	0.3022
86	0.0294	0.0471	0.0595	0.0782	0.1099	0.1490	0.2552	0.3009
87	0.0290	0.0466	0.0589	0.0774	0.1089	0.1479	0.2539	0.2997

	5 μm Insulating Plane (Conical)							
μm away	5 μm	10 μm	15 μm	25 μm	50 μm	100 μm	500 μm	1000 μm
88	0.0287	0.0461	0.0583	0.0767	0.1080	0.1468	0.2527	0.2985
89	0.0284	0.0457	0.0577	0.0759	0.1071	0.1457	0.2515	0.2973
90	0.0281	0.0452	0.0571	0.0752	0.1062	0.1446	0.2502	0.2961
91	0.0278	0.0447	0.0566	0.0745	0.1053	0.1435	0.2491	0.2949
92	0.0275	0.0443	0.0560	0.0738	0.1044	0.1425	0.2479	0.2938
93	0.0272	0.0439	0.0555	0.0732	0.1035	0.1414	0.2467	0.2927
94	0.0270	0.0434	0.0550	0.0725	0.1027	0.1404	0.2456	0.2915
95	0.0267	0.0430	0.0544	0.0718	0.1018	0.1394	0.2444	0.2904
96	0.0264	0.0426	0.0539	0.0712	0.1010	0.1385	0.2433	0.2893
97	0.0262	0.0422	0.0534	0.0706	0.1002	0.1375	0.2422	0.2883
98	0.0259	0.0418	0.0530	0.0700	0.0994	0.1365	0.2411	0.2872
99	0.0257	0.0414	0.0525	0.0694	0.0986	0.1356	0.2400	0.2861
100	0.0254	0.0410	0.0520	0.0688	0.0979	0.1347	0.2390	0.2851

APPENDIX C

DUMMY CELL RESULTS

The results of current interruption experiments on 16 different dummy cells, which was used to check the accuracy of the experiments. The electrode and solution resistances were measured using an ohmmeter. The experimental solution resistances were determined by measuring the instantaneous voltage drop of the current interruption experiments and dividing this voltage by the applied current for that experiment. The current interruption experiments were performed at 0.5, 1.0, 1.5 and 2 μA for each dummy cell. There was less than a 2.5 % difference in experimental solution resistance values for the four different currents tested. Experiments for each dummy cell at the different currents were repeated 10 or more times with less than a 5 % difference between each individual experiment and the average for that dummy cell; the average for the current interruption experiments is shown in table 12 below.

Table 12. Experimental results for dummy cells of various resistances.

Dummy Cell #	Measured Electrode Resistance	Measured Solution Resistance	Experimental Solution Resistance	Measured Experimental
1	486 kΩ	4.75 kΩ	5.1 kΩ	0.93
2	496 kΩ	22.33 kΩ	22.2 kΩ	1.01
3	1.01 MΩ	24.81 kΩ	24.9 kΩ	1.00
4	490 kΩ	23.50 kΩ	23.9 kΩ	0.98
5	1.11 MΩ	10.15 kΩ	10.3 kΩ	0.99
6	1.03 MΩ	4.69 kΩ	5.1 kΩ	0.92
7	1.04 MΩ	23.92 kΩ	23.7 kΩ	1.01
8	1.06 MΩ	10.51 kΩ	10.8 kΩ	0.97
9	10.11 MΩ	1.02 MΩ	951 kΩ	1.07
10	10.45 MΩ	481 kΩ	445 kΩ	1.08
11	9.32 MΩ	715 kΩ	676 kΩ	1.06
12	2.79 MΩ	720 kΩ	700 kΩ	1.03
13	23.03 MΩ	990 kΩ	918 kΩ	1.08
14	1.71 MΩ	484 kΩ	453 kΩ	1.07
15	2.75 MΩ	219 kΩ	206 kΩ	1.07
16	5.07 MΩ	480 kΩ	468 kΩ	1.03

EXAMPLES OF THE TWO DIFFERENT TYPES OF SIMULATIONS

Table 13. **The two types of computer simulations for several different actual microelectrodes of various lengths.**

Distance from Tip (μm)	11.5 μm long electrode		14.5 μm long electrode		16.8 μm long electrode	
	Potential in Solution (V)		Potential in Solution (V)		Potential in Solution (V)	
	1 V Potential	Current	1 V Potential	Current	1 V Potential	Current
1	0.75200933	0.75187016	0.76358443	0.76364416	0.77057594	0.7704884
2	0.70825607	0.70812494	0.7215581	0.72161454	0.72983223	0.7297493
3	0.6661121	0.6659888	0.6810662	0.6811195	0.6903134	0.690235
4	0.62655985	0.62644386	0.6428608	0.6429111	0.6529803	0.6529062
5	0.58989924	0.58979005	0.6071963	0.60724384	0.6180991	0.61802894
6	0.55604565	0.5559427	0.57427347	0.5743184	0.58579904	0.5857326
7	0.5248402	0.5247431	0.5438461	0.5438887	0.5559145	0.5558515
8	0.4960352	0.49594343	0.51590574	0.5159462	0.52844	0.5283801
9	0.47005334	0.46996638	0.49041122	0.49044967	0.5033093	0.50325227
10	0.44621432	0.4461318	0.46691072	0.46694735	0.48012298	0.4800686
11	0.4243775	0.424299	0.44536212	0.44539705	0.45879856	0.4587466
12	0.40435886	0.40428406	0.42560634	0.42563975	0.43921787	0.43916816
13	0.3859912	0.3859198	0.4073232	0.4073552	0.4209963	0.42094865
14	0.36920384	0.36913556	0.3905944	0.39062506	0.40421587	0.40417013
15	0.35359183	0.35352644	0.3747937	0.37482312	0.3887162	0.38867223
16	0.33916047	0.33909777	0.3602479	0.3602762	0.3742176	0.37417525
17	0.32590982	0.32584956	0.34687537	0.3469026	0.3607095	0.3606687
18	0.31364617	0.31358817	0.33453742	0.3345637	0.34812942	0.34809005
19	0.30211073	0.30205488	0.32286578	0.32289118	0.3363605	0.3363225
20	0.29135042	0.29129654	0.3118605	0.31188503	0.32535398	0.3253172
21	0.2814418	0.2813898	0.30150992	0.3015336	0.31505537	0.31501976
22	0.27211964	0.27206933	0.2918537	0.29187664	0.30536327	0.30532876
23	0.2632811	0.26323244	0.282973	0.28299525	0.2961796	0.29614612

Distance from Tip (μm)	11.5 μm long electrode Potential in Solution (V)		14.5 μm long electrode Potential in Solution (V)		16.8 μm long electrode Potential in Solution (V)	
24	0.25492626	0.25487915	0.27450782	0.27452943	0.2875043	0.2874718
25	0.24705505	0.2470094	0.26645818	0.26647913	0.27933738	0.27930582
26	0.23966752	0.23962322	0.25882408	0.25884444	0.2716142	0.27158353
27	0.23277506	0.23273204	0.2516055	0.25162533	0.26433328	0.26430342
28	0.22628096	0.22623914	0.24480249	0.24482176	0.2573827	0.2573536
29	0.22009869	0.22005802	0.23841502	0.23843378	0.2507772	0.2507489
30	0.21419801	0.21415843	0.23222739	0.23224565	0.24453294	0.24450533
31	0.20857966	0.20854111	0.22644812	0.22646594	0.23861732	0.23859037
32	0.20324901	0.20321146	0.22095636	0.22097376	0.23294942	0.23292312
33	0.19820726	0.19817065	0.2156865	0.21570347	0.2275264	0.2275007
34	0.19343354	0.1933978	0.21063843	0.21065502	0.2223417	0.2223166
35	0.18885414	0.18881924	0.20581226	0.20582847	0.21736273	0.21733819
36	0.18447325	0.18443917	0.20120792	0.20122376	0.21266018	0.21263617
37	0.18029276	0.18025945	0.19682543	0.19684093	0.20812736	0.20810387
38	0.17631266	0.17628008	0.19264898	0.19266415	0.2037643	0.2037413
39	0.17253296	0.17250109	0.18859842	0.18861328	0.199571	0.19954847
40	0.16893227	0.16890107	0.18472397	0.18473852	0.19554745	0.19552536
41	0.16545416	0.1654236	0.1810274	0.18104166	0.19169363	0.191672
42	0.16209564	0.16206568	0.17746142	0.1774754	0.18800959	0.18798837
43	0.15885663	0.15882729	0.1740195	0.17403321	0.18449056	0.18446974
44	0.15573724	0.15570846	0.17072245	0.1707359	0.18107662	0.18105619
45	0.15273672	0.1527085	0.1675365	0.1675497	0.1777746	0.17775454
46	0.1498587	0.14983101	0.1644617	0.16447465	0.17458312	0.17456342
47	0.14711891	0.14709173	0.161498	0.16151072	0.17150217	0.17148282
48	0.14446384	0.14443715	0.15864542	0.15865792	0.16853175	0.16851273
49	0.14188966	0.14186345	0.15590397	0.15591626	0.16567184	0.16565314
50	0.13939638	0.13937064	0.15326616	0.15327823	0.16290669	0.1628883
51	0.13698399	0.13695869	0.15067814	0.15069002	0.16022773	0.16020966
52	0.13465251	0.13462764	0.14821441	0.1482261	0.1576357	0.15761793
53	0.13240585	0.13238138	0.14582121	0.1458327	0.15513055	0.15511306
54	0.1302486	0.13022454	0.14349854	0.14350985	0.15270114	0.15268391
55	0.12815869	0.12813501	0.14124638	0.14125751	0.15034534	0.15032838
56	0.12614085	0.12611754	0.13906474	0.1390757	0.14806317	0.14804646
57	0.12417789	0.12415495	0.13695364	0.13696443	0.14585464	0.14583817
58	0.12227065	0.12224806	0.13491303	0.13492367	0.14371997	0.14370376
59	0.12041918	0.12039693	0.13291614	0.13292661	0.14164248	0.1416265
60	0.11862348	0.11860157	0.1309746	0.13098493	0.13961864	0.13960288
61	0.11688355	0.11686195	0.12909307	0.12910324	0.13764842	0.13763289
62	0.11519938	0.1151781	0.12728733	0.12729737	0.13573185	0.13571653
63	0.11357097	0.11354999	0.12552442	0.12553431	0.13386889	0.1338538
64	0.11198941	0.11196873	0.12380435	0.12381411	0.13205981	0.13204491
65	0.11044609	0.11042569	0.12212713	0.12213676	0.13030626	0.13029157
66	0.10894124	0.10892112	0.12049274	0.12050224	0.12859833	0.12858383
67	0.10747486	0.10745502	0.11890119	0.11891056	0.12693077	0.12691647
68	0.10604699	0.1060274	0.11735247	0.11736172	0.12530361	0.12528948

Distance from Tip (μm)	11.5 μm long electrode Potential in Solution (V)		14.5 μm long electrode Potential in Solution (V)		16.8 μm long electrode Potential in Solution (V)	
69	0.10465761	0.10463828	0.11584661	0.11585575	0.12371684	0.12370288
70	0.1033067	0.10328762	0.11438358	0.11439259	0.12217043	0.12215666
71	0.10199095	0.10197211	0.11295932	0.11296822	0.12066441	0.1206508
72	0.10071169	0.10069308	0.11156827	0.11157706	0.11919876	0.11918532
73	0.09946705	0.09944869	0.1102145	0.11022319	0.1177735	0.11776021
74	0.09824952	0.09823138	0.10888933	0.10889791	0.11637829	0.11636517
75	0.09705908	0.09704115	0.10759282	0.10760131	0.11501312	0.11500014
76	0.09589572	0.09587801	0.10632667	0.10633505	0.11367964	0.11366682
77	0.09475946	0.09474196	0.10509011	0.1050984	0.11237786	0.11236519
78	0.09365064	0.09363335	0.10388315	0.10389134	0.11110777	0.11109525
79	0.0925695	0.09255241	0.10270577	0.10271387	0.10986696	0.10985458
80	0.09151605	0.09149915	0.10155799	0.10156599	0.10865214	0.10863989
81	0.09049028	0.09047357	0.10043979	0.10044771	0.1074645	0.10745239
82	0.08948469	0.08946817	0.09934786	0.09935569	0.1063045	0.10629252
83	0.08850376	0.08848741	0.09827672	0.09828447	0.1051702	0.10515834
84	0.08754105	0.08752488	0.09722637	0.09723403	0.10405941	0.10404769
85	0.08659756	0.08658157	0.09619679	0.09620437	0.10297215	0.10296053
86	0.08567418	0.08565836	0.09518801	0.09519551	0.10190842	0.10189692
87	0.0847709	0.08475525	0.09420002	0.09420744	0.10086666	0.10085528
88	0.08388773	0.08387224	0.09323281	0.09324016	0.09984643	0.09983517
89	0.08302464	0.08300931	0.09228639	0.09229367	0.09884767	0.09883653
90	0.08218167	0.08216649	0.09136076	0.09136796	0.09786706	0.09785603
91	0.08135727	0.08134224	0.09045544	0.09046258	0.09690649	0.09689556
92	0.08054711	0.08053224	0.0895681	0.08957516	0.09596625	0.09595543
93	0.07975155	0.07973682	0.08869709	0.08870409	0.09504636	0.09503564
94	0.07897093	0.07895635	0.08784249	0.08784942	0.09414186	0.09413124
95	0.07820567	0.07819123	0.08700427	0.08701114	0.09325318	0.09324267
96	0.07745557	0.07744126	0.08618246	0.08618926	0.09238174	0.09237132
97	0.07672062	0.07670645	0.08537704	0.08538377	0.09152758	0.09151726
98	0.07600084	0.0759868	0.08458802	0.0845947	0.09068988	0.09067965
99	0.07529622	0.07528231	0.0838154	0.08382201	0.08986862	0.08985849
100	0.07460675	0.07459297	0.08305918	0.08306573	0.08906381	0.08905377

115

Distance from Tip (μm)	18.1 μm long electrode Potential in Solution (V)		21.8 μm long electrode Potential in Solution (V)		27.8 μm long electrode Potential in Solution (V)	
	1 V Potential	Current	1 V Potential	Current	1 V Potential	Current
1	0.77419776	0.77433324	0.78328997	0.7835681	0.7938129	0.7939377
2	0.73388505	0.7340135	0.7446041	0.7448686	0.75681406	0.75693315
3	0.69491243	0.6950341	0.7066354	0.7068864	0.7210834	0.72119695
4	0.6580507	0.65816593	0.6708991	0.6711374	0.6865534	0.6866616
5	0.62353927	0.62364846	0.6375021	0.6377286	0.65441704	0.65452015
6	0.5915456	0.59164923	0.60627013	0.60648555	0.62445337	0.62455183
7	0.5620105	0.562109	0.5774424	0.5776477	0.59659636	0.5966904
8	0.53483456	0.5349283	0.5509304	0.5511262	0.57099366	0.5710838
9	0.50987715	0.5099665	0.5264259	0.52661306	0.54717183	0.5472582
10	0.4868443	0.48692966	0.503929	0.5041082	0.52515614	0.52523905
11	0.46563768	0.46571934	0.48306203	0.48323378	0.5049373	0.5050171
12	0.44610757	0.44618583	0.4637925	0.46395746	0.48622128	0.4862981
13	0.42803708	0.42811215	0.44593135	0.44608995	0.468646	0.46872008
14	0.41128045	0.4113526	0.42928427	0.42943698	0.45222571	0.45229724
15	0.39569297	0.3957624	0.41378972	0.4139369	0.4370563	0.43712544
16	0.38123563	0.38130254	0.39943516	0.39957726	0.4227189	0.4227858
17	0.36783585	0.36790043	0.38593203	0.38606936	0.40946952	0.4095343
18	0.35525745	0.35531983	0.373275	0.37340784	0.3969461	0.39700893
19	0.34347138	0.3435317	0.36140603	0.36153463	0.38514864	0.38520965
20	0.3323537	0.33241206	0.35036272	0.3504874	0.37400886	0.3740681
21	0.32193932	0.32199585	0.33990455	0.3400255	0.3635399	0.36359748
22	0.31217572	0.31223056	0.33000848	0.33012593	0.35364085	0.35369688
23	0.30295798	0.30301118	0.32066178	0.32077593	0.34424213	0.3442967
24	0.29427376	0.29432544	0.31186447	0.31197548	0.33535057	0.33540374
25	0.2860519	0.28610215	0.30361	0.3037181	0.32690415	0.32695597
26	0.2782924	0.2783413	0.29572043	0.2958257	0.3188647	0.31891525
27	0.27092862	0.27097622	0.28815588	0.28825846	0.31126004	0.3113094
28	0.26400125	0.26404762	0.2809669	0.28106695	0.3039895	0.3040377
29	0.25735745	0.25740266	0.27415353	0.27425113	0.2970516	0.29709873
30	0.2509972	0.2510413	0.2677157	0.267811	0.29039416	0.29044023
31	0.24492149	0.24496454	0.26155946	0.2616526	0.28406894	0.28411403
32	0.23914425	0.23918627	0.2556309	0.25572193	0.27798635	0.27803046
33	0.23366915	0.23371021	0.24997883	0.25006783	0.27216482	0.272208
34	0.2284781	0.22851826	0.24457552	0.2446626	0.26657656	0.26661885
35	0.22343193	0.2234712	0.239397	0.23948225	0.26121178	0.26125324
36	0.21866748	0.21870591	0.23440912	0.2344926	0.2560704	0.25611106
37	0.21407136	0.21410899	0.22963294	0.22971472	0.25113848	0.25117835
38	0.20964356	0.20968041	0.22507802	0.22515817	0.24633563	0.24637474
39	0.20538409	0.20542018	0.22069576	0.22077437	0.24175966	0.24179804
40	0.20129293	0.20132832	0.21643929	0.21651638	0.23733903	0.23737672
41	0.1973701	0.1974048	0.21240771	0.21248336	0.23315214	0.23318917

Distance from Tip (μm)	18.1 μm long electrode Potential in Solution (V)		21.8 μm long electrode Potential in Solution (V)		27.8 μm long electrode Potential in Solution (V)	
42	0.1936156	0.19364963	0.20849873	0.20857298	0.22908287	0.22911924
43	0.19002499	0.1900584	0.20471232	0.20478523	0.22513118	0.22516693
44	0.18652835	0.18656115	0.20104852	0.20112014	0.22129713	0.22133228
45	0.18316081	0.18319301	0.1975073	0.19757766	0.21758068	0.21761523
46	0.1799221	0.17995374	0.1940887	0.19415784	0.21398185	0.21401586
47	0.17680812	0.1768392	0.19079268	0.19086064	0.21050063	0.21053408
48	0.17379068	0.17382124	0.18761925	0.18768609	0.20713702	0.20716994
49	0.17086609	0.17089613	0.18457451	0.18464027	0.20389746	0.20392987
50	0.16803746	0.16806701	0.1816719	0.18173662	0.20079614	0.20082805
51	0.16529888	0.16532795	0.17880514	0.17886885	0.19775029	0.19778171
52	0.16264968	0.16267827	0.17602736	0.17609008	0.19481248	0.19484344
53	0.16008985	0.160118	0.1733263	0.17338803	0.19195126	0.19198176
54	0.15761103	0.15763874	0.17070194	0.17076275	0.18916664	0.1891967
55	0.15520523	0.15523252	0.16815428	0.1682142	0.1864586	0.18648826
56	0.15287244	0.15289932	0.16568336	0.16574238	0.18382719	0.18385641
57	0.15061268	0.15063916	0.16328914	0.16334732	0.18127237	0.18130119
58	0.14842652	0.14845262	0.16097164	0.161029	0.17879413	0.17882256
59	0.14629857	0.1463243	0.15873085	0.1587874	0.17639251	0.17642055
60	0.14422542	0.14425078	0.15656477	0.15662055	0.17406662	0.17409429
61	0.14220706	0.14223206	0.15443821	0.15449323	0.17179413	0.17182146
62	0.1402435	0.14026816	0.15236269	0.15241697	0.1695739	0.16960087
63	0.1383347	0.13835904	0.1503382	0.15039176	0.16740589	0.16743252
64	0.13648157	0.13650557	0.14836475	0.14841762	0.16529012	0.1653164
65	0.13468635	0.13471004	0.14644237	0.14649455	0.1632266	0.16325256
66	0.13293648	0.13295986	0.144571	0.14462252	0.16121532	0.16124095
67	0.13122746	0.13125055	0.14274777	0.14279865	0.15925038	0.1592757
68	0.12955932	0.1295821	0.1409754	0.14102563	0.15733817	0.15736319
69	0.12793206	0.12795457	0.13925408	0.1393037	0.15547857	0.1555033
70	0.12634566	0.12636788	0.13757476	0.13762377	0.15365888	0.15368332
71	0.12480012	0.12482207	0.13592996	0.13597839	0.1518769	0.15190105
72	0.12329546	0.12331715	0.13431925	0.13436711	0.15013668	0.15016057
73	0.12183165	0.12185308	0.13274743	0.13279472	0.1484369	0.14846052
74	0.12039971	0.12042089	0.13121451	0.13126126	0.14677759	0.14680094
75	0.11899927	0.11902019	0.12972048	0.1297667	0.14515872	0.1451818
76	0.11763072	0.11765141	0.12826535	0.12831105	0.14358029	0.14360313
77	0.11629408	0.11631454	0.12684941	0.12689461	0.14204319	0.1420658
78	0.11498934	0.11500957	0.12546334	0.12550806	0.14053829	0.14056066
79	0.11371472	0.11373472	0.12410318	0.1241474	0.13906094	0.13908307
80	0.11246656	0.11248635	0.12276892	0.12281267	0.13761117	0.13763307
81	0.11124536	0.11126493	0.12146057	0.12150386	0.13618895	0.13621062
82	0.11005112	0.11007047	0.12017813	0.12022096	0.1347943	0.13481574
83	0.10888463	0.10890378	0.11892161	0.11896399	0.1334272	0.13344842
84	0.10774255	0.1077615	0.11769098	0.11773292	0.13208766	0.13210867
85	0.10662442	0.10664317	0.11648636	0.11652786	0.13077542	0.13079624
86	0.10553024	0.10554881	0.11530955	0.11535064	0.12949014	0.12951075

117

Distance from Tip (μm)	18.1 μm long electrode Potential in Solution (V)		21.8 μm long electrode Potential in Solution (V)		27.8 μm long electrode Potential in Solution (V)	
87	0.10446003	0.1044784	0.11416084	0.11420152	0.12823416	0.12825456
88	0.10341073	0.10342892	0.11303925	0.11307953	0.12700742	0.12702765
89	0.10238121	0.10239923	0.11193705	0.11197694	0.1258034	0.12582341
90	0.101372	0.10138984	0.11085382	0.11089333	0.1246194	0.12463924
91	0.10038354	0.1004012	0.109791	0.10983013	0.12345676	0.12347641
92	0.09941576	0.09943326	0.10874751	0.10878627	0.1223147	0.12233416
93	0.09846868	0.09848601	0.10772336	0.10776174	0.12119322	0.12121251
94	0.09753733	0.09755449	0.10671855	0.10675658	0.12009234	0.12011146
95	0.09662202	0.09663902	0.10573307	0.10577075	0.11901205	0.11903099
96	0.09572421	0.09574105	0.10476693	0.10480427	0.11795235	0.11797112
97	0.09484423	0.09486092	0.10382012	0.10385712	0.11691323	0.11693183
98	0.09398131	0.09399784	0.10289266	0.10292933	0.11589471	0.11591316
99	0.09313542	0.09315181	0.10198454	0.10202088	0.11489678	0.11491507
100	0.09230657	0.09232281	0.10109574	0.10113177	0.11391944	0.11393757

Distance from Tip (μm)	34.8 μm long electrode		55.7 μm long electrode		73.9 μm long electrode	
	Potential in Solution (V)		Potential in Solution (V)		Potential in Solution (V)	
	1 V Potential	Current	1 V Potential	Current	1 V Potential	Current
1	0.80362093	0.8032984	0.8213357	0.82126266	0.83128744	0.83167595
2	0.7678145	0.7675065	0.788984	0.78891397	0.8004321	0.80080634
3	0.7333455	0.73305136	0.75756794	0.7575009	0.7706913	0.7710518
4	0.700325	0.70004416	0.7273016	0.72723734	0.74224705	0.7425945
5	0.66944116	0.66917276	0.6988454	0.69878376	0.7151665	0.7155015
6	0.64071417	0.6404574	0.6723211	0.67226195	0.68980706	0.6901303
7	0.6139085	0.61366254	0.6475734	0.64751655	0.66628706	0.66659945
8	0.5890207	0.5887848	0.6244989	0.6244442	0.6442824	0.64458466
9	0.56593907	0.5657124	0.60310054	0.6030478	0.6240176	0.6243105
10	0.54455847	0.54434043	0.58326566	0.5832147	0.6050112	0.6052953
11	0.5247834	0.52457327	0.5646893	0.56464005	0.5872473	0.5875232
12	0.50651866	0.50631595	0.54742974	0.54738206	0.5707153	0.5709836
13	0.48936895	0.48917308	0.5314002	0.531354	0.5551552	0.5554163
14	0.47332576	0.47313637	0.51627135	0.5162266	0.540562	0.5408163
15	0.45838916	0.45820576	0.50202847	0.50198495	0.52691066	0.5271586
16	0.44439217	0.4442144	0.48862907	0.4885868	0.5140867	0.5143287
17	0.43126708	0.43109462	0.47611344	0.4760723	0.5018523	0.50208867
18	0.41888338	0.4187159	0.4642339	0.46419385	0.49031	0.490541
19	0.40721574	0.40705293	0.45291582	0.45287678	0.4794538	0.47967973
20	0.39611736	0.39595902	0.4421982	0.44216013	0.46912426	0.4693454
21	0.38573492	0.38558072	0.4321164	0.43207923	0.45925066	0.4594672
22	0.3758783	0.37572807	0.422412	0.4223757	0.44983295	0.4500451
23	0.3664631	0.36631662	0.41327998	0.4132445	0.44084215	0.44105014
24	0.35755366	0.3574108	0.40452048	0.4044858	0.43226779	0.43247178
25	0.34912318	0.34898368	0.39613354	0.39609963	0.42404288	0.42424306
26	0.3410524	0.34091616	0.3881192	0.38808596	0.41616753	0.416364
27	0.33334056	0.3332074	0.38045022	0.38041767	0.40864164	0.40883464
28	0.32598758	0.32585737	0.37309033	0.37305844	0.40140688	0.4015965
29	0.31893748	0.3188101	0.36605573	0.36602446	0.39447498	0.39466137
30	0.31216842	0.31204376	0.35928643	0.3592558	0.3877762	0.38795948
31	0.30573547	0.30561337	0.352779	0.35274893	0.38131353	0.38149378
32	0.29955545	0.29943582	0.34653333	0.34650382	0.3750989	0.37527627
33	0.29362842	0.29351118	0.34053972	0.34051076	0.3691251	0.36929965
34	0.28793716	0.2878222	0.33474436	0.3347159	0.363345	0.36351687
35	0.2824535	0.28234074	0.32913938	0.32911143	0.35775408	0.35792333
36	0.277177	0.27706635	0.32372472	0.3236972	0.3523523	0.35251904
37	0.27209997	0.27199134	0.3184825	0.31845546	0.3471236	0.34728786
38	0.26718146	0.2670748	0.31340042	0.31337383	0.34202126	0.34218317
39	0.26252496	0.26242015	0.30851606	0.3084899	0.33710754	0.33726713
40	0.25803244	0.25792944	0.30377248	0.30374676	0.3323281	0.33248547
41	0.25366354	0.25356227	0.29923123	0.29920587	0.3277697	0.32792494

Distance from Tip (μm)	34.8 μm long electrode Potential in Solution (V)		55.7 μm long electrode Potential in Solution (V)		73.9 μm long electrode Potential in Solution (V)	
42	0.24941818	0.24931863	0.29480734	0.2947824	0.32332075	0.3234739
43	0.24529637	0.24519847	0.2905008	0.2904762	0.3189812	0.3191323
44	0.24129815	0.24120186	0.28631163	0.28628743	0.31475112	0.31490025
45	0.23742348	0.23732874	0.2822398	0.28221595	0.31063047	0.31077766
46	0.23367241	0.23357916	0.27828538	0.27826187	0.3066193	0.3067646
47	0.23004489	0.22995308	0.27444828	0.27442512	0.3027175	0.302861
48	0.22654092	0.22645053	0.27072856	0.27070573	0.2989252	0.2990669
49	0.22317186	0.22308281	0.267135	0.26711246	0.2952481	0.29538807
50	0.21995577	0.219868	0.26368397	0.26366174	0.29169843	0.29183674
51	0.21676467	0.21667817	0.26027212	0.26025018	0.28819332	0.28832996
52	0.21367532	0.21359007	0.25694674	0.2569251	0.2847814	0.28491646
53	0.21066423	0.21058019	0.2537034	0.25368202	0.2814515	0.28158498
54	0.20773126	0.2076484	0.25054204	0.25052094	0.27820355	0.2783355
55	0.20487642	0.20479469	0.24746267	0.24744186	0.27503756	0.27516806
56	0.20209973	0.2020191	0.24446532	0.24444474	0.27195355	0.2720826
57	0.19940116	0.19932161	0.24154995	0.24152964	0.26895154	0.26907918
58	0.19678071	0.19670221	0.23871659	0.23869652	0.2660287	0.26615497
59	0.1942384	0.19416091	0.23595116	0.23593132	0.2631639	0.26328883
60	0.1917742	0.1916977	0.23324132	0.23322172	0.26035538	0.26047897
61	0.18937373	0.1892982	0.23058772	0.23056836	0.2576031	0.2577254
62	0.18702577	0.18695118	0.2279904	0.22797126	0.25490713	0.25502813
63	0.18473062	0.18465693	0.22544904	0.22543012	0.25226727	0.25238705
64	0.18248832	0.18241554	0.22295763	0.22293893	0.24968132	0.24979988
65	0.18029888	0.18022697	0.22052512	0.22050661	0.24715333	0.2472707
66	0.17816226	0.17809121	0.2181663	0.21814802	0.24468744	0.24480365
67	0.17606884	0.17599861	0.21585843	0.21584034	0.2422709	0.24238597
68	0.17403011	0.1739607	0.21359634	0.21357845	0.23990156	0.24001552
69	0.17204648	0.17197786	0.21138005	0.21136235	0.23757942	0.23769228
70	0.17010592	0.17003809	0.20920952	0.209192	0.23530446	0.23541625
71	0.16820353	0.16813646	0.20708476	0.20706743	0.23307668	0.23318742
72	0.16634473	0.16627839	0.20500578	0.20498861	0.2308961	0.2310058
73	0.16452798	0.16446237	0.20297258	0.20295559	0.2287627	0.2288714
74	0.16275327	0.16268837	0.20098045	0.20096365	0.22666967	0.22677739
75	0.16102062	0.16095641	0.19902281	0.19900616	0.22460887	0.22471562
76	0.15933003	0.1592665	0.19710313	0.19708665	0.2225859	0.2226917
77	0.15768097	0.1576181	0.1952313	0.19521497	0.22060543	0.22071029
78	0.15606381	0.15600158	0.19340345	0.19338728	0.21866365	0.2187676
79	0.15447553	0.15441394	0.19160514	0.19158912	0.21675302	0.21685608
80	0.15291615	0.15285517	0.18983637	0.18982051	0.21487357	0.21497573
81	0.15138565	0.15132529	0.18809715	0.18808144	0.21302526	0.21312656
82	0.14988403	0.14982428	0.18638748	0.18637191	0.21120812	0.21130855
83	0.14841132	0.14835215	0.18470736	0.18469194	0.20942216	0.20952174
84	0.14696749	0.1469089	0.18305679	0.1830415	0.20766732	0.20776609
85	0.14555262	0.1454946	0.18143559	0.18142045	0.20594369	0.20604163
86	0.14416835	0.14411087	0.17984438	0.17982936	0.20425276	0.2043499

120

Distance from Tip (μm)	34.8 μm long electrode Potential in Solution (V)		55.7 μm long electrode Potential in Solution (V)		73.9 μm long electrode Potential in Solution (V)	
87	0.14281495	0.14275801	0.17828506	0.17827019	0.20259519	0.20269156
88	0.1414914	0.14143498	0.176759	0.17674427	0.20096892	0.20106451
89	0.14018959	0.1401337	0.1752615	0.17524688	0.1993644	0.19945922
90	0.1389092	0.13885383	0.1737867	0.1737722	0.19778396	0.19787805
91	0.13765189	0.13759702	0.17233598	0.1723216	0.19622955	0.1963229
92	0.13641624	0.13636185	0.17090851	0.17089425	0.19469914	0.19479176
93	0.13520224	0.13514835	0.16950427	0.16949014	0.19319274	0.19328465
94	0.13400993	0.1339565	0.16812332	0.16810931	0.19171037	0.19180158
95	0.13283926	0.13278632	0.1667656	0.16675171	0.190252	0.19034253
96	0.13169028	0.13163778	0.16543114	0.16541736	0.18881766	0.1889075
97	0.13056295	0.1305109	0.16411991	0.16410625	0.18740731	0.1874965
98	0.1294573	0.12940569	0.16283198	0.16281842	0.18602102	0.18610954
99	0.1283733	0.12832212	0.16156727	0.16155382	0.18465872	0.18474661
100	0.12731098	0.12726022	0.16032581	0.16031247	0.18332045	0.1834077

Distance	117.3 μm long electrode		142.1 μm long electrode	
from Tip (μm)	Potential in Solution (V)		Potential in Solution (V)	
	1 V		1 V	
	Potential	Current	Potential	Current
1	0.8459419	0.8455183	0.8515667	0.85161185
2	0.8178378	0.8174286	0.8241739	0.82421815
3	0.79022133	0.7898264	0.7976902	0.7977335
4	0.7640175	0.76363605	0.77252626	0.7725687
5	0.7393184	0.73894954	0.7486725	0.748714
6	0.7161354	0.7157785	0.72611934	0.72616005
7	0.69445795	0.6941121	0.7051856	0.7052256
8	0.67416686	0.67383146	0.68561286	0.68565214
9	0.6553522	0.65502644	0.6673159	0.66735446
10	0.6377907	0.63747394	0.65037477	0.65041274
11	0.62131095	0.6210026	0.6344794	0.6345168
12	0.605933	0.6056326	0.61950755	0.6195444
13	0.59151727	0.5912242	0.6056054	0.60564166
14	0.57792777	0.5776416	0.59242654	0.5924623
15	0.56517136	0.5648917	0.58004934	0.58008456
16	0.5531199	0.55284643	0.5683114	0.56834614
17	0.5417122	0.5414446	0.55730754	0.5573419
18	0.53088045	0.5306183	0.54678327	0.5468172
19	0.520605	0.52034813	0.5367385	0.536772
20	0.51083356	0.5105816	0.52717334	0.5272065
21	0.50147784	0.50123066	0.51808774	0.51812047
22	0.4925438	0.49230114	0.5094276	0.50946
23	0.48403418	0.48379582	0.501145	0.501177
24	0.47590402	0.4756698	0.4931694	0.49320105
25	0.4680755	0.46784526	0.4854893	0.48552063
26	0.46054736	0.46032092	0.47811797	0.47814894
27	0.45331466	0.45309186	0.47105536	0.47108603
28	0.44635633	0.44613707	0.46428436	0.46431473
29	0.43965873	0.43944284	0.45773798	0.45776805
30	0.43319738	0.43298477	0.45141014	0.45143992
31	0.42695704	0.4267476	0.44528973	0.4453192
32	0.42093766	0.42073125	0.4393767	0.43940595
33	0.41513935	0.41493583	0.43367118	0.43370014
34	0.40953988	0.4093392	0.42816088	0.42818958
35	0.4040928	0.40389484	0.42280462	0.42283306
36	0.39880627	0.39861098	0.41760135	0.41762954
37	0.39368036	0.39348766	0.4125511	0.41257903
38	0.38867077	0.38848057	0.4076205	0.4076482
39	0.38383707	0.38364932	0.4028551	0.40288258
40	0.37913606	0.37895066	0.39821544	0.39824268
41	0.3746201	0.374437	0.39374593	0.39377296

Distance from Tip (μm)	117.3 μm long electrode Potential in Solution (V)		142.1 μm long electrode Potential in Solution (V)	
42	0.3702065	0.3700256	0.3893766	0.3894034
43	0.36589518	0.36571646	0.38510746	0.38513404
44	0.36168623	0.3615096	0.38093853	0.3809649
45	0.35757953	0.35740495	0.37686974	0.3768959
46	0.3535752	0.3534026	0.37290117	0.37292713
47	0.34967318	0.34950253	0.36903277	0.36905852
48	0.34587345	0.34570473	0.36526456	0.36529014
49	0.3421819	0.342015	0.36160398	0.36162937
50	0.3386103	0.3384452	0.35806447	0.35808966
51	0.33508775	0.33492443	0.3545602	0.3545852
52	0.3316778	0.33151615	0.35113665	0.35116148
53	0.32833073	0.32817075	0.3477842	0.34780884
54	0.32504338	0.32488507	0.34450284	0.3445273
55	0.32181737	0.32166067	0.34129253	0.34131682
56	0.31865707	0.31850195	0.3381533	0.33817744
57	0.3155625	0.3154089	0.33508515	0.3351091
58	0.31253356	0.31238148	0.33208808	0.3321119
59	0.30957037	0.30941975	0.3291546	0.32917824
60	0.30667284	0.30652368	0.3262728	0.32629627
61	0.30384105	0.3036933	0.32344255	0.32346588
62	0.30107495	0.30092856	0.3206639	0.32068706
63	0.2983745	0.2982295	0.31793648	0.3179595
64	0.29573312	0.2955894	0.31525254	0.3152754
65	0.29310533	0.2929629	0.31262156	0.31264427
66	0.29054648	0.2904053	0.3100488	0.31007135
67	0.28803685	0.28789696	0.3075225	0.30754495
68	0.28557134	0.28543264	0.30504048	0.30506277
69	0.28314987	0.2830124	0.3026027	0.30262485
70	0.28077248	0.2806362	0.30020913	0.30023113
71	0.27843916	0.278304	0.29785982	0.29788166
72	0.2761499	0.27601588	0.2955547	0.29557645
73	0.2739047	0.27377182	0.29329386	0.29331544
74	0.2716987	0.2715669	0.29106888	0.29109034
75	0.269525	0.26939428	0.2888718	0.28889313
76	0.26738724	0.26725757	0.28671023	0.28673145
77	0.2652927	0.26516408	0.28459144	0.28461254
78	0.2632386	0.263111	0.28251255	0.2825335
79	0.26121435	0.26108772	0.28046295	0.28048378
80	0.25921986	0.2590942	0.27844268	0.2784634
81	0.25725517	0.2571305	0.2764517	0.2764723
82	0.2553203	0.2551966	0.27449003	0.2745105
83	0.25341523	0.25329247	0.27255768	0.27257806
84	0.25153998	0.25141814	0.27065465	0.27067488
85	0.24969442	0.2495735	0.26878083	0.26880097
86	0.24787931	0.24775928	0.26693714	0.26695716

Distance from Tip (μm)	117.3 μm long electrode		142.1 μm long electrode	
	Potential in Solution (V)		Potential in Solution (V)	
87	0.24609606	0.24597692	0.2651245	0.2651444
88	0.24434477	0.24422649	0.2633423	0.2633621
89	0.24261926	0.24250183	0.26158392	0.26160362
90	0.24091671	0.24080011	0.25984836	0.25986797
91	0.23923853	0.23912276	0.2581371	0.2581566
92	0.23758394	0.23746899	0.2564491	0.2564685
93	0.23595291	0.23583877	0.25478438	0.25480363
94	0.2343455	0.23423214	0.2531429	0.2531621
95	0.23276167	0.23264909	0.2515247	0.25154376
96	0.23120141	0.2310896	0.24992976	0.24994874
97	0.22966474	0.2295537	0.24835807	0.24837695
98	0.22815168	0.22804138	0.24680968	0.24682845
99	0.22666219	0.22655262	0.24528453	0.24530321
100	0.22519629	0.22508743	0.24378265	0.24380124

124

APPENDIX E

EXAMPLE CALCULATIONS FOR THE PREDICTED CURRENT NEEDED TO

ELECTROPORATE

Table 14. **Example calculations of the current needed to electroporate for 5 different microelectrodes used in experiments.**

Exported from Simulation		16.5 μm Long Microelectrode		
Distance (m)	Potential (V)	Current Needed for 1 Volt Drop in Solution is 40.53 μA		
1.32E-23	0.81149817	Microelectrode 5 μm Away from Cell		
-1.00E-06	0.77037114	Cell Dia. (μm)	Current (μA) Needed to Epore	Potential (V) Drop Across Cell
-2.00E-06	0.7290294	0		
-3.00E-06	0.68938506	1	312.0	0.03247736
-4.00E-06	0.65209883	2	162.7	0.06229387
-5.00E-06	0.6171184	3	112.6	0.0899756
-6.00E-06	0.58464104	4	88.0	0.1150876
-7.00E-06	0.55482453	5	73.3	0.13822548
-8.00E-06	0.5271428	6	63.4	0.15974985
-9.00E-06	0.5020308	7	56.5	0.17943643
-1.00E-05	0.47889292	8	51.3	0.19750146
-1.10E-05	0.45736855	9	47.3	0.21441833
-1.20E-05	0.43768197	10	44.1	0.2299912
-1.30E-05	0.41961694	11	41.4	0.24463717
-1.40E-05	0.40270007	12	39.3	0.2578541
-1.50E-05	0.3871272	13	37.5	0.27036683
-1.60E-05	0.37248123	14	35.9	0.28221188
-1.70E-05	0.3592643	15	34.5	0.29338918
-1.80E-05	0.34675157	16	33.3	0.30383916
-1.90E-05	0.33490652	17	32.3	0.31351886
-2.00E-05	0.32372922	18	31.4	0.32242994
-2.10E-05	0.31327924	19	30.6	0.33105527

Exported from Simulation		16.5 μm Long Microelectrode		
Distance (m)	Potential (V)	Current Needed for 1 Volt Drop in Solution is 40.53 μA		
		Microelectrode 5 μm Away from Cell		
		Cell Dia. (μm)	Current (μA) Needed to Epore	Potential (V) Drop Across Cell
-2.20E-05	0.30359954	20	29.9	0.3391692
-2.30E-05	0.29468846	21	29.2	0.34688608
-2.40E-05	0.28606313	22	28.6	0.3542584
-2.50E-05	0.2779492	23	28.0	0.36125557
-2.60E-05	0.27023232	24	27.5	0.36787757
-2.70E-05	0.26286	25	27.1	0.37412443
-2.80E-05	0.25586283	26	26.7	0.37999613
-2.90E-05	0.24924083	27	26.3	0.38555118
-3.00E-05	0.24299397	28	25.9	0.39090629
-3.10E-05	0.23712227	29	25.6	0.39605029
-3.20E-05	0.23156722	30	25.3	0.40098314
-3.30E-05	0.22621211	31	25.0	0.40570487
-3.40E-05	0.22106811	32	24.7	0.41028987
-3.50E-05	0.21613526	33	24.4	0.41467295
-3.60E-05	0.21141353	34	24.2	0.4187623
-3.70E-05	0.20682853	35	24.0	0.42267885
-3.80E-05	0.20244545	36	23.8	0.42647807
-3.90E-05	0.1983561	37	23.6	0.43015997
-4.00E-05	0.19443955	38	23.4	0.43372453
-4.10E-05	0.19064033	39	23.2	0.43717177
-4.20E-05	0.18695843	40	23.0	0.44050167
-4.30E-05	0.18339387	41	22.8	0.44371424
-4.40E-05	0.17994663	42	22.7	0.44680948
-4.50E-05	0.17661673	43	22.5	0.44978739
-4.60E-05	0.17340416	44	22.4	0.45263736
-4.70E-05	0.17030892	45	22.3	0.45534153
-4.80E-05	0.16733101	46	22.1	0.45800513
-4.90E-05	0.16448104	47	22.0	0.46057528
-5.00E-05	0.16177687	48	21.9	0.46307258
-5.10E-05	0.15911327	49	21.8	0.46549742
-5.20E-05	0.15654312	50	21.7	0.46784979

Exported from Simulation		14.9 μm Long Microelectrode		
Distance (m)	Potential (V)	Current Needed for 1 Volt Drop in Solution is 38.36 μA		
1.70E-22	0.80759925	Microelectrode 5 μm Away from Cell		
		Cell Dia. (μm)	Current (μA) Needed to Epore	Potential (V) Drop Across Cell
-1.00E-06	0.7653277			
-2.00E-06	0.7236725	0		
-3.00E-06	0.6832021	1	291.7	0.03287563
-4.00E-06	0.645243	2	152.0	0.0631065
-5.00E-06	0.6096007	3	105.4	0.0909593
-6.00E-06	0.57672507	4	82.3	0.11655176
-7.00E-06	0.5464942	5	68.5	0.13996635
-8.00E-06	0.5186414	6	59.4	0.16154826
-9.00E-06	0.49304894	7	52.9	0.18128402
-1.00E-05	0.46963435	8	48.1	0.19957114
-1.10E-05	0.44805244	9	44.3	0.21652154
-1.20E-05	0.42831668	10	41.3	0.23200492
-1.30E-05	0.41002956	11	38.9	0.24655933
-1.40E-05	0.39307916	12	36.9	0.2596924
-1.50E-05	0.37759578	13	35.2	0.27216265
-1.60E-05	0.36304137	14	33.8	0.28397015
-1.70E-05	0.3499083	15	32.5	0.29511485
-1.80E-05	0.33743805	16	31.4	0.3055145
-1.90E-05	0.32563055	17	30.4	0.31515942
-2.00E-05	0.31448585	18	29.6	0.32405475
-2.10E-05	0.3040862	19	28.8	0.33262555
-2.20E-05	0.29444128	20	28.2	0.3406453
-2.30E-05	0.28554595	21	27.5	0.3482246
-2.40E-05	0.27697515	22	27.0	0.3554364
-2.50E-05	0.2689554	23	26.5	0.36228066
-2.60E-05	0.2613761	24	26.0	0.36875737
-2.70E-05	0.2541643	25	25.6	0.37486658
-2.80E-05	0.24732004	26	25.2	0.38070442
-2.90E-05	0.24084333	27	24.8	0.38625132
-3.00E-05	0.23473412	28	24.5	0.39160299
-3.10E-05	0.22889628	29	24.2	0.39673115
-3.20E-05	0.22334938	30	23.9	0.40162324
-3.30E-05	0.21799771	31	23.6	0.40627936
-3.40E-05	0.21286955	32	23.4	0.41069945
-3.50E-05	0.20797746	33	23.1	0.41488353
-3.60E-05	0.20332134	34	22.9	0.41884842
-3.70E-05	0.19890125	35	22.7	0.42268453
-3.80E-05	0.19471717	36	22.5	0.42640277
-3.90E-05	0.19075228	37	22.3	0.43000313
-4.00E-05	0.18691617	38	22.1	0.43348563
-4.10E-05	0.18319793	39	22.0	0.43685026
-4.20E-05	0.17959757	40	21.8	0.44009703

Exported from Simulation		14.9 μm Long Microelectrode		
Distance (m)	Potential (V)	Current Needed for 1 Volt Drop in Solution is 38.36 μA		
		Microelectrode 5 μm Away from Cell		
		Cell Dia. (μm)	Current (μA) Needed to Epore	Potential (V) Drop Across Cell
-4.30E-05	0.17611507	41	21.6	0.4432259
-4.40E-05	0.17275044	42	21.5	0.44623692
-4.50E-05	0.16950367	43	21.4	0.44913007
-4.60E-05	0.1663748	44	21.2	0.45189188
-4.70E-05	0.16336378	45	21.1	0.45450299
-4.80E-05	0.16047063	46	21.0	0.4570982
-4.90E-05	0.15770882	47	20.9	0.459601
-5.00E-05	0.15509771	48	20.8	0.4620297
-5.10E-05	0.1525025	49	20.7	0.46438535
-5.20E-05	0.1499997	50	20.5	0.46666793

Exported from Simulation		14.5 μm Long Microelectrode		
Distance (m)	**Potential (V)**	**Current Needed for 1 Volt Drop in Solution is 37.80 μA**		
1.32E-23	0.80593854	**Microelectrode 5 μm Away from Cell**		
-1.00E-06	0.76364416	**Cell Dia. (μm)**	**Current (μA) Needed to Epore**	**Potential (V) Drop Across Cell**
-2.00E-06	0.72161454	0		
-3.00E-06	0.6811195	1	287.0	0.03292544
-4.00E-06	0.6429111	2	149.2	0.06335514
-5.00E-06	0.60724384	3	103.5	0.09129764
-6.00E-06	0.5743184	4	80.9	0.11679417
-7.00E-06	0.5438887	5	67.4	0.14029649
-8.00E-06	0.5159462	6	58.4	0.16184679
-9.00E-06	0.49044967	7	52.0	0.18160409
-1.00E-05	0.46694735	8	47.3	0.19988864
-1.10E-05	0.44539705	9	43.6	0.21661878
-1.20E-05	0.42563975	10	40.7	0.23242072
-1.30E-05	0.4073552	11	38.3	0.24696764
-1.40E-05	0.39062506	12	36.3	0.26034124
-1.50E-05	0.37482312	13	34.7	0.27268014
-1.60E-05	0.3602762	14	33.2	0.28435266
-1.70E-05	0.3469026	15	32.0	0.29535881
-1.80E-05	0.3345637	16	30.9	0.30571024
-1.90E-05	0.32289118	17	30.0	0.3153672
-2.00E-05	0.31188503	18	29.1	0.32424859
-2.10E-05	0.3015336	19	28.4	0.33271441
-2.20E-05	0.29187664	20	27.7	0.34076471
-2.30E-05	0.28299525	21	27.1	0.3483994
-2.40E-05	0.27452943	22	26.6	0.35561851
-2.50E-05	0.26647913	23	26.1	0.36242208
-2.60E-05	0.25884444	24	25.6	0.36881006
-2.70E-05	0.25162533	25	25.2	0.37499819
-2.80E-05	0.24482176	26	24.8	0.3807779
-2.90E-05	0.23843378	27	24.5	0.38627008
-3.00E-05	0.23224565	28	24.1	0.39154037
-3.10E-05	0.22646594	29	23.8	0.39658882
-3.20E-05	0.22097376	30	23.5	0.40141537
-3.30E-05	0.21570347	31	23.3	0.40602008
-3.40E-05	0.21065502	32	23.0	0.41040291
-3.50E-05	0.20582847	33	22.8	0.41457969
-3.60E-05	0.20122376	34	22.6	0.41863056
-3.70E-05	0.19684093	35	22.4	0.42250532
-3.80E-05	0.19266415	36	22.2	0.42620218
-3.90E-05	0.18861328	37	22.0	0.42976844
-4.00E-05	0.18473852	38	21.8	0.43321063
-4.10E-05	0.18104166	39	21.6	0.43650794
-4.20E-05	0.1774754	40	21.5	0.43969414

Exported from Simulation		14.5 μm Long Microelectrode		
Distance (m)	Potential (V)	Current Needed for 1 Volt Drop in Solution is 37.80 μA		
		Microelectrode 5 μm Away from Cell		
		Cell Dia. (μm)	Current (μA) Needed to Epore	Potential (V) Drop Across Cell
-4.30E-05	0.17403321	41	21.3	0.44276919
-4.40E-05	0.1707359	42	21.2	0.44573312
-4.50E-05	0.1675497	43	21.1	0.44858592
-4.60E-05	0.16447465	44	20.9	0.45132758
-4.70E-05	0.16151072	45	20.8	0.45396561
-4.80E-05	0.15865792	46	20.7	0.45655382
-4.90E-05	0.15591626	47	20.6	0.45901774
-5.00E-05	0.15327823	48	20.5	0.46141114
-5.10E-05	0.15069002	49	20.4	0.46373399
-5.20E-05	0.1482261	50	20.3	0.46598633

Exported from Simulation		11.5 μm Long Microelectrode		
Distance (m)	Potential (V)	Current Needed for 1 Volt Drop in Solution is 33.50 μA		
2.28E-22	0.7963699	Microelectrode 5 μm Away from Cell		
-1.00E-06	0.75187016	Cell Dia. (μm)	Current (μA) Needed to Epore	Potential (V) Drop Across Cell
-2.00E-06	0.70812494	0		
-3.00E-06	0.6659888	1	247.4	0.03384735
-4.00E-06	0.62644386	2	128.8	0.06504695
-5.00E-06	0.58979005	3	89.2	0.09384662
-6.00E-06	0.5559427	4	69.9	0.11982367
-7.00E-06	0.5247431	5	58.3	0.14365825
-8.00E-06	0.49594343	6	50.6	0.16549105
-9.00E-06	0.46996638	7	45.1	0.18550599
-1.00E-05	0.4461318	8	41.1	0.20387025
-1.10E-05	0.424299	9	38.0	0.22065449
-1.20E-05	0.40428406	10	35.4	0.23626361
-1.30E-05	0.3859198	11	33.4	0.25069228
-1.40E-05	0.36913556	12	31.7	0.26394049
-1.50E-05	0.35352644	13	30.3	0.27620188
-1.60E-05	0.33909777	14	29.1	0.28773517
-1.70E-05	0.32584956	15	28.1	0.29849351
-1.80E-05	0.31358817	16	27.2	0.30840025
-1.90E-05	0.30205488	17	26.4	0.31772072
-2.00E-05	0.29129654	18	25.6	0.32655761
-2.10E-05	0.2813898	19	25.0	0.3349109
-2.20E-05	0.27206933	20	24.4	0.34278065
-2.30E-05	0.26323244	21	23.9	0.35016683
-2.40E-05	0.25487915	22	23.5	0.35705801
-2.50E-05	0.2470094	23	23.0	0.36355091
-2.60E-05	0.23962322	24	22.7	0.36973203
-2.70E-05	0.23273204	25	22.3	0.37563162
-2.80E-05	0.22623914	26	22.0	0.38124894
-2.90E-05	0.22005802	27	21.7	0.38657859
-3.00E-05	0.21415843	28	21.4	0.3916194
-3.10E-05	0.20854111	29	21.1	0.39639225
-3.20E-05	0.20321146	30	20.9	0.40097081
-3.30E-05	0.19817065	31	20.7	0.40535088
-3.40E-05	0.1933978	32	20.5	0.4095306
-3.50E-05	0.18881924	33	20.3	0.41350997
-3.60E-05	0.18443917	34	20.1	0.41728896
-3.70E-05	0.18025945	35	19.9	0.42088898
-3.80E-05	0.17628008	36	19.7	0.42436645
-3.90E-05	0.17250109	37	19.6	0.42772437
-4.00E-05	0.16890107	38	19.4	0.43096276
-4.10E-05	0.1654236	39	19.3	0.43408159
-4.20E-05	0.16206568	40	19.2	0.43708155

Exported from Simulation		11.5 μm Long Microelectrode		
Distance (m)	Potential (V)	Current Needed for 1 Volt Drop in Solution is 33.50 μA		
		Microelectrode 5 μm Away from Cell		
		Cell Dia. (μm)	Current (μA) Needed to Epore	Potential (V) Drop Across Cell
-4.30E-05	0.15882729	41	19.0	0.43995904
-4.40E-05	0.15570846	42	18.9	0.44269832
-4.50E-05	0.1527085	43	18.8	0.4453529
-4.60E-05	0.14983101	44	18.7	0.4479266
-4.70E-05	0.14709173	45	18.6	0.45041941
-4.80E-05	0.14443715	46	18.5	0.45283136
-4.90E-05	0.14186345	47	18.4	0.45516241
-5.00E-05	0.13937064	48	18.3	0.45740867
-5.10E-05	0.13695869	49	18.2	0.45956551
-5.20E-05	0.13462764	50	18.1	0.46165504

Exported from Simulation		6.8 μm Long Microelectrode		
Distance (m)	Potential (V)	Current Needed for 1 Volt Drop in Solution is 26.05 μA		
0	0.7740783	Microelectrode 5 μm Away from Cell		
-1.00E-06	0.7252247	Cell Dia. (μm)	Current (μA) Needed to Epore	Potential (V) Drop Across Cell
-2.00E-06	0.67786264	0		
-3.00E-06	0.6321581	1	180.7	0.03603856
-4.00E-06	0.5897931	2	93.9	0.06938944
-5.00E-06	0.5508276	3	65.8	0.098953
-6.00E-06	0.51478904	4	51.9	0.12540946
-7.00E-06	0.48143816	5	43.5	0.14958803
-8.00E-06	0.4518746	6	37.9	0.17174114
-9.00E-06	0.42541814	7	33.9	0.19192613
-1.00E-05	0.40123957	8	31.0	0.21014295
-1.10E-05	0.37908646	9	28.8	0.22647906
-1.20E-05	0.35890147	10	27.0	0.24161447
-1.30E-05	0.34068465	11	25.5	0.25563774
-1.40E-05	0.32434854	12	24.2	0.26859046
-1.50E-05	0.30921313	13	23.2	0.28032897
-1.60E-05	0.29518986	14	22.4	0.29111416
-1.70E-05	0.28223714	15	21.6	0.30128314
-1.80E-05	0.27049863	16	21.0	0.31079128
-1.90E-05	0.25971344	17	20.4	0.31962565
-2.00E-05	0.24954446	18	19.9	0.32778629
-2.10E-05	0.24003632	19	19.4	0.33527314
-2.20E-05	0.23120195	20	19.0	0.34236141
-2.30E-05	0.22304131	21	18.7	0.34906998
-2.40E-05	0.21555446	22	18.3	0.35537841
-2.50E-05	0.20846619	23	18.0	0.3613272
-2.60E-05	0.20175762	24	17.7	0.36693924
-2.70E-05	0.19544919	25	17.5	0.3722146
-2.80E-05	0.1895004	26	17.3	0.37715616
-2.90E-05	0.18388836	27	17.1	0.38185842
-3.00E-05	0.178613	28	16.9	0.38633827
-3.10E-05	0.17367144	29	16.7	0.39059664
-3.20E-05	0.16896918	30	16.5	0.39465054
-3.30E-05	0.16448933	31	16.3	0.39850488
-3.40E-05	0.16023096	32	16.2	0.40213201
-3.50E-05	0.15617706	33	16.1	0.40560754
-3.60E-05	0.15232272	34	15.9	0.40893354
-3.70E-05	0.14869559	35	15.8	0.41211001
-3.80E-05	0.14522006	36	15.7	0.41513697
-3.90E-05	0.14189406	37	15.6	0.41804824
-4.00E-05	0.13871759	38	15.5	0.42085505
-4.10E-05	0.13569063	39	15.4	0.42355453
-4.20E-05	0.13277936	40	15.3	0.42611751

Exported from Simulation		6.8 μm Long Microelectrode		
Distance (m)	Potential (V)	Current Needed for 1 Volt Drop in Solution is 26.05 μA		
0	0.7740783	Microelectrode 5 μm Away from Cell		
-1.00E-06	0.7252247	Cell Dia. (μm)	Current (μA) Needed to Epore	Potential (V) Drop Across Cell
-4.30E-05	0.12997255	41	15.2	0.42857491
-4.40E-05	0.12727307	42	15.1	0.43094406
-4.50E-05	0.12471009	43	15.0	0.43322495
-4.60E-05	0.12225269	44	15.0	0.435417585
-4.70E-05	0.11988354	45	14.9	0.437521964
-4.80E-05	0.11760265	46	14.8	0.43954519
-4.90E-05	0.115410015	47	14.8	0.441507176
-5.00E-05	0.113305636	48	14.7	0.44340848
-5.10E-05	0.11128241	49	14.6	0.4452491
-5.20E-05	0.109320424	50	14.6	0.447028786

CELL DEATH FACTORS ANOVA

Table 15. The ANOVA analysis of the various cell death factors.

Anova: Single Factor						
SUMMARY						
Groups	*Count*	*Sum*	*Average*	*Variance*		
Control	10	7.932236	0.793224	0.222894		
Iso Solution	10	11.8167	1.18167	0.564636		
Light Exposure	5	4.500913	0.900183	0.483261		
Thioglo-1	5	5.922175	1.184435	0.08584		
Light Exposure + Thioglo-1	5	4.200677	0.840135	0.253465		
Iso Solution + Thioglo-1	5	12.14646	2.429292	1.523271		
Iso Solution + Light Exposure	5	11.54297	2.308595	1.005059		
Iso Solution + Light Exposure + Thioglo-1	5	11.1079	2.22158	1.499781		
ANOVA						
Source of Variation	*SS*	*df*	*MS*	*F*	*P-value*	*F crit*
Between Groups	19.99325	7	2.856179	4.528401	0.00078	2.23707
Within Groups	26.49048	42	0.630726			
Total	46.48373	49				

Anova: Single Factor						
SUMMARY						
Groups	*Count*	*Sum*	*Average*	*Variance*		
Control	10	7.932236	0.793224	0.222894		
Iso Solution	10	11.8167	1.18167	0.564636		
ANOVA						
Source of Variation	*SS*	*df*	*MS*	*F*	*P-value*	*F crit*
Between Groups	0.754454	1	0.754454	1.916	0.183221	4.413873
Within Groups	7.08777	18	0.393765			
Total	7.842224	19				

Anova: Single Factor
SUMMARY

Groups	Count	Sum	Average	Variance		
Control	10	7.932236	0.793224	0.222894		
Light Exposure	5	4.500913	0.900183	0.483261		

ANOVA

Source of Variation	SS	df	MS	F	P-value	F crit
Between Groups	0.038134	1	0.038134	0.125852	0.728461	4.667193
Within Groups	3.93909	13	0.303007			
Total	3.977224	14				

Anova: Single Factor
SUMMARY

Groups	Count	Sum	Average	Variance		
Control	10	7.932236	0.793224	0.222894		
Thioglo-1	5	5.922175	1.184435	0.08584		

ANOVA

Source of Variation	SS	df	MS	F	P-value	F crit
Between Groups	0.510155	1	0.510155	2.822842	0.116788	4.667193
Within Groups	2.34941	13	0.180724			
Total	2.859565	14				

Anova: Single Factor
SUMMARY

Groups	Count	Sum	Average	Variance		
Control	10	7.932236	0.793224	0.222894		
Light Exposure + Thioglo-1	5	4.200677	0.840135	0.253465		

ANOVA

Source of Variation	SS	df	MS	F	P-value	F crit
Between Groups	0.007336	1	0.007336	0.031579	0.861695	4.667193
Within Groups	3.019909	13	0.232301			
Total	3.027245	14				

136

Anova: Single Factor
SUMMARY

Groups	Count	Sum	Average	Variance		
Control	10	7.932236	0.793224	0.222894		
Iso Solution + Thioglo-1	5	12.14646	2.429292	1.523271		

ANOVA

Source of Variation	SS	df	MS	F	P-value	F crit
Between Groups	8.922402	1	8.922402	14.32144	0.002274	4.667193
Within Groups	8.09913	13	0.62301			
Total	17.02153	14				

Anova: Single Factor
SUMMARY

Groups	Count	Sum	Average	Variance		
Control	10	7.932236	0.793224	0.222894		
Iso Solution + Light Exposure	5	11.54297	2.308595	1.005059		

ANOVA

Source of Variation	SS	df	MS	F	P-value	F crit
Between Groups	7.6545	1	7.6545	16.51242	0.001342	4.667193
Within Groups	6.026283	13	0.46356			
Total	13.68078	14				

Anova: Single Factor
SUMMARY

Groups	Count	Sum	Average	Variance		
Control	10	7.932236	0.793224	0.222894		
Iso Solution + Light Exposure + Thioglo-1	5	11.1079	2.22158	1.499781		

ANOVA

Source of Variation	SS	df	MS	F	P-value	F crit
Between Groups	6.800674	1	6.800674	11.04395	0.005496	4.667193
Within Groups	8.005173	13	0.615783			
Total	14.80585	14				

BIBLIOGRAPHY

1. Allbritton, N.L., et al., *Fast controllable laser lysis of cells for analysis*, in *PCT Int. Appl.* 1999, (The Regents of the University of California, USA). World. p. 40 pp.

2. Bergquist, J., et al., *Analysis of Human Cerebrospinal Fluid by Capillary Electrophoresis with Laser-Induced Fluorescence Detection.* Analytical Chemistry, 1994. **66**(20): p. 3512-18.

3. Bergquist, J., et al., *Measurements of catecholamine-mediated apoptosis of immunocompetent cells by capillary electrophoresis.* Electrophoresis, 1997. **18**(10): p. 1760-1766.

4. Han, F., et al., *Fast Electrical Lysis of Cells for Capillary Electrophoresis.* Analytical Chemistry, 2003. **75**(15): p. 3688-3696.

5. Sims, C.E., et al., *Laser-Micropipet Combination for Single-Cell Analysis.* Analytical Chemistry, 1998. **70**(21): p. 4570-4577.

6. Krylov, S.N. and N.J. Dovichi, *Single-cell analysis using capillary electrophoresis: influence of surface support properties on cell injection into the capillary.* Electrophoresis, 2000. **21**(4): p. 767-773.

7. Heller, R., *The development of electroporation.* Science (Washington, DC, United States), 2002. **295**(5553): p. 277.

8. Prasanna, G.L. and T. Panda, *Electroporation. Basic principles, practical considerations and applications in molecular biology.* Bioprocess Engineering, 1997. **16**(5): p. 261-264.

9. Olofsson, J., et al., *Single-cell electroporation.* Current Opinion in Biotechnology, 2003. **14**(1): p. 29-34.

10. Mosharov, E.V., et al., *Intracellular patch electrochemistry: Regulation of cytosolic catecholamines in chromaffin cells.* Journal of Neuroscience, 2003. **23**(13): p. 5835-5845.

11. Ryttsen, F., et al., *Characterization of single-cell electroporation by using patch-clamp and fluorescence microscopy.* Biophysical Journal, 2000. **79**(4): p. 1993-2001.

12.   Weaver, J.C., *Electroporation of cells and tissues.* IEEE Transactions on Plasma Science, 2000. **28**(1): p. 24-33.

13.   Riske, K.A. and R. Dimova, *Electro-deformation and poration of giant vesicles viewed with high temporal resolution.* Biophysical Journal, 2005. **88**(2): p. 1143-1155.

14.   Glaser, R.W., et al., *Resversible electrical breakdown of lipid bilayers: formation and evoluton of pores.* Biochem. Biophys. Acta., 1988. **940**: p. 275 - 287.

15.   Kakorin, S. and E. Neumann, *Electrooptical relaxation spectrometry of membrane electroporation in lipid vesicles.* Colloids and Surfaces, A: Physicochemical and Engineering Aspects, 2002. **209**(2-3): p. 147-165.

16.   Teissie, J. and T.Y. Tsong, *Electric field induced transient pores in phospholipid bilayer vesicles.* Biochemistry, 1981. **20**: p. 1548 - 1554.

17.   Griese, T., S. Kakorin, and E. Neumann, *Conductometric and electrooptic relaxation spectrometry of lipid vesicle electroporation at high fields.* Physical Chemistry Chemical Physics, 2002. **4**(7): p. 1217-1227.

18.   Seger, U., et al., *Towards single-cell-controlled electroporation in a microfluidic device.* Micro Total Analysis Systems 2002, Proceedings of the mTAS 2002 Symposium, 6th, Nara, Japan, Nov. 3-7, 2002, 2002. **2**: p. 796-798.

19.   Lin, Y.-C. and M.-Y. Huang, *Electroporation microchips for in vitro gene transfection.* Journal of Micromechanics and Microengineering, 2001. **11**(5): p. 542-547.

20.   Lin, Y.-C. and M.-Y. Huang, *Electroporation microchips for gene transfection.* Micro Total Analysis Systems 2001, Proceedings mTAS 2001 Symposium, 5th, Monterey, CA, United States, Oct. 21-25, 2001, 2001: p. 250-252.

21.   Huang, Y. and B. Rubinsky, *Microfabricated electroporation chip for single cell membrane permeabilization.* Sensors and Actuators, A: Physical, 2001. **A89**(3): p. 242-249.

22.   Nolkrantz, K., et al., *Electroporation of single cells and tissues with an electrolyte-filled capillary.* Analytical Chemistry, 2001. **73**(18): p. 4469-4477.

23.   Wilson, C.F., et al., *Nanoengineered structures for holding and manipulating liposomes and cells.* Analytical Chemistry, 2001. **73**(4): p. 787-791.

24.   Banga, A.K. and M.R. Prausnitz, *Assessing the potential of skin electroporation for the delivery of protein- and gene-based drugs.* Trends in Biotechnology, 1998. **16**(10): p. 408-412.

25.   Baron, S., et al., *Electroporation of antibodies, DNA, and other macromolecules into cells: a highly efficient method.* Journal of Immunological Methods, 2000. **242**(1-2): p. 115-126.

26.   Gothelf, A., L.M. Mir, and J. Gehl, *Electrochemotherapy: results of cancer treatment using enhanced delivery of bleomycin by electroporation.* Cancer Treatment Reviews, 2003. **29**(5): p. 371-387.

27.   Heller, R., R. Gilbert, and M.J. Jaroszeski, *Clinical trials for solid tumors using electrochemotherapy.* Methods in Molecular Medicine, 2000. **37**: p. 137-156.

28.   Jaroszeski, M.J., et al., *Toxicity of anticancer agents mediated by electroporation in vitro.* Anti-Cancer Drugs, 2000. **11**(3): p. 201-208.

29.   Zewert, T.E., et al., *Creation of transdermal pathways for macromolecule transport by skin electroporation and a low toxicity, pathway-enlarging molecule.* Bioelectrochemistry and Bioenergetics, 1999. **49**(1): p. 11-20.

30.   Drury, M.D. and E.B. Kmiec, *DNA pairing is an important step in the process of targeted nucleotide exchange.* Nucleic Acids Research, 2003. **31**(3): p. 899-910.

31.   Greco, O., et al., *Cancer gene therapy: 'delivery, delivery, delivery'.* Frontier in Bioscience, 2002. **7**(84): p. 1516-24.

32.   Jaroszeski, M.J., et al., *In vivo gene delivery by electroporation.* Advanced Drug Delivery Reviews, 1999. **35**(1): p. 131-137.

33.   Li, S. and Z. Ma, *Nonviral gene therapy.* Current Gene Therapy, 2001. **1**(2): p. 201-26.

34.   Neumann, E. and S. Kakorin, *Digression on membrane electroporation for drug and gene delivery.* Technology in Cancer Research & Treatment, 2002. **1**(5): p. 329-339.

35.   Cemazar, M., et al., *Effective gene transfer to solid tumors using different nonviral gene delivery techniques: electroporation, liposomes, and integrin-targeted vector.* Cancer Gene Therapy, 2002. **9**(4): p. 399-406.

36.   Golzio, M., J. Teissie, and M.-P. Rols, *Direct visualization at the single-cell level of electrically mediated gene delivery.* Proceedings of the National Academy of Sciences of the United States of America, 2002. **99**(3): p. 1292-1297.

37.   Golzio, M., J. Teissie, and M.-P. Rols, *Cell synchronization effect on mammalian cell permeabilization and gene delivery by electric field.* Biochimica et Biophysica Acta, Biomembranes, 2002. **1563**(1-2): p. 23-28.

38.   Golzio, M., J. Teissie, and M.P. Rols, *Control by membrane order of voltage-induced permeabilization, loading and gene transfer in mammalian cells.* Bioelectrochemistry, 2001. **53**(1): p. 25-34.

39.   Nicolau, C.Y., et al., *In vivo electroporation of cells for use in gene therapy*, in *PCT Int. Appl.* 1997, (Cbr Laboratories, Inc., USA; University of South Florida). World. p. 19 pp.

40.   Somiari, S., et al., *Theory and in vivo application of electroporative gene delivery.* Molecular Therapy, 2000. **2**(3): p. 178-187.

41.   Gehl, J., *Electroporation: Theory and methods, perspectives for drug delivery, gene therapy and research.* Acta Physiologica Scandinavica, 2003. **177**(4): p. 437-447.

42.   Canatella, P.J., et al., *Quantitative study of electroporation-mediated molecular uptake and cell viability.* Biophysical Journal, 2001. **80**(2): p. 755-764.

43.   Jaroszeski, M.J., et al., *Effects of electrochemotherapy with bleomycin on normal liver tissue in a rat model.* European Journal of Cancer, 2001. **37**(3): p. 414-421.

44.   Jaroszeski, M.J., R. Gilbert, and R. Heller, *Electrochemotherapy: an emerging drug delivery method for the treatment of cancer.* Advanced Drug Delivery Reviews, 1997. **26**(2,3): p. 185-197.

45.   Jaroszeski, M.J., et al., *Enhanced effects of multiple treatment electrochemotherapy.* Melanoma Research, 1996. **6**(6): p. 427-433.

46.   Neumann, E.S.-R., W.Y.; Hofschneider, P.H., *Gene transfer into mouse lyoma cell by electroporation in high electric fields.* The EMBO Journal, 1982. **1**(7): p. 841 - 845.

47.   Dayball, K., et al., *Electroporation enables plasmid vaccines to elicit CD8+ T cell responses in the absence of CD4+ T cells.* Journal of Immunology, 2003. **171**(7): p. 3379-3384.

48.   Lin, Y.-C., et al., *Flow-type electroporation chips for gene transfection.* Proceedings of SPIE-The International Society for Optical Engineering, 2000. **4177**(Microfluidic Devices and Systems III): p. 194-198.

49.   Wells, J.M., et al., *Electroporation-enhanced gene delivery in mammary tumors.* Gene Therapy, 2000. **7**(7): p. 541-547.

50.   Sugar, I.P. and E. Neumann, *Stochastic model for electric field-induced membrane pores. Electroporation.* Biophysical Chemistry, 1984. **19**(3): p. 211-25.

51.   Saarinen-Savolainen, P., et al., *Method for evaluating drug release from liposomes in sink conditions.* International Journal of Pharmaceutics, 1997. **159**(1): p. 27-33.

52.   Schulte, A. and R.H. Chow, *Cylindrically Etched Carbon-Fiber Microelectrodes for Low-Noise Amperometric Recording of Cellular Secretion.* Analytical Chemistry, 1998. **70**(5): p. 985-990.

53.   Vargha-Butler, E.I. and E.L. Hurst, *Study of liposomal drug delivery systems. 1. Surface characterization of steroid loaded MLV liposomes.* Colloids and Surfaces, B: Biointerfaces, 1995. **3**(5): p. 287-95.

54. Weiss, D.J., et al., *Computer Simulation of Charge-Selective Electrochemistry of Catechols at High-Surface-Area Carbon Fibers.* Analytical Chemistry, 1999. **71**(17): p. 3712-3720.

55. Solak, A.O., et al., *Modified Carbon Surfaces as \"Organic Electrodes\" That Exhibit Conductance Switching.* Analytical Chemistry, 2003. **75**(2): p. 296-305.

56. Maeda, H., Y. Yamauchi, and H. Ohmori, *Electrochemical preparation of chemically modified carbon electrodes and their applications to electroanalytical chemistry.* Current Topics in Analytical Chemistry, 2001. **2**: p. 121-133.

57. Maeda, H., *Preparation of chemically modified carbon electrodes by anodization in 1-alkanols and their application to electrochemical analysis.* Yakugaku Zasshi, 2000. **120**(2): p. 170-182.

58. Martel, D., et al., *The effect of modification of carbon electrodes with hybrid inorganic/organic monolayers on morphology and electrocatalytic activity of platinum deposits.* Electrochimica Acta, 2001. **46**(26-27): p. 4197-4204.

59. Malinauskas, A., T. Ruzgas, and L. Gorton, *Electrochemical study of glassy carbon electrodes modified with zirconium phosphate and some azine-type redox dyes.* Journal of Solid State Electrochemistry, 2001. **5**(4): p. 287-292.

60. Lojou, E., et al., *Poly(ester-sulfonic acid): modified carbon electrodes for the electrochemical study of c-type cytochromes.* Electrochimica Acta, 1999. **44**(19): p. 3341-3352.

61. Demel, R., E. Dotterl, and A. Merz, *Catalytic electrochemical reduction of 1,2-dibromocyclohexane derivatives at carbon electrodes modified with cobalt porphyrin siloxane films.* Acta Chemica Scandinavica, 1999. **53**(11): p. 1038-1042.

62. Downard, A.J., *Electrochemically assisted covalent modification of carbon electrodes.* Electroanalysis, 2000. **12**(14): p. 1085-1096.

63. Kulkarni, S.B. and E.I. Vargha-Butler, *Effect of bilayer additives on encapsulation of steroids in MLV liposomes.* International Journal of Pharmaceutical Advances, 1996. **1**(4): p. 408-413.

64. Kulkarni, S.B. and E.I. Vargha-Butler, *Study of liposomal drug delivery systems. Encapsulation efficiencies of some steroids in MLV liposomes.* Colloids and Surfaces, B: Biointerfaces, 1995. **4**(2): p. 77-85.

65. Weaver, J.C. and Y.A. Chizmadzhev, *Theory of electroporation: A review.* Bioelectrochemistry and Bioenergetics, 1996. **41**(2): p. 135-160.

66. Rols, M.-P. and J. Teissie, *Electropermeabilization of mammalian cells to macromolecules: control by pulse duration.* Biophysical Journal, 1998. **75**(3): p. 1415-1423.

67.   Gabriel, B. and J. Teissie, *Control by electrical parameters of short- and long-term cell death resulting from electropermeabilization of Chinese hamster ovary cells.* Biochimica et Biophysica Acta, Molecular Cell Research, 1995. **1266**(2): p. 171-178.

68.   Wruck, W.J., R.M. Machado, and T.W. Chapman, *Current interruption - Instrumentation and applications.* Journal of the Electrochemical Society, 1987. **134**(3): p. 539-46.

69.   Baruzzi, A.M. and J. Uehlken, *Current interruption potentiostat for elimination of the IR drop in four-electrode systems.* Journal of Electroanalytical Chemistry and Interfacial Electrochemistry, 1990. **282**(1-2): p. 267-73.

70.   Brown, W.B., *Current-interruption method of electrodepositing paints.* Journal of Paint Technology, 1975. **47**(605): p. 43-7.

71.   Bard, A.J., et al., *Scanning electrochemical microscopy. Introduction and principles.* Analytical Chemistry, 1989. **61**(2): p. 132-8.

72.   Frysz, C.A. and D.D.L. Chung, *Improving the electrochemical behavior of carbon black and carbon filaments by oxidation.* Carbon, 1997. **35**(8): p. 1111-1127.

73.   Michael, A.C. and J.B. Justice, Jr., *Oxidation of dopamine and 4-methylcatechol at carbon fiber disk electrodes.* Analytical Chemistry, 1987. **59**(3): p. 405-10.

74.   Sujaritvanichpong, S., et al., *Electrochemical behavior of dopamine at carbon fiber electrodes.* Journal of Electroanalytical Chemistry and Interfacial Electrochemistry, 1986. **198**(1): p. 195-203.